Chapter 16

Model-Based Parameter Identification for Helicopter Main Rotor Balancing and Tracking Using Once-per-Revolution Vibration Data

Chapter details

Chapter DOI:

https://doi.org/10.4322/978-65-86503-83-8.c16

Chapter suggested citation / reference style:

Jorge, Ariosto B., et al. (2022). "Model-Based Parameter Identification for Helicopter Main Rotor Balancing and Tracking Using Once-per-Revolution Vibration Data". *In* Jorge, Ariosto B., et al. (Eds.) *Fundamental Concepts and Models for the Direct Problem*, Vol. II, UnB, Brasilia, DF, Brazil, pp. 519–616. Book series in Discrete Models, Inverse Methods, & Uncertainty Modeling in Structural Integrity.

P.S.: DOI may be included at the end of citation, for completeness.

Book details

Book: Fundamental Concepts and Models for the Direct Problem

Edited by: Jorge, Ariosto B., Anflor, Carla T. M., Gomes, Guilherme F., & Carneiro, Sergio H. S.

Volume II of Book Series in:

Discrete Models, Inverse Methods, & Uncertainty Modeling in Structural Integrity

Published by: UnB City: Brasilia, DF, Brazil Year: 2022

DOI: https://doi.org/10.4322/978-65-86503-83-8

Model-Based Parameter Identification for Helicopter Main Rotor Balancing and Tracking Using Once-per-Revolution Vibration Data

Ariosto B. Jorge[1*], Rafael de A. González[2],

Bento S. de Mattos[3], and Ronaldo V. Cruz[3]

[1]Post-Graduate Program - Integrity of Engineering Materials, University of Brasilia, Brazil. E-mail: ariosto.b.jorge@gmail.com
[2]Naval Studies Coordination Center in São Paulo, Brazilian Navy, Brazil. E-mail: rafaelgonzalez.eng@gmail.com
[3]Instituto Tecnológico de Aeronáutica, Brazil. E-mail: bmattos@ita.br; ronaldoc@ita.br

*Corresponding author

Abstract

This chapter presents a compilation of the research work accomplished by authors and collaborators on the topics of model-based balancing and tracking of the helicopter main rotor using once-per-revolution vibration data. Simplified analytical modeling is presented for the analysis of vibration signal in the monitored structure of any rotorcraft for the detection of defects, equivalent to a hub blade unbalancing and out-of-tracking blades. Those degradations are common in the main rotor and are the greatest source of periodic excitations transmitted to the fuselage. The vibratory responses under analysis are limited to the one-per-rev fundamental frequency of the main rotor and were numerically simulated both in FORTRAN and in MATLAB^(R) environments. The direct problem is presented in two parts: The rotor-fuselage system is initially modeled as isotropic, and then anisotropies are introduced in the formulation, to simulate defects that generate vibration information (in amplitude and phase) at the selected points where accelerometers were located. The application of the model involves comparisons of the results from the obtained non-linear system of equations with either the information contained in the maintenance manual (for the case study of a four-blade main rotor helicopter) or with preliminary experimental data obtained by flight tests (for the case study of a three-blade main rotor helicopter. The comparison between the simulation results and either the maintenance manual information or the flight test measurements considered the accelerometers placed at the points of the fuselage as defined in the flight manual by the aircraft manufacturer.

Keywords: vibration of the helicopter rotor; vibration analysis; helicopter dynamic components

1 Helicopter vibration reduction techniques of balancing and tracking of the main rotor: introduction and chapter outline

This chapter discusses helicopter vibration reduction techniques focused on balancing and tracking the helicopter rotors and concentrated on a discussion of model-based parameter identification for balancing and tracking a helicopter's main rotor using once-per-revolution vibration data.

Signal-based vibration analysis techniques and the use of a framework of Health and Usage Monitoring Systems (HUMS) for helicopter dynamic components and aircraft engines are discussed in a separate chapter. Some HUMS systems include built-in features for the use of vibration data to help main-rotor and tail-rotor balancing and tracking.

1.1 Introduction

In the study of helicopter dynamics, rotor-induced vibration can be seen to arise from flapping and lead-lag blade motion, in different flight conditions. For detailed discussions on helicopter aerodynamics and dynamics, see references (Bramwell et al., 2001), (Bielawa, 2006), (Johnson, 2013a), (Venkatesan, 2015), (Padfield, 2018). Throughout the operational life cycle of a helicopter, routine corrective maintenance - reactive to the failure that has already occurred - is carried out to counter problems of maladjustment and misalignment of its rotating systems, including also problems due to other components secondarily degraded as a result of these defects in the rotor system. These maintenance procedures increase the helicopter operating costs, i. e., material, man-hours, and execution of test flights, including the loss of profit associated with the aircraft's unavailability. Mass unbalance and blade tip trajectory misalignment (out-of tracking) are the most common degradations foreseen in the main rotor, which are, for dynamic reasons, the source that contributes the most to the periodic excitations transmitted to the fuselage. For references on main rotor balancing and tracking models and procedures, see (Rosen & Ben-Ari, 1997), (Ben-Ari & Rosen, 1997), (Ventres & Hayden, 2000), (Wang & Danai, 2003), (Wang et al., 2005), (Miller & Kunz, 2008). For references on tail rotor balancing and tracking models and procedures, see (Kunz & Newkirk, 2009), (Damy, 2017).

1.1.1 Dynamics of structures: some concepts on vibration

In engineering, the term “structure” can be described as a system created to support loads, which are vector quantities, and, as such, it is a necessary and sufficient condition that they are defined by their magnitude, direction, and point of application. A load is said to be dynamic when any of these vector characteristics are functions of time, and thus the structure is also said to be dynamic. Deterministic dynamic loads can assume periodic forms, that is, they are repeated in time (harmonic or not), or non-periodic forms (transient or arbitrary). This study is restricted to deterministic periodic harmonic response loads. In the sense of state variation (position, velocity, etc.), the dynamic displacement associated with the second problem, in its most basic form, is represented by the harmonic function (sine or cosine trigonometric function). This function is the product of the amplitude of motion X_0 by a periodic function whose argument is the phase (composed of the initial phase at t=0) added to the product of time and the linear frequency f: $X = X_0 \sin(\Omega t)$. Figure 1(a) shows a representation in time and frequency, in which the displacement “X” of a point refers to a linear quantity of length.

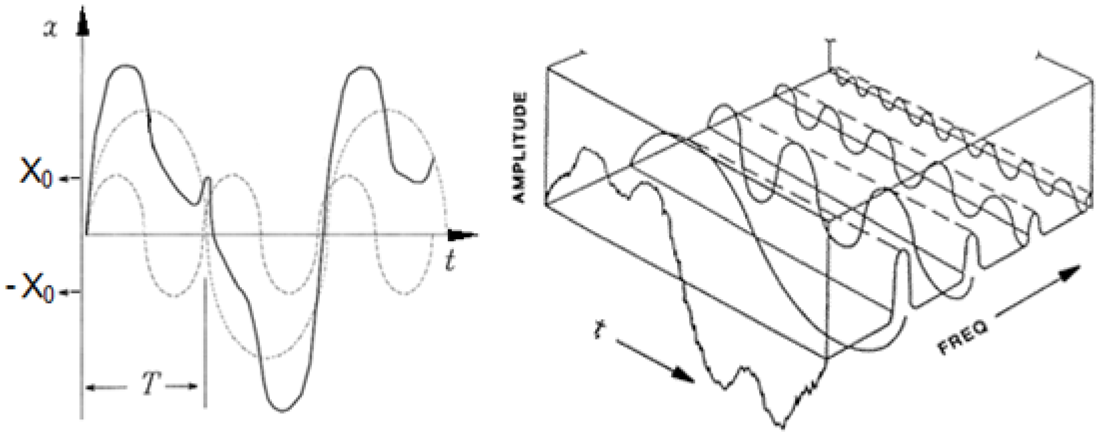

(a) (b)

Figure 1: (a) Discrete (harmonics - dashed lines) and total (solid line) vibration curves in the time domain; (b) Representations in the time domain (on the left) and the frequency domain (on the right) - adapted from (Mobley, 1999)

These displacement profiles can be presented in the time domain (abscissa in s, for example) or frequency domain (abscissa in Hz, for example), as can be inferred from Figure 1(b). Their conversion takes place by techniques based on the application of the Fourier Transform.

When vibration information is plotted as amplitude or phase versus time, it is the time domain information profile, also called the global method for seeing the composition of all frequencies. However, these data are difficult to use in continuous systems modeled as multibody ones, as they represent the total displacement. This time-domain representation makes it difficult to verify the contribution of each oscillation source even after discretization as multiple degrees of freedom. And when the complex signal is composed of several sources and harmonics, one might have the effect of masking the defects. In obtaining graphical information, approximate methods of graphical analysis such as peak value, peak-to-peak, or peak RMS value can be used. Meanwhile, in the frequency domain, everything is clearer through the identification of amplitude and phase, which refer to the Theory of Complex Numbers associated with the solution of the governing differential equations of the oscillating systems.

1.1.2 Vibration: peculiarities of rotary-wing aircraft

Since helicopter engineering demands a dynamic set composed of a large number of rotating elements (in constant change of position in time), such as motors, transmission shafts, pumps, and fans, in addition to the rotors themselves, the helicopter is subject to a wide spectrum of vibration. In this chapter, the study is limited to working with vibrations associated only with the main rotor.

Helicopter rotor vibrations are evidence of the aeroelastic phenomena related to the dynamics of the rotating movement of the blades, submitted to the complex interaction of periodic inertial and aerodynamic forces of a non-linear nature with their flexible and damped structures. As they greatly influence the flight qualities, together with the structural loads, they delineate the boundaries of the operational flight envelope as shown in Figure 2.

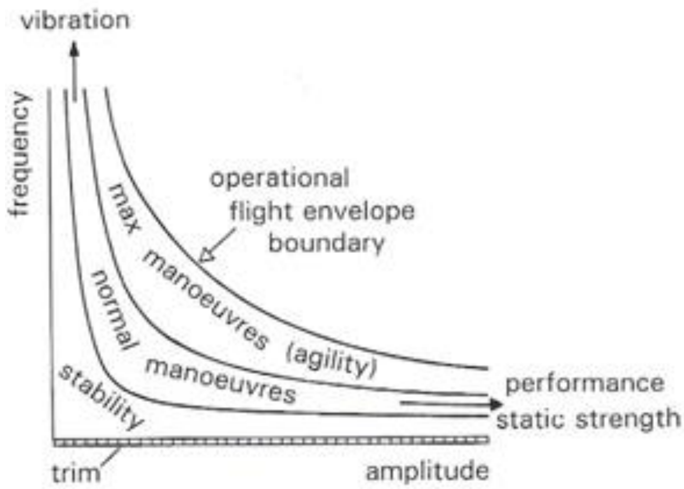

Figure 2: Vibrations (in terms of frequency and amplitude), delineating limits to flight envelopes in flight mechanics modeling - adapted from (Padfield, 2007)

The main rotor, due to its dimensions and vibration emission spectrum, is the main source of vibration, whose transmitted frequencies are multiples of the product of the number of blades “N” by the angular frequency of rotation “Ω”. The amplitude of the periodic efforts decreases as their harmonic frequencies are increased, that is, multiples of the fundamental frequency. The blades' responses to the aerodynamic and inertia forces (forces and moments) that excite them interfere at the level of the rotor hub, where they are joined. Therefore, it acts as a filter during the transmission of forced vibrations (resulting from all blades) to the fuselage, adding and subtracting amplitudes. The fuselage, generally of a semi-monocoque design (which is a structure consisting of thin coverings fixed to frames and spars), reacts according to its flexible vibratory modes (in flexion and torsion). The vibration at a particular point in the helicopter depends on the fuselage's response to these forces transmitted by the rotor hub. To calculate the fuselage response it is necessary to know the frequencies and the modal shapes of the fuselage, which are difficult to obtain. Helicopter rotors are subject to high periodic forces due to the highly flexible blades and the severity of the non-stationarity of the aerodynamic environment, which leads to the wear of critical components to the airworthiness of these aircraft (Ganguli et al., 1998). The generation of oscillating aerodynamic loads at frequencies multiples of the rotational speed are fundamental to the rotor's operation in forwarding flight, and therefore these forced vibrations cannot be eliminated. Figure 3(i) illustrates the different velocity components that make up the linear velocity, as well as its variations throughout the blade rotation cycle, with the variation of lift on the blade. This behavior characterizes the lift asymmetry of the rotor when moving forward, which also brings the phenomena, shown in Figure 3(ii) that limit its performance under high displacement speeds (Müller et al., 1999). Among these are the disturbing interaction of vortices at the tip of the predecessor blade, detachments on the leading blade (due to shock wave rides linked to air compressibility) and reverse flow in the trailing blade (flow from the trailing edge to the leading edge), with temporal loss of sustain-dynamic stall (Padfield, 2007). Added to this is the Gyroscope Effect (manifestation of the Principle of Conservation of the Angular Momentum of the rotating system), of an inertial nature, which forces the design of the chain of command/cyclic platters to compensate for the displacement of the rotor response, in its majority, at 90º about the command input.

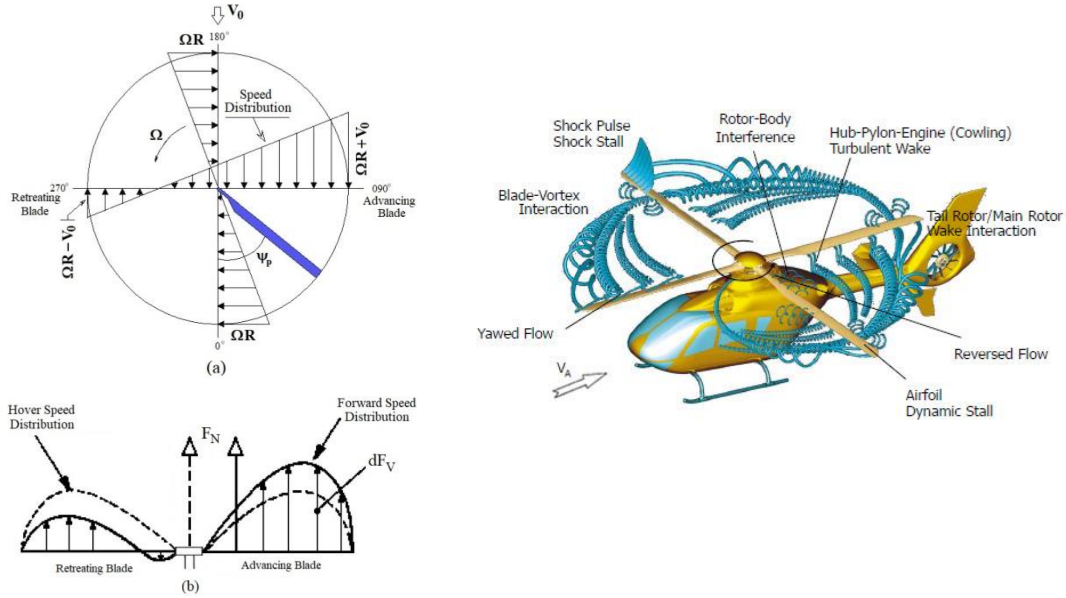

(i) (ii)

Figure 3: (i) For forwarding flight, distributions of (a) speed components in the rotor plane; (b) support on the blade at 90º and 270º of azimuthal angle - adapted from (Prouty, 1985); (ii) Limiting phenomena of rotor performance in high-speed flights - adapted from (EUROCOPTER, 2012)

Vibrations at the fundamental frequency of once-per-rev (1/rev), the focus of this research, are distributed in the vertical and lateral (rotational) planes. Another effect, the Coriolis effect, is related to the Coriolis force, acting on a rotating body and applied tangentially to its rotation. Thus, acting by flapping on the blade, creates the lead-lag motion. This effect is present by the tendency of the body to maintain its angular momentum (hence it's another inertial force) when simultaneously some of its mass elements are being moved radially in the plane of the disk, as a component in the blade flapping movement. For the detection of rotor defects, it is necessary to know the relationship between a defective blade and the response behavior of the aircraft. This knowledge can be numerically obtained by computer simulations of models based on the dynamics of these systems, where techniques based on artificial intelligence, until a properly trained artificial neural network, can be implemented permanently embedded in an aircraft to detect and identify damage (Ganguli et al., 1998). The literature reports several works regarding the detection of defects through vibration, as well as solutions to absorb or isolate unwanted permanent vibrations not associated with damage to systems. In (Ganguli et al., 1998) an aeroelastic analysis is presented based on finite elements in time and space to simulate a defective articulated rotor, both in hover and in flight in front of an SH-60 aircraft, validated through flight tests. In that work, it is stated that only localized structural damage such as cracks and delamination in the blades are not detectable by the global methodology. Several defect simulations indicate that global faults, such as lag damper defects, tab damage, pitch-link mismatches, or imbalances along the blade string, are detectable by remote measurements of global parameters such as fuselage vibration and deflection of the blades. Hence, those authors cite those special methods such as robust laser interferometer, photoelastic and ultrasonic techniques, and application of acoustic emission sensors complement these methods.

The combination of these approaches allows the design of devices for monitoring the condition of systems of this type. Simulated faults can be primary (only one type of rotor fault) or composite (a combination of more than one). The detection of the latter is important to highlight catastrophic failures such as cracks among the other fault types (Ganguli et al., 1998). However, for simplicity's sake, only primary faults are numerically simulated, such as rotor unbalance and maladjustment (out-of-tracking) of the blade tip trajectory, on one blade at a time.

1.1.3 Rotor unbalance and blade tracking problems

The oscillatory movement under consideration in this study presents itself as a vibration of lateral and vertical components (in 1Ω) and is associated with the imbalance and tracking misfits. However, for completeness, it is worth mentioning other less common causes, for example: in articulated rotor helicopters (such as in Sikorsky's Sea King helicopter), defective dampers can cause the blades to be out of phase, producing the same effect. The lateral and vertical vibrations acting on the rotor interact in a complex way, in such a way that the practice recommends correcting the trajectory of the blades first, followed by the balancing of the masses, according to the procedures described in the maintenance manual (MET, in the case of this study) and with the aid of specialized equipment that suggests corrections from the processing measures the vibration amplitude (the accelerometer), its phase angle (the "phasor") and the difference in the trajectory of the blades (the "strobex"). The correction of vibrations due to unbalance occurs in the phases of hovering inside the ground effect (IGE) and outside the ground (OGE), while the corresponding correction by trajectory difference (tracking) occurs in displacements in maximum continuous power (MCP) – straight and level flight, and also a curve at 45º. In the hover phases, the ground effect can occur, in which the presence of the ground changes the intensity and direction of the airflow around the rotor (IGE). With the rotor at a height of one rotor diameter, there is no more ground effect (OGE).

Main rotor imbalance issues

Unbalance is the most common cause of vibration. The main rotor is statically unbalanced when its center of gravity is outside the axis of rotation of this rotor. Among the two adjustment alternatives, there is the so-called single-plane balancing, which involves changing the axis of the bearing supports (impractical) or changing the rotor masses (Figure 4-A). The other case is the dynamic unbalance, established when its main axis of inertia (which contains its center of gravity) does not coincide with the structural axis of its tree due to the eccentric mass(es). In this situation, when the centrifugal forces and associated moments overcome the opposing forces of reaction in the bearings, the flexibility of the shaft allows oscillatory displacements in 1Ω in the plane of the main rotor (longitudinal and lateral). The corrective actions consecrated as a maintenance solution to carry out the balancing (said in two planes) consist of the redistribution of weights in the rotor (generally acting on the blade handle, according to the decomposition of the balancing mass, and according to the number of blades) in such a way that those two axes coincide (Figure 4-B). The second case can compromise the first, however, if the former is satisfied, then the latter is also resolved (which alone does not guarantee the latter).

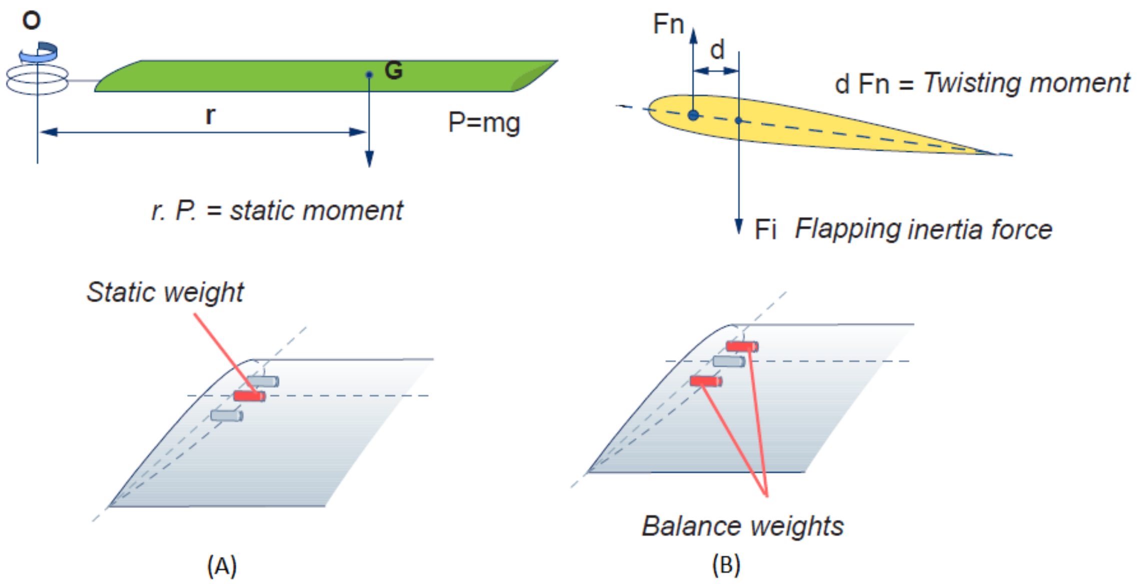

Figure 4: Blade adjustments for unbalance: (A) static moment and (B) dynamic moment - adapted from (EUROCOPTER, 2010)

Main rotor blade tracking issues

The maladjustment (out-of-tracking) in the trajectory of the tip of the blades referring to the plane of rotation is related to differences in lift between the blades. These differences result from changes in the blade's pitch angle and generate vertical vibrations at 1Ω. However, these height variations create the Coriolis Effect, arising from components of the instantaneous mass distribution, changed radially in that plane, thus also generating lateral vibrations. Due to this effect and the difference in drag of the blades, the trajectory of the blades is first corrected, to later conduct the balancing of the masses. Corrective actions aim to intervene in the blade height through the blade pitch angle by intervening in the length of the blade pitch control rod (pitch link), which promotes a uniform rotation throughout the blade around its pitch axis and/or by modifying the position of the compensators (or tab) available for this (changes the bowing of the blade profile, generally, in its outermost sections, promoting structural twists around the elastic axis of the blade by the action of aerodynamic forces resulting from the alteration of the blade lift distribution, therefore dependent on the azimuthal position, whose effect reverses that undesirable height of the blade. In the present work, for simplicity in the adopted modeling, there is no torsional degree of freedom for the blade. Hence, tab adjustment cannot be a corrective action in this case.

1.2 Chapter outline

Section 2 presents a discussion and details of vibration reduction techniques for helicopter rotors, from the point of view of the operational user and the technical maintenance of the helicopter. Section 3 presents a discussion and details of model-based helicopter main rotor balancing and tracking (case study: a 4-blade helicopter), including a subsection with perspectives on the inverse problem. Section 4 presents a discussion and details of model-based helicopter main rotor balancing and tracking (case study: a 3-blade helicopter), with modeling adapted from the previous 4-blade helicopter case. Section 5 presents some concluding remarks.

2 Vibration reduction techniques for helicopter rotors

This section is based on the article (Jorge & Torres Filho, 1989), presented at "XI Simpósio de Segurança de Aviação da MB", SIPAERM, 1989, Rio de Janeiro, RJ.

2.1 Vibration reduction for rotors

The vibration reduction techniques available for the helicopter users are concentrated in the correction of the trajectory traveled by the blade tips (adjustment of the blade "track") of the main and tail rotors, and/or in the correction of any imbalance present in these rotors. The statement of the problem, at the user level, is detailed below. In addition to vibration reduction techniques, some details of the equipment used for these purposes are described, as well as some prospects for the future.

2.2 Objectives of the Vibration Reduction

The reduction of vibrations has, among others, the objectives of:

a) Reduce the probability of failures in structural components before useful life expires. Components have an estimated life based on a certain magnitude of cyclic loads. In this way, considering that there is a direct relationship between the vibration level of the structure and the cyclic loads acting, a high level of vibration shows that the structural components of the helicopter are being subjected to unforeseen efforts consequently, present a high probability of in-service fatigue failures.

b) Minimize the effects of tiredness and fatigue on the crew. Prolonged and repeated exposure to vibrations of different frequencies, amplitudes, and directions can cause various types of aggressions that essentially consist of headaches, tinnitus, general malaise, feeling of drowsiness, general weakness, irritability, a reduction in the will and the ability to concentrate, a reduction in reflexes, a psychic depression as well as fatigue of the eyes and ears. These disturbances, depending on their intensity and persistence, can decisively contribute to pilot fatigue, as well as helicopter accidents.

Just for illustration, helicopter main rotors typically rotate between 3 and 7 Hz and the main vibrations perceived in the structure vary between 3 and 22 Hz; tail rotors and other accessories rotate at higher frequencies.

2.3 Causes of Vibration in helicopter rotors

The most common causes for the occurrence of vibration are categorized in 2 groups, according to operator procedures to mitigate the efforts that caused the vibration:

a) Unavoidable causes:

I. The variable aerodynamic forces resulting from the cyclic movement of the blades are necessary for translational flight. It is found that such forces predominantly induce vibrations at the multiple frequencies of the aircraft's main rotor rotation times the number of blades, that is, for a 4-blade helicopter with a main rotor rotation speed of 340 RPM (5.7 Hz), the cyclical variation of the pitch of this rotor blades will cause efforts that will induce vibrations in the frequencies of 22.8 Hz, 45.6 Hz, 91.2 Hz, etc., in the aircraft. These efforts increase with the aircraft's translational speed.

II. Centrifugal forces resulting from CG variation from the flapping motion of the blades, are necessary to maintain translational flight. The resulting vibration occurs in the plane of the rotor, at the rotation frequency of the main rotor.

III. Aerodynamic forces arise from the airflow over the rotors, acting on the helicopter fuselage, or from turbulence and gusts on the aircraft.

b) Avoidable causes

I. Unbalance of rotating parts and rotors: unbalance always exists, to a greater or lesser degree, in any set or rotating part and is characterized by vibration that occurs once per rotation as shown in Figure 5.

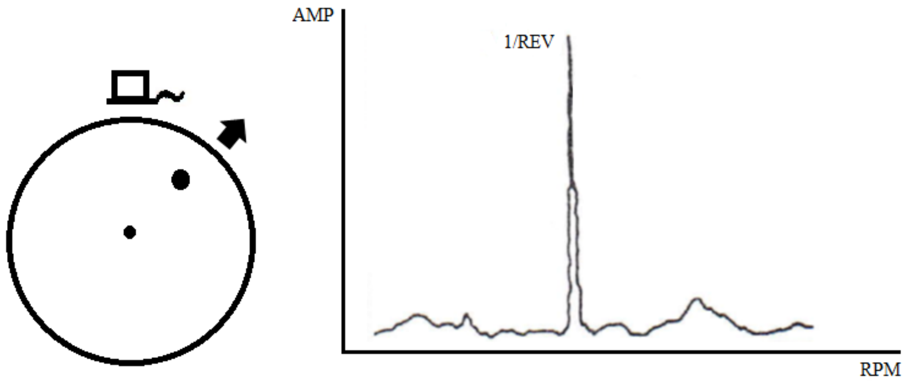

Figure 5: Unbalance (rotating parts / rotors) [Adapted from (Jorge & Torres Filho, 1989)]

Imbalance occurs when the center of mass of the rotating body is different from, or farther from, the center of rotation of that body. If the center of mass and the center of rotation are equal, the system is said to be balanced. As the center of rotation cannot be moved, the solution is to move the center of mass, adding weights in opposition to the inertia force produced by the imbalance, which is of form $F = M.r.\omega^2$, where: (i) F = Force produced by unbalancing; (ii) M = Mass of the set; (iii) r = Radius (radial position of the center of mass); and (iv) ω = Angular Velocity.

Vibration at the frequency of once per revolution is not always due to unbalance but could be indicative of another problem (such as mechanical backlash). The characteristics of unbalance are: (i) the vibration occurs at the frequency of once per revolution; (ii) the phase is stable. For example, if we are trying to balance a tail rotor that exceeds established vibration limits and the phase indication is not stable, this could be an indication of mechanical clearances rather than unbalance; and (iii) the amplitude of vibration increases with increasing rotational speed.

II. Helicopter rotor blades

1. Flying out-of-track causes elevated levels of vibration in the direction perpendicular to the rotor's plane of rotation at a frequency of once per revolution. The fact that all the blades are flying in the same plane does not always mean, however, that the aircraft will fly smoothly. Other aerodynamic forces may be involved and adjusting the blades to fly slightly out of the plane could as appropriate, counterbalance these dynamic forces to provide a smoother flight for the aircraft.

   The rotor blades of a helicopter must always travel the same path, which often does not occur, causing the aircraft to vibrate. If each blade on a rotor were identical in profile, torsion, weight distribution, stiffness distribution, and head installation, then, in steady flight, it would fly along the same path as the blade that preceded it in motion. In practice, however, not all blades are identical in these characteristics and the loss of track can always be related to effects classified as aerodynamic, dynamic, or a combination of the two, which is indeed aeroelasticity.

The major cause for out-of-track blades is when identical blades present unequal itch angles rotor and therefore generates different lifts. As this can easily occur, all helicopters have pitch control rods whose length can be adjusted in small increments between the rotating swashplate and the blades. Another common source of track loss is when the blades are attached to the head with the same collective pitch angle but produce different lifts because they are not identical. In this case, an adjustment to the pitch control rod may or may not bring the blade into the perfect track. If the differences between the blades are in the airfoil profile or the torsion distribution, adjustments are made to the trailing edge of the blade, slightly tilting an appropriate trim tab or the trailing edge itself, when possible. These changes have two effects: they change the zero-lift angle of the airfoil and produce a local pitching moment during flight, which tends to twist the blade to a different torsion distribution when in forward flight when compared to the existing torsion distribution of the blade when at rest.

The fact that the blades are out of track can also sometimes be related to a difference in balance along the chord between two otherwise identical blades. Centrifugal forces, operating on the mass elements close to the leading and trailing edges, produce a torque whose pitching moment tends to decrease the angle of attack of the blade profile, causing it to fly low. If this effect is greater on one blade than the other, due to the different weight distribution, that blade will twist downward more than the other and therefore have a lower lift in flight.

2. Unbalanced: cause vibration problems in the rotor plane at the frequency of once per revolution, as seen above (Avoidable Causes, item I). Thus, for the main rotor we will have vibrations in the lateral and longitudinal directions, and for the tail rotor, in the vertical and longitudinal directions.
3. With defects in the assembly, components, or installation: if the defect affects only one blade, we will have a vibration at the frequency of once per revolution. An indication of this type of defect appears in situations where, when trying to balance or track, the phase becomes unstable before we reach a specified threshold. If the defect occurs in items or installations that affect all rotor blades, we will have high levels of vibration at foot pass frequencies (2, 3, 4, etc. times per rotation, depending on the number of rotor blades).

2.4 Vibration Reduction Techniques for helicopter rotors

a) Balancing the main rotor

1) Amplitude and phase of vibration.

Helicopter vibrations are caused by external forces, due to unbalanced rotors. These efforts are periodic and generate a vibratory movement at all points on the aircraft. For this case of forced vibrations, the amplitudes of displacement (X), velocity (V), and acceleration (A), for a given excitation frequency, are related in the form $A = \omega V = \omega^2 X$, where ω is the vibration frequency.

In terms of phase, we have that acceleration is 90 degrees out of phase with velocity and 180 degrees out of phase with displacement. For a given frequency, the time delay between the forced response (vibration at a point of the structure, in a given direction) and the excitation (an external effort that caused this vibration) can be expressed in terms of the clockwise phase, whose angular value (measured in degrees or hours of a watch) can be measured directly on the rotor, by using vibration sensors (accelerometers) and synchronism signal generating devices at that frequency (magnetic pick-up, optical pickup, etc. .) or reference points (such as reflective tape).

2) Types of Balancing

Unbalance only occurs in the rotor plane (the plane perpendicular to the rotor's axis of rotation) and, therefore, it is sufficient to apply static balancing techniques. Normally, field balancing is chosen, with the rotor installed in the aircraft and its normal rotation regime, with the following advantages: (i) the removal of aircraft rotors is avoided; (ii) inaccuracies resulting from friction in the static balance benches are avoided; and (iii) the vibration measuring equipment is portable.

3) Field balancing methods

a) *Balance chart*. The amplitude and phase of vibration are measured and plotted on suitable balance charts, which provide the values of the necessary balance masses, as well as their installation position on the rotor. However, it may be necessary to make corrections to the balance chart to adapt it to the aircraft, because the vibration amplitude and phase vary as a function of the mass and stiffness of the structure. Thus, differences may occur between the "average" aircraft used by the manufacturer in determining the chart and the aircraft whose rotor is being balanced. The correction in the chart is made by direct comparison between the results obtained and those predicted.

b) *Method of the two measures*. The method consists of obtaining the vibration amplitude and phase values before and after the addition of a known balancing mass at a defined location on the rotor and, from these data, the position and value of the balancing mass to be placed are graphically or analytically determined.

c) *Three-mass method (four measures).* This method is used when the measuring equipment of the vibration phase is not available. The method consists of placing a known balance mass in three angular positions: 0, 90, and 180 degrees and using the difference of the vibration phase and amplitude values about the initially measured value, to determine the position and value of the balance mass.

During the balancing procedure, any unexpected phase change after the addition of balancing masses may represent the existence of gaps in the set to be balanced (Avoidable Causes, item V, above). In this situation, the balancing process must be interrupted until the origin of the gap is found and the problem corrected since the existence of gaps prevents the use of Balance Charts and the 2- or 4- measurement methods.

b) Equalization of the lift force of the main rotor blades (adjustment of a track)

Equalization is performed by changing the length of the rotor pitch control rods, which modifies the angle of attack equally along the length of the blade and, consequently, the blade lift; or by changing the angle of the blade tab (sometimes known as trim tab), which changes the blade pitch incrementally along its length, due to the variation in its torsion. A rod length adjustment modifies the blade lift force in all flight conditions, while a tab adjustment only works when the aircraft is moving at higher forward speeds. While for the first case the angular variation of the blade pitch is of mechanical origin, for the second case this angular variation of the blade pitch is of aerodynamic origin. Thus, the variation in the blade torsion introduced by the tab is proportional to the air displacement over the blade section, the pitch angular variation becomes dependent on the forward flight speed. Figure 6 shows the variation in the position of the tip of the blades of a helicopter as the flight conditions change. For each blade, we have the position of the aircraft on the ground, in hover, and at 3 forward flight speeds. If the blade tends to fly high or low in all flight conditions, the typical adjustment will be at the control rod. If the blade tends to go out of track as forward flight speed increases, the typical adjustment will be in the tab.

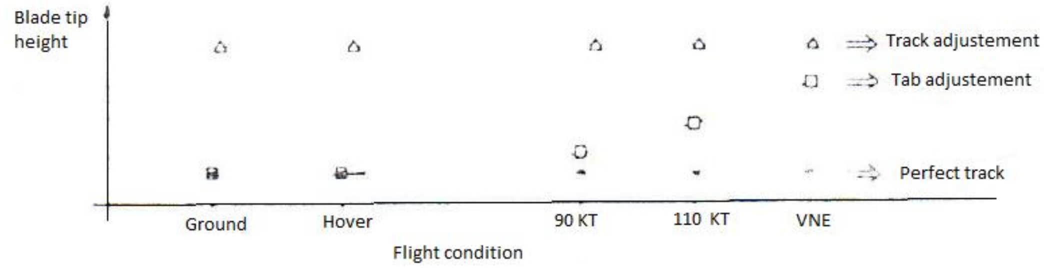

Figure 6: Blade tip path versus flight condition: a visualization of required adjustments – adapted from (Jorge & Torres Filho, 1989)

c) Main rotor blades: coupling between balancing and equalization of the lift force

If the main rotor blades do not produce the same lift force (*L*), they will be in equilibrium with different flap angles (θ), as shown in Figure 7. Thus, the loss of track is characterized by the blade tips rotating in different planes (different θ angles).

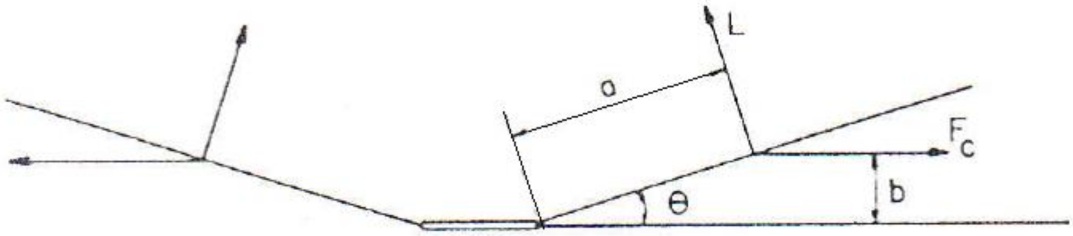

Figure 7: Blade equilibrium conditions – adapted from (Jorge & Torres Filho, 1989)

With $L.a = F_c.b$ and $\sin\theta = b/a = L/F_c$. Equal blades (same Lift L) lead to the same F_c, and thus to the same angle θ, which means that the blade's track is perfect. Blades with different L (that is, different blades) lead to different F_c, and thus the angle θ will be different for each blade, which means that the blades are out of track. The center of gravity of the blade which is flying higher (than the other blades) approaches the axis of rotation of the rotor. Thus, blades of the identical static moment (first moment of cross-sectional area) may have different centrifugal forces and therefore appear to be unbalanced, when they were producing different lift forces. Figure 6 also illustrates the case of blades with different static moments, but with the same lift. These blades will be out of track and may induce vertical vibration at the main rotor frequency of 1Ω, due to the difference in the vertical components of their lift forces. Therefore, the lift balancing and equalization operations must be carried out interspersed, until satisfactory results are obtained, for vertical and lateral vibration levels at 1Ω.

d) Balancing and equalization of the lift force of the tail rotor blades

The same theoretical considerations and techniques described for the case of the main rotor are applied in the case of the tail rotor. The existence of problems of lift difference is less common in the tail rotor case, due to the fixed-pitch adjustment of the blades and the lower susceptibility to aeroelastic effects. Normally, it is sufficient to statically balance the blades or field balance the rotor with the aircraft on the ground, or both, depending on the aircraft model.

By way of illustration, we describe the characteristics of two cases (Jorge & Torres Filho, 1989):

1. AS 332 SUPER PUMA: a tail rotor malfunction originates a vibration characterized by three times the rotation of the main rotor when in forward flight (frequency coupling).
2. AS 350 SQUIRREL: the tail rotor resonant frequency occurs when the main rotor rotation is around 310 RPM, and therefore, at start-up and final cut-off, the tail rotor passes through this frequency. If the vibration level measured near the tail rotor is greater than 1 IPS (inches per second) during this transient, the tail rotor must be statically balanced before field balancing is applied.

3 Model-based parameter identification for unbalanced and out-of-track helicopter rotor blades: a case study of a 4-blade main rotor

This section is based on the Master's Thesis (Jorge, 1992), for the Specialized Masters Program in Helicopter Techniques at ENSICA, Toulouse, France, 1992.

Case study of a 4-blade main rotor: model development and comparison with maintenance manual (Jorge, 1992)

Helicopter vibrations are one of the problems that require a lot of maintenance effort. Various practical procedures already exist relating the measured vibrations to the possible corrections to be introduced at the main rotor head. This work formulates a theoretical background that leads, from corrections, to the vibrations measured at the fuselage. The problem was split into two parts: the calculation of the isotropic rotor equilibrium and, then, the introduction of the defects from this equilibrium position.

The model here considered defects that generate vibrations in 1Ω (one-per-revolution), 2-D aerodynamics, rigid blades, articulated rotor, a rigid fuselage, and flight conditions without load factor. From the equations found, a software was created for different flight conditions and configurations of weight and balance. The results obtained were consistent with those from the aircraft's maintenance manual (MET) The algorithm obtained can be inserted into an on-board software, as part of a system of the HUMS type, providing information on rotor defects to reduce the maintenance time and cost.

3.1 Introduction

GENERAL

Vibration is, for a helicopter, one of the problems that require the most effort, either for the designers and manufacturers or for the users. In the design offices, during the conceptual design of the aircraft, a complete set of methods is used to tackle the problem, the origin of the vibratory forces, its transmission to the fuselage, and the response of the fuselage to this excitation.

When the helicopter is delivered to the user, it is already tuned and balanced. However, during its operational life, problems of maladjustment and unbalance appear on the various rotating systems, which requires a maintenance effort on the part of the user, with periodic adjustment procedures with, therefore, a very high maintenance cost, due to the maintenance flight hours required to perform the tasks of the various adjustments until an acceptable vibration level, measured at the fuselage, is reached. The necessary maintenance flight hours have an intrinsic or direct cost (fuel consumption, etc.) and a cost associated with the unavailability of the aircraft for its operational use, and therefore must be minimized.

The purpose of this study is the conceptual design of a system that can detect various defects at the rotor head, using fuselage vibration measurements, during normal or operational use of the helicopter, and that also can propose the adjustments or corrective procedures to be conducted at the next shutdown of the aircraft. Such a system leads to a reduction in maintenance time since it can replace maintenance flight hours for fault finding by flight hours in operational use.

This system also leads to an increase for in-flight safety, since it will detect faults when they appear, while in the current adjustment procedures (which are scheduled, with some periodicity), it will be necessary to reach a scheduled moment in the life of the device to be able to detect a fault. In this way, without such a system, a helicopter could fly for a certain time in a degraded configuration, with a defect in its rotor which could increase the risk of the appearance of various problems, such as the appearance of cracks in rotating parts subjected to alternating efforts and even, at the limit, a reduction in the operational performance of the crew due to human fatigue in a more degraded vibration environment. This study of vibration problems generated by faults in the main rotor can be generalized to vibration problems generated by faults in other rotating systems such as the tail rotor or the engines. Such a fault detection system can be installed onboard a helicopter in the context of HUMS (Health and Usage Monitoring Systems) type systems.

MODELING

Within the framework of sensitivity studies on the vibratory level of a helicopter, in all directions, due to the forces at the rotor head caused by defects of a geometric, kinematic, structural nature, etc... and of any origin (manufacture, maladjustment, wear, damage, etc.), a simulation will be performed of these defects on a helicopter rotor-structure model, to obtain the vibration level at different locations of the structure, to be able to carry out, in a next step, the inverse problem, i.e., from the vibrations measured at known points of the fuselage, being able to capture to the rotor defects.

The hypotheses

The model will study defects that generate vibrations in 1Ω (one-per-revolution), that is, once the rotation of the main rotor. This frequency, lower than 6 Hz (as is the case of some aircraft from Airbus Helicopters - former Eurocopter France), being lower than the first resonance frequency of the fuselage (around 12 Hz for the Super Puma, for example), allows us to have a model where we will retain: (i) the 6 degrees of freedom of the fuselage, seen as a rigid body; and (ii) the degrees of freedom in flapping, drag, and pitch of each blade, also seen as a rigid body linked to the main rotor through the joints.

The application case, for comparison between the model results and practical results, will be the Super Puma (AS 332 MKI long version and AS 332 MKII) helicopter. For the calculation of the aerodynamic forces, the approach will retain a two-dimensional steady-state aerodynamic model, with the hypotheses of small angles of incidence, flapping, drag, and pitch. In this model, two flight conditions with zero load factor will be considered: (i) hover; and (ii) stabilized level flight.

The settings
The parameters relating to the device, considered as "a priori" known data, necessary to initialize the system are: (i) the mass of the aircraft; (ii) the mass center; (iii) forward flight speed; and (iv) atmospheric density. These are the parameters necessary to establish a particular flight condition, where one can calculate the pitch, the flapping, and the drag of a rotor considered to be isotropic, without defects. From this flight condition, defects will be introduced on the different blades of the rotor.

Faults and possible corrections on a blade
Possible defects: (i) mass imbalance on one or more blades or even on the hub-rotor mast assembly; (ii) "detracking" (blade flying out of position) in flapping and/or drag; (iii) incorrect or inadequate twisting on a blade; (iv) the maladjustment of a pitch control rod and/or a slack/mechanical clearance of this rod; (v) the loss of stiffness and/or damping on a drag adapter of a blade; (vi) incorrect adjustment or locking of the tabs of a blade, etc... For all problems, whatever their origin, the Maintenance Manual offers the user only two options: (i) perform possible corrections and adjustments on a blade; or (ii) change the defective element, in the cases provided for, where it is no longer possible to adjust.

The modeling of the inverse problem must consider the maximum admissible values of the corrections to be introduced, to determine whether the calculated correction should be carried out or a replacement of a defective element (correction exceeding a threshold). The possible corrections and adjustments on a blade are: (i) the variation of the collective pitch of a blade from the variation in the length of the pitch control rod; (ii) the variation of the mass of a blade (and, consequently, of its static moment and of its inertia in flapping and in drag) by introducing or removing balancing weights (at the point of attachment between sleeve and blade, in our case study, i.e., the Super Puma); and (iii) The variation of the bracketing of the tab located most at the end of the blade.

The assumption in this model is that the various defects can be reduced to "equivalent defects" at the points where the corrections will be introduced. This "equivalence" means that a defect will generate a vibration in the fuselage equal to that which would be generated by the "equivalent defect(s)". The goal to be achieved is to introduce a correction (i.e., an "equivalent defect" of the same amplitude but opposite sign to the one just detected) to balance the rotor (if it is possible) and not to find the exact origin of the actual defect. Thus, the model is not going to simulate the real defect, but, instead, its "equivalent defect" at the points of introduction of the corrections.

PROJECT STAGES

Study of the equilibrium of the isotropic rotor

Initially, the model will take into account a so-called "isotropic" rotor, ie, without defects. All the blades being considered equal, we will have: (i) from the balance of moments around the joint, the equations of the movements of the blade, in flapping and in drag, which will be functions of 1 Ω; (ii) through the integration of the elementary forces on a current element of the blade, we will have the force of a blade on the rotor head; (iii) the summation of the forces of all the blades on the hub, including the moments introduced by the frequency adapters, gives us the wrench of the forces at the rotor head, which is constant concerning the azimuthal position of the blades (and, therefore, concerning in time) due to the hypothesis of an isotropic rotor that restricts in this study to the frequency 1 Ω; (iv) from the forces at the rotor head and other forces external to the helicopter, we will have the balance of the fuselage for this flight condition. We will retain, as external forces: the thrust of the rear rotor, the own weight of the helicopter, the drag of the fuselage, and the downforce of the horizontal stabilizer. From the equations of the balance of the fuselage, we will obtain the longitudinal attitudes (in pitch), roll, and yaw. In addition to the assumption of stabilized flight (zero acceleration, that is to say, constant attitudes over time) we will assume that the flight is not skidded and that the yaw attitude is zero, retaining, instead, as unknown, the tail rotor thrust necessary to obtain this zero attitude.

Study of the effect of the introduction of defects

"Equivalent defects" will be introduced into the model, which is consistent with the reality, to study their effect: (i) on the rotor head forces; (ii) on the acceleration of the center of gravity of the fuselage; and (iii) on the acceleration of any point of the fuselage where it is planned to install accelerometers. The equations of the balance of the fuselage will no longer be equations in static equilibrium but dynamic equilibrium. The forces at the rotor head will no longer be constants, but functions of 1Ω, which brings us to inertial forces and, therefore, accelerations of the fuselage, also in 1Ω, neglecting the higher harmonics of the fuselage movement, which could be originated from the rotor head excitations in 1Ω.

Study of the inverse problem

The model

We have seen that, from the position of the equilibrium and the defects, one can obtain the forces at the rotor head and also the acceleration of the fuselage. For the inverse problem, we need to know the position of the equilibrium (as before) and the accelerations of the fuselage. The full motion of the fuselage, which was assumed to be rigid, is measured by accelerometers which record the fuselage's 6 degrees of freedom. The measurements of the accelerometers are then brought back to the movement of the center of gravity of the fuselage, through a formulation step which is the inverse of that which was previously made. This inversion is always possible. The movement of the fuselage is passed from the helicopter frame to the fixed rotor frame and then to the rotating rotor frame, so that: (i) the movement of the blade will therefore be its displacement plus the displacement of the fuselage; and (ii) the rotor head forces will be the sum of the constant forces, obtained from the balance of the isotropic rotor, plus the variable forces in the frequency 1Ω. As the model has more unknowns (defects) than information obtained from the accelerometers, certain restrictions must be imposed and the transformation can be called a “pseudo-inverse”.

The optimization

The optimization will consist of seeking the optimal distribution of the accelerometers to minimize the calculations for obtaining the inverse of the “pseudo-inverse”. For that, one must look for: (i) either defect decoupling or minimum coupling; (ii) harmonization of the orders of magnitude between the various "defect-acceleration" pairs; and (iii) the minimum number of calculation operations.

The application

The transition from simulation software to embedded software

Here, it is necessary to consider constraints and to operational limitations: (i) maximum collective pitch; (ii) maximum admissible movements in flapping and in drag; (iii) maximum admissible forces in connecting rods; (iv) maximum bracketing of tabs; (v) maximum balancing weight that can be inserted in the sleeve (in the rotor head); and (vi) accelerometer limitations: sensitivity, threshold, accuracy.

The expert system

This software can be inserted into a more complete embedded system, such as the HUMS, with: (i) setting of priorities and rules for the corrections to be introduced; (ii) the choice between the corrections or the replacement of the defective component; (iii) the use of this acceleration and force information for updating the calculation of the service life of vital parts; and (iv) the information on flight safety. For helicopters with a system for measuring the pitch of the blades, it is possible to consider, as an option, the pitch input as a parameter of the system, instead of the speed of forward flight. This system, in its first stage, i.e., the calculation of the balance of the isotropic rotor, could, therefore, provide us, in addition, the speed of flight, functioning as an anemometer, for example, for low speeds where conventional anemometry systems are inaccurate.

3.2 Balance study of the system: main rotor plus fuselage study of the articulated rotor in flapping and drag

Introduction

In this part, we will study a rotor composed of blades articulated in flapping and dragging. We are going to attack more particularly the establishment of the analytical expression of the wrench of the efforts in the rotor head. The assumption made was that the blade had a flapping angular movement (β) independent of the dragging angular movement (δ), followed by a small dragging movement $\delta = \delta_0 + \delta_{1C} \cos \psi_1 t + \delta_{1S} \sin \psi_1 t$, which is a function of the flapping angular movement.

Calculation of rotor head efforts

Each of the blades that constitute the rotor is subjected to inertia and aerodynamic forces. As a resultant effect, the fundamental principle of dynamics applied to the blade gives: the resultant of the efforts of connections at the level of the flapping joint is determined by the preceding relationship, which gives:

$\vec{R}_{\text{blade}\to\text{hub}} = \vec{R}_{\text{aerodynamic}} - \int_e^R \gamma \vec{M}.dm_i$. On the other hand, to calculate the moments at the rotor head, the Dynamic Moment Theorem is applied at the hub: $\vec{\delta^\circ}_{\text{hub}/Rg} = \vec{M}_{\text{blade}\to\text{hub}} + \vec{M}_{\text{fuselage}\to\text{hub}}$. As the rotor hub is rotating at a constant speed, the dynamic moment δ° $_{\text{cube}/Rg}$ is zero and: $\vec{M}_{\text{hub}\to\text{fuselage}} = \vec{M}_{\text{blade}\to\text{hub}}$. We will note in the sequence the components of the wrench of efforts in the rotor head: $\{T_{eff}\}_0 = \begin{Bmatrix} \vec{R}_{\text{blade}\to\text{hub}} \\ \vec{M}_{\text{blade}\to\text{hub}} \end{Bmatrix}_0 = \begin{Bmatrix} F_x.\vec{X} + F_y.\vec{Y} + F_z.\vec{Z} \\ M_x.\vec{X} + M_y.\vec{Y} + M_z.\vec{Z} \end{Bmatrix}_0$. Let's now calculate these components for a blade. We will then make the sum according to the number of blades to obtain the wrench of the efforts of the complete rotor.

Calculation of the dynamic resultant

The blade is simply articulated in flapping and drag. Let *M* be a current point of the blade of radial coordinate r. The coordinates are represented in Figure 8.

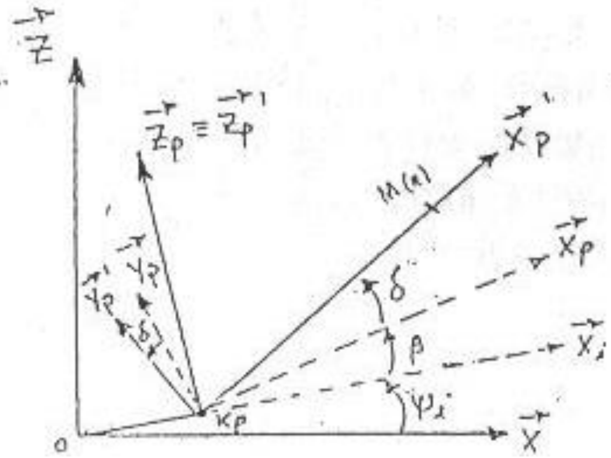

Figure 8: Representation of the coordinates – adapted from (Jorge, 1992)

We will calculate the acceleration of this point *M* in the fixed rotor frame and then integrate the obtained expressions along the blade. We have, in the fixed rotor frame:

$$\overrightarrow{OM} = \begin{bmatrix} e\cos\psi_i + (r-e)\cos\delta\,\cos\beta\,\cos\psi_i - (r-e)\sin\delta\,\sin\psi_i \\ e\sin\psi_i + (r-e)\cos\delta\,\cos\beta\,\sin\psi_i + (r-e)\sin\delta\,\cos\psi_i \\ (r-e)\cos\delta\,\sin\beta \end{bmatrix} \qquad (1)$$

Notation: $\frac{d\beta}{dt} = \dot{\beta}_t$ e $\frac{d^2\beta}{dt^2} = \ddot{\beta}_{t.t}$; rotor constant speed $\dot{\psi}_i = \Omega$, what gives us:

$$\frac{d^2\overrightarrow{OM}}{dt^2} = \begin{bmatrix} -e\Omega^2\cos\psi_i + 2(r-e)\Omega\dot{\beta}_t\cos\delta\sin\beta\sin\psi_i - (r-e)\ddot{\beta}_{t.t}\cos\delta\sin\beta\cos\psi_i \\ -(r-e)\dot{\beta}_t^{\,2}\cos\delta\cos\beta\cos\psi_i - (r-e)\Omega^2\cos\delta\cos\beta\cos\psi_i + 2(r-e)\Omega\dot{\delta}_t\sin\delta\cos\beta\sin\psi_i \\ +2(r-e)\dot{\delta}_t\dot{\beta}_t\sin\delta\sin\beta\cos\psi_i - (r-e)\dot{\delta}_t^{\,2}\cos\delta\cos\beta\cos\psi_i - (r-e)\ddot{\delta}_{t.t}\sin\delta\cos\beta\cos\psi_i \\ +(r-e)\dot{\delta}_t^{\,2}\sin\delta\sin\psi_i - (r-e)\ddot{\delta}_{t.t}\cos\delta\sin\psi_i - 2(r-e)\dot{\delta}_t\Omega\cos\delta\cos\psi_i \\ +(r-e)\Omega^2\sin\delta\sin\psi_i \\[1em] -e\Omega^2\sin\psi_i - 2(r-e)\Omega\dot{\beta}_t\cos\delta\sin\beta\cos\psi_i - (r-e)\ddot{\beta}_{t.t}\cos\delta\sin\beta\sin\psi_i \\ -(r-e)\dot{\beta}_t^{\,2}\cos\delta\cos\beta\sin\psi_i - (r-e)\Omega^2\cos\delta\cos\beta\sin\psi_i - 2(r-e)\Omega\dot{\delta}_t\sin\delta\cos\beta\cos\psi_i \\ +2(r-e)\dot{\delta}_t\dot{\beta}_t\sin\delta\sin\beta\sin\psi_i - (r-e)\dot{\delta}_t^{\,2}\cos\delta\cos\beta\sin\psi_i - (r-e)\ddot{\delta}_{t.t}\sin\delta\cos\beta\sin\psi_i \\ -(r-e)\dot{\delta}_t^{\,2}\sin\delta\cos\psi_i + (r-e)\ddot{\delta}_{t.t}\cos\delta\cos\psi_i - 2(r-e)\dot{\delta}_t\Omega\cos\delta\sin\psi_i \\ -(r-e)\Omega^2\sin\delta\cos\psi_i \\[1em] (r-e)\ddot{\beta}_{t.t}\cos\delta\cos\beta - (r-e)\dot{\beta}_t^{\,2}\cos\delta\sin\beta - 2(r-e)\dot{\delta}_t\dot{\beta}_t\sin\delta\cos\beta - (r-e)\dot{\delta}_t^{\,2}\cos\delta\sin\beta \\ -(r-e)\ddot{\delta}_{t.t}\sin\delta\sin\beta \end{bmatrix} \qquad (2)$$

As β and δ are small angles, the following assumptions will be made: sinβ ≈ β; sinδ ≈ δ; cosβ ≈ 1-(β^2/2); cosδ ≈ 1; sinβsinδ ≈ 0; cosβsinδ ≈ δ (noting that, if taking cosβ ≈ 1, then terms that are not negligible will not be taken into account), leading to:

$$\begin{aligned}\ddot{\gamma}_x = & -e\Omega^2\cos\psi_i + 2(r-e)\Omega\dot{\beta}_t\beta\sin\psi_i - (r-e)\ddot{\beta}_{t.t}\beta\cos\psi_i - (r-e)\dot{\beta}_t^2\left(1-\frac{\beta^2}{2}\right)\cos\psi_i \\ & -(r-e)\Omega^2\left(1-\frac{\beta^2}{2}\right)\cos\psi_i + 2(r-e)\Omega\dot{\delta}_t\delta\sin\psi_i - (r-e)\dot{\delta}_t^2\cos\psi_i - (r-e)\ddot{\delta}_{t.t}\delta\cos\psi_i \\ & +(r-e)\dot{\delta}_t^2\delta\sin\psi_i - (r-e)\ddot{\delta}_{t.t}\sin\psi_i - 2(r-e)\dot{\delta}_t\Omega\cos\psi_i + (r-e)\Omega^2\delta\sin\psi_i\end{aligned}$$

$$\begin{aligned}\ddot{\gamma}_y = & -e\Omega^2\sin\psi_i - 2(r-e)\Omega\dot{\beta}_t\beta\cos\psi_i - (r-e)\ddot{\beta}_{t.t}\beta\sin\psi_i - (r-e)\dot{\beta}_t^2\left(1-\frac{\beta^2}{2}\right)\sin\psi_i \\ & -(r-e)\Omega^2\left(1-\frac{\beta^2}{2}\right)\sin\psi_i - 2(r-e)\Omega\dot{\delta}_t\delta\cos\psi_i - (r-e)\dot{\delta}_t^2\sin\psi_i - (r-e)\ddot{\delta}_{t.t}\delta\sin\psi_i \\ & -(r-e)\dot{\delta}_t^2\delta\cos\psi_i + (r-e)\ddot{\delta}_{t.t}\cos\psi_i - 2(r-e)\dot{\delta}_t\Omega\sin\psi_i - (r-e)\Omega^2\delta\cos\psi_i\end{aligned}$$

$$\ddot{\gamma}_z = (r-e)\ddot{\beta}_{t.t}\left(1-\frac{\beta^2}{2}\right) - (r-e)\dot{\beta}_t^2\beta - 2(r-e)\dot{\delta}_t\dot{\beta}_t\delta - (r-e)\dot{\delta}_t^2\beta$$

The final expression of the blade acceleration is obtained in the fixed rotor frame by integrating the acceleration of an element of mass *dmi*:

$$m_i\gamma_i = \int_e^R \ddot{\gamma}_x\, dm_i$$

$$m_i\gamma_i = \int_e^R \ddot{\gamma}_x\, dm_i \quad \text{Avec} \int_e^R (r-e)\, dm_i = m_{si}$$

$$m_i\gamma_i = \int_e^R \ddot{\gamma}_x\, dm_i$$

What gives us:

$$\begin{aligned}m_{i\gamma x} = & -m_i e\Omega^2\cos\psi_i + m_{si}\left[2\beta\dot{\beta}_t\Omega\sin\psi_i - \dot{\beta}_t^2\left(1-\frac{\beta^2}{2}\right)\cos\psi_i - \beta\ddot{\beta}_{t.t}\cos\psi_i - \Omega^2\left(1-\frac{\beta^2}{2}\right)\cos\psi_i\right] \\ & + m_{si}\left[2\Omega\dot{\delta}_t\delta\sin\psi_i - \dot{\delta}_t^2\cos\psi_i - \ddot{\delta}_{t.t}\delta\cos\psi_i + \dot{\delta}_t^2\delta\sin\psi_i - \ddot{\delta}_{t.t}\sin\psi_i - 2\dot{\delta}_t\Omega\cos\psi_i + \Omega^2\delta\sin\psi_i\right]\end{aligned}$$

$$\begin{aligned}m_{i\gamma y} = & -m_i e\Omega^2\sin\psi_i + m_{si}\left[2\beta\dot{\beta}_t\Omega\cos\psi_i - \dot{\beta}_t^2\left(1-\frac{\beta^2}{2}\right)\sin\psi_i - \beta\ddot{\beta}_{t.t}\sin\psi_i - \Omega^2\left(1-\frac{\beta^2}{2}\right)\sin\psi_i\right] \\ & + m_{si}\Big[2\Omega\dot{\delta}_t\delta\cos\psi_i - \dot{\delta}_t^2\sin\psi_i - \ddot{\delta}_{t.t}\delta\sin\psi_i + \dot{\delta}_t^2\delta\cos\psi_i - \ddot{\delta}_{t.t}\cos\psi_i - 2\dot{\delta}_t\Omega\sin\psi_i \\ & + \Omega^2\delta\cos\psi_i\Big]\end{aligned}$$

$$m_{i\gamma z} = m_{si}\left[\ddot{\beta}_{t.t}\left(1-\frac{\beta^2}{2}\right) - \beta\dot{\beta}_t^2\right] + m_{si}\left[-2\dot{\delta}_t\dot{\beta}_t\delta - \dot{\delta}_t^2\beta\right]$$

Aerodynamic loads

We are now interested in the aerodynamic forces generated in flight. Figure 9 shows the wind direction concerning the fixed rotor frame as well as the decomposition of the wind velocity into velocity tangential to the rotor plane (and perpendicular to the blade span) (U_T), and velocity perpendicular to the rotor plane (U_P).

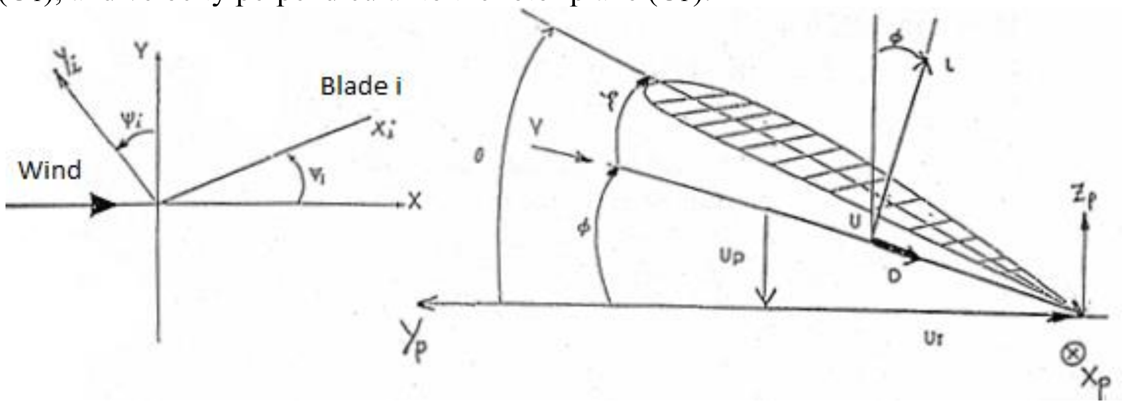

Figure 9: Representation of the forces acting on a blade – adapted from (Jorge, 1992)

The resulting speed is $U = \sqrt{U_T^2 + U_P^2}$ and $\tan\varphi \approx \varphi \approx U_P/U_T$. Additional notation adopted: $\dot{\beta}_t = \frac{d\beta}{dt} = \frac{d\beta}{d\psi}\frac{d\psi}{dt} = \Omega\dot{\beta}$, with $\dot{\beta} = \frac{d\beta}{d\psi}$.

Let us first calculate the velocity of a current point M (r) of the blade about the Galilean frame of reference (a reference frame where $\vec{V}_{ar/Rg} = \overrightarrow{VX}_g$), leading to: $\vec{V}_{\text{M blade/Rg}} = \vec{V}_{\text{M blade/fixed rotor}} + \vec{V}_{\text{M fixed rotor/air}} + \vec{V}_{\text{M air/Rg}}$. The velocity of the current point of the blade can be obtained as the sum of the velocity due to blade rotation, flapping, and drag $\vec{V}_{\text{blade}}\ \Omega, \beta, \delta$ plus the velocity due to forward flight $\vec{V}_{\text{blade V}}$, plus the velocity component due to the induced velocity $\vec{V}_{\text{blade V}_i}$, where

$$\left(\vec{V}_{\text{blade}\Omega\beta\delta}\right)_{R_f} = \left(\frac{d\overrightarrow{OM}}{dt}\right)_{R_f} = \left(\frac{d\overrightarrow{OM}}{dt}\right)_{R_f} + \vec{\Omega}\left(R_f / R_f\right) \wedge \overrightarrow{OM} \tag{3}$$

with: R_f: fixed rotor reference frame
R_t: rotating rotor reference frame
R_p: blade reference frame
$\overrightarrow{OM}$: in the R_f reference frame

What gives us:

$$\left(\frac{d\overrightarrow{OM}}{dt}\right)_{Rf} = \begin{bmatrix} (r-e)\left[-\sin\delta\,\dot{\delta}_t\cos\beta\cos\psi_i - \cos\delta\,\cos\beta\ \dot{\beta}_t\cos\psi_i - \cos\delta\,\dot{\delta}_t\sin\psi_i\right] \\ (r-e)\left[-\sin\delta\,\dot{\delta}_t\cos\beta\sin\psi_i - \cos\delta\sin\beta\ \dot{\beta}_t\sin\psi_i - \cos\delta\,\dot{\delta}_t\cos\psi_i\right] \\ (r-e)\left[-\sin\delta\,\dot{\delta}_t\sin\beta + \cos\delta\cos\beta\,\dot{\beta}_t\right] \end{bmatrix}$$
$$+ \begin{bmatrix} 0 \\ 0 \\ \Omega \end{bmatrix} \wedge \begin{bmatrix} e\cos\psi_i + (r-e)\cos\delta\cos\beta\cos\psi_i - (r-e)\sin\delta\sin\psi_i \\ e\sin\psi_i + (r-e)\cos\delta\cos\beta\sin\psi_i + (r-e)\sin\delta\cos\psi_i \\ (r-e)\cos\delta\sin\beta \end{bmatrix}$$

and, subsequently:

$$\left(\overrightarrow{V_{\text{blade }\Omega\beta\delta}}\right)_{R_f} = \left[\begin{array}{l} -(r-e)\dot{\beta}_t \cos\delta\cos\beta\cos\psi_i - \Omega\sin\psi_i\left[(r-e)\cos\delta\cos\beta+e\right] \\ \quad -(r-e)\left(\Omega\sin\delta\cos\psi_i + \dot{\delta}_t\sin\delta\cos\beta\cos\psi_i + \dot{\delta}_t\cos\delta\sin\psi_i\right) \\ \\ -(r-e)\dot{\beta}_t \cos\delta\sin\beta\sin\psi_i + \Omega\cos\psi_i\left[(r-e)\cos\delta\cos\beta+e\right] \\ \quad +(r-e)\left(-\Omega\sin\delta\sin\psi_i - \dot{\delta}_t\sin\delta\cos\beta\sin\psi_i + \dot{\delta}_t\cos\delta\cos\psi_i\right) \\ \\ (r-e)\dot{\beta}_t\cos\delta\cos\beta - (r-e)\dot{\delta}_t\sin\delta\sin\beta \end{array}\right. \quad (4)$$

The same treatment can be done to the velocity due to forward flight: $\left(\overrightarrow{V_{\text{blade}_V}}\right)_{R_a} = \left|\begin{array}{l} -V \\ 0 \\ 0 \end{array}\right.$

in the aerodynamic reference frame (Ra). A rotation (α_D) around $\overrightarrow{Ya} = \vec{Y}$ leads us to R_f

$$\left(\dot{V}_{blade_V}\right)_{R_f} = \begin{bmatrix} \cos\alpha_0 & 0 & \sin\alpha_0 \\ 0 & 1 & 0 \\ -\sin\alpha_0 & 0 & \cos\alpha_0 \end{bmatrix} \begin{bmatrix} -V \\ 0 \\ 0 \end{bmatrix} = \begin{bmatrix} -V\cos\alpha_0 \\ 0 \\ +V\sin\alpha_0 \end{bmatrix} \quad (5)$$

A rotation ($-\psi_i$) around $\vec{Z} \equiv \vec{Z_i}$ leads ($\overrightarrow{V_{pá\ \Omega,\beta,\delta}} + \overrightarrow{V_{pá\ V}}$) from R_f to R_t

$$\left(\overrightarrow{V_{\text{blade }\Omega.\beta.\delta}}\right)_{R_t} + \left(\overrightarrow{V_{\text{blade V}}}\right)_{R_t} = \left|\begin{array}{l} -(r-e)\dot{\beta}_t\cos\delta\sin\beta - (r-e)\Omega\sin\delta - (r-e)\dot{\delta}_t\sin\delta\cos\beta - V\cos\alpha_0\cos\psi_i \\ \\ \Omega\left[(r-e)\cos\delta\cos\beta+e\right] + (r-e)\dot{\delta}_t\cos\delta + V\cos\alpha_0\sin\psi_i \\ \\ (r-e)\dot{\beta}_t\cos\delta\cos\beta - (r-e)\dot{\delta}_t\sin\delta\sin\beta + V\sin\alpha_0 \end{array}\right.$$

A rotation of (β) around $\overrightarrow{Y_i} = \overrightarrow{Y'_p}$ leads us to R'p, with flapping by:

$$\left(\overrightarrow{V_{\text{blade }\Omega.\beta.\delta}}\right)_{R'_p} + \left(\overrightarrow{V_{\text{blade V}}}\right)_{R'_p} = \left|\begin{array}{l} -(r-e)\Omega\sin\delta\cos\beta - (r-e)\dot{\delta}_t\sin\delta - V\cos\alpha_D\cos\psi_i\cos\beta - V\sin\alpha_D\sin\beta \\ \\ \Omega\left[(r-e)\cos\delta\cos\beta+e\right] + (r-e)\dot{\delta}_t\cos\delta + V\cos\alpha_D\sin\psi_i \\ \\ (r-e)\dot{\beta}_t\cos\delta + (r-e)\Omega\sin\delta\sin\beta + V\cos\alpha_D\cos\psi_i\sin\beta + V\sin\alpha_D\cos\beta \end{array}\right.$$

A rotation of (-δ) around $\overrightarrow{Z'}_p \equiv \overrightarrow{Z}_p$ leads us to R_p (flapping followed by drag motion)

$$\left(\overrightarrow{V_{blade\ \Omega.\beta.\delta}}\right)_{R_p} + \left(\overrightarrow{V_{blade\ V}}\right)_{R_p} = \begin{bmatrix} e\Omega\sin\delta - V\cos\alpha_D\cos\psi_i\cos\beta\cos\delta + V\sin\alpha_D\sin\beta\cos\delta + V\cos\alpha_D\sin\delta \\ \\ e\Omega\cos\delta + (r-e)\Omega\cos\beta + (r-e)\dot{\delta}_t + V\cos\alpha_D\sin\psi_i\cos\delta \\ +V\cos\alpha_D\cos\psi_i\cos\beta\sin\delta - V\sin\alpha_D\sin\beta\cos\delta \\ \\ (r-e)\dot{\beta}_t\cos\delta + (r-e)\Omega\sin\delta\sin\beta + V\cos\alpha_D\cos\psi_i\cos\beta + V\sin\alpha_D\sin\beta \end{bmatrix} \tag{6}$$

Finally, the relative motion of the blade due to the induced velocity is:

$$\left(\overrightarrow{V_{blade_{Vi}}}\right)_{R_p} = \begin{bmatrix} 0 \\ 0 \\ V_i \end{bmatrix} \tag{7}$$

The blade velocity is:

$$\left(\overrightarrow{V_{blade}}\right)_{R_p} = \left(\overrightarrow{V_{blade_{\Omega,\beta,\delta}}}\right)_{R_p} + \left(\overrightarrow{V_{blade_V}}\right)_{R_p} + \left(\overrightarrow{V_{blade_{Vi}}}\right)_{R_p} \tag{8}$$

The relative wind velocity is:

$$\left(\vec{U}\right)_{R_p} = \begin{bmatrix} U_{xp} \\ U_{yp} \\ U_{zp} \end{bmatrix} = -\left(\overrightarrow{V_{blade}}\right)_{R_p} \tag{9}$$

One can see that there is a third component of U along the blade span, that is, along with Xp, thus one can assume that its contribution to lift (L) and drag (D) is negligible. Assuming a two-dimensional aerodynamics problem for the profile of the current point of the blade, with the direction of U_P and U_T shown in the figure above. The wind velocity U will be taken as the composition of U_T and U_P. Therefore, we have tangential and vertical components of the velocity given as $U_T = -U_{yp}$; $U_p = -U_{zp}$ (Note: U_{xp} gives negligible aerodynamic efforts and is neglected). One has, finally:

$$U_T = V\cos\alpha_D\sin\psi_i\cos\delta + V\cos\alpha_D\cos\psi_i\cos\beta\sin\delta$$
$$+ V\sin\alpha_D\sin\beta\sin\delta + \Omega\,[(r-e)\cos\beta + e\cos\delta]$$
$$U_p = V\cos\alpha_D\cos\psi_i\sin\beta + V\sin\alpha_D\cos\beta + V_i$$
$$+ (r-e)\dot{\beta}_t\cos\delta + (R-e)\Omega\sin\delta\sin\beta$$

Let $\sin\beta \approx \beta$; $\sin\delta \approx \delta$; $\cos\beta \approx 1$; $\cos\delta \approx 1$; $\sin\beta\sin\delta \approx 0$; $(r\text{-}e)\cos\beta + e\cos\delta \approx r$, then:

$$\begin{cases} U_T = r\Omega + V\cos\alpha_D\sin\psi_i + V\cos\alpha_D\cos\psi_i\delta \\ U_p = (r\text{-}e)\dot{\beta}_t + V\cos\alpha_D\beta\cos\psi_i + V\sin\alpha_D + V_i \end{cases} \tag{10}$$

$$\text{with}\quad \dot{\beta}_t = \Omega\dot{\beta}$$

The U_T speed is the sum of the speeds due to (i) the blade rotation (Ω r) and (ii) the translation of the helicopter The U_P speed is the sum of the speeds due to (i) the induced speed ($V\,.\,\sin\alpha_D + V_i$), (ii) the flapping speed $\left[\frac{d\beta}{dt}(r-e)\right]$,and (iii) the translation of the helicopter ($V\,.\,\cos\alpha_D\,.\,\cos\psi_i\,\beta$).

Also, as $\frac{d\beta}{dt} = \dot{\beta}_t = \Omega\dot{\beta}$, then:

$U_T = \Omega r + V\cos\alpha_D \sin\psi_i + V\cos\alpha_D \cos\psi_i \delta$

$U_p = V\sin\alpha_D + V_i + (r - e)\dot{\beta}\Omega + V.\cos\alpha_D \cos\psi_i \ \beta$. The lift (L) and drag (D) forces for the element are, respectively, perpendicular and parallel to the plane of velocity U.

$$\begin{aligned} L &= \frac{\rho}{2}U^2 \ ca\,(\theta - \phi)\ dr \\ D &= \frac{\rho}{2}U^2 \ c\,C_{d0}\ dr \end{aligned} \tag{11}$$

Figure 9 shows us the lift and drag forces for the element. In the reference frame R_p, we have, for blade *i*:

$$\left[d\vec{F}_i^{a}\right]_{R_p} = \begin{bmatrix} 0 \\ L\sin\xi \ - \ D\ \cos\xi \\ L\cos\xi \ + \ D\sin\xi \end{bmatrix} \tag{12}$$

A rotation of (δ) leads us to R'_p:

$$\left[dF_i^{a}\right]_{R'_p} = \begin{bmatrix} \cos\delta & -\sin\delta & 0 \\ \sin\delta & \cos\delta & 0 \\ 0 & 0 & 1 \end{bmatrix} \begin{bmatrix} 0 \\ L\ \text{sen}\xi \ - \ D\ \cos\xi \\ L\ \cos\xi \ + \ D\ \text{sen}\xi \end{bmatrix} = \begin{bmatrix} -\left(L\sin\xi \ - \ D\cos\xi\right)\sin\delta \\ \left(L\sin\xi - D\cos\xi\right)\cos\delta \\ L\ \cos\xi \ + \ D\ \text{sen}\xi \end{bmatrix}$$

A rotation of (-β) leads us to R_t:

$$\left[dF_i^{a}\right]_{R_t} = \begin{bmatrix} -\left(L\ \text{sen}\xi\ -\ D\ \cos\xi\right)\text{sen}\delta\ \cos\beta\ -\left(L\ \cos\xi\ +\ D\ \text{sen}\xi\right)\text{sen}\beta \\ \left(L\ \text{sen}\xi - D\cos\xi\right)\cos\delta \\ -\left(L\ \text{sen}\xi\ -\ D\ \cos\xi\right)\text{sen}\delta\ \text{sen}\beta + \left(L\ \cos\xi\ +\ D\ \text{sen}\xi\right)\cos\beta \end{bmatrix}$$

ξ, β and δ being small angles, we have: $\sin\xi \approx \xi = \theta-\phi \approx \theta-\tan\phi = \theta-U_p/U_T$; $\cos\xi \approx 1$; $\sin\beta \approx \beta$; $\sin\delta \approx \delta$; $\cos\beta \approx 1$; $\cos\delta \approx 1$; $\sin\xi \sin\delta \approx 0$; $\sin\delta \sin\beta \approx 0$; $\sin\xi \sin\beta \approx 0$. Assuming: $U^2 = U_T^2 + U_p^2 \approx U_T^2$, as $U_p << U_T$, and $a + C_{d0} \approx a$, as $C_{d0} << a$, leads to:

$$\left\{dF^{a}\right\}_{R_t} = \begin{bmatrix} -L\beta + D\delta \\ L\left(\theta - \phi\right) - D \\ L + D\left(\theta - \phi\right) \end{bmatrix} \tag{13}$$

What gives:

$$\begin{cases} dF_{xi}^{\ a} = -\dfrac{\rho\beta aC}{2}\ (U_T^{\ 2}\theta\ -\ U_p U_T)\ dr + \dfrac{\rho c C_{d0}}{2}\ U_T^{\ 2}\ \delta\ dr \\ dF_{yi}^{\ a} = \dfrac{\rho aC}{2}\ \left[U_T^{\ 2}\theta\ -\ 2U_p U_T \theta + U_p^{\ 2}\right]\ dr + \dfrac{\rho c C_{d0}}{2}\ U_T^{\ 2}\ dr \\ dF_{zi}^{\ a} = \dfrac{\rho aC}{2}\ \left[U_T^{\ 2}\theta\ -\ U_p U_T\right]\ dr \end{cases} \tag{14}$$

Introducing the following coefficients:

$\mu = \; = \dfrac{V\cos\alpha_D}{\Omega R}$ is called the advance coefficient, which is the relationship between the component of velocity over the disc and the velocity at the tip of the blade; and

$\lambda = \; = \dfrac{V\mathrm{sen}\alpha_D + V_i}{\Omega R}$ is the axial flow parameter, which is the relationship between the component of velocity perpendicular to the disk and the velocity at the tip of the blade;

- $\chi = \dfrac{r}{R}$ e $\chi_e = \dfrac{e}{R}$; $\theta = \theta_{con} + \dfrac{r}{R}\theta_{tw}$ (θ_{tw}: twist); $\theta_{con} = \theta_0 + \theta_{1c}\cos\psi_i + \theta_{1s}\,\mathrm{sen}\psi_i$. Thus:

$$dF_{xi}{}^{a} = \rho ac(\Omega R)^2\left\{-\frac{\beta}{2}[\theta(\chi + \mu sen\psi_i + \mu\delta\cos\psi_i)^2 - (\lambda + (\chi - \chi_e)\beta + \beta\mu\cos\psi_i)(\chi + \mu sen\psi_i + \mu\delta\, sen\psi_i)] + \frac{C_{d0}}{2a}\delta(\chi + \mu sen\psi_i + \mu\delta\cos\psi_i)^2\right\}dr \tag{15}$$

$$dF_{yi}{}^{a} = \rho ac(\Omega R)^2\left\{-\frac{1}{2}[2\theta(\chi + \mu sen\psi_i + \mu\delta\cos\psi_i)(\lambda + (\chi - \chi_e)\beta + \beta\mu\cos\psi_i) - (\chi + \mu sen\psi_i + \mu\delta\cos\psi_i)^2\theta^2 - (\lambda + (\chi - \chi_e)\beta + \beta\mu cos()^2)] - \frac{C_{d0}}{2a}(\chi + \mu sen\psi_i + \mu\delta\cos\psi_i)^2\right\}\Bigg]$$

$$dF_{zi}{}^{a} = \frac{\rho ac}{2}(\Omega R)^2\left\{\theta\left(\chi + \mu sen\psi_i + \mu\delta\cos\psi_i\right)^2 - \left(\chi + \mu sen\psi_i + \mu\delta\cos\psi_i\right)\left(\lambda + (\chi - \chi_e)\beta + \beta\mu\cos\psi_i\right)\right\}dr$$

For the evaluation of the axial flux parameter λ, the Meijer-Drees modeling is used (Meijer Drees, 1949). This allows the consideration of a cyclic variation of the parameter λ. The Meijer-Drees formulation leads us to:

$$\begin{aligned}\lambda &= \lambda_0 + \lambda_{1c}\chi\cos\psi_i + \lambda_{1s}\chi\mathrm{sen}\psi_i \\ &= \mu\mathrm{tg}\alpha_D + \frac{C_T}{2\left(1 - \frac{3}{2}\mu^2\right)\sqrt{\mu^2 + \lambda^2}}\left(1 + K_x\chi\cos\psi_i + K_y\chi\mathrm{sen}\psi_i\right)\end{aligned} \tag{16}$$

Where

$$\begin{aligned}K_x &= \frac{4}{3}\left[\left(1 - 1{,}8\mu^2\right)\sqrt{1 + \left[\frac{\lambda}{\mu}\right]^2} - \frac{\lambda}{\mu}\right] \\ K_y &= -2\mu\end{aligned} \tag{17}$$

Which gives the cyclic components:

$$\begin{aligned}\lambda_0 &= \mu tg\alpha_D + \frac{C_T}{2\left(1 - \frac{3}{2}\mu^2\right)\sqrt{\lambda^2 + \mu^2}} \\ \lambda_{1c} &= \frac{2\mu C_T}{3\left(1 - \frac{3}{2}\mu^2\right)}\left[\frac{1}{\sqrt{\lambda^2 + \mu^2}\left(\sqrt{\lambda^2 + \mu^2} + \lambda\right)} - 1{,}8\right]\end{aligned} \tag{18}$$

$$\lambda_{1s} = -\frac{\mu C_T}{\left(1-\frac{3}{2}\mu^2\right)\sqrt{\lambda^2+\mu^2}}$$

λ_0 is calculated by an iterative method (Meijer Drees, 1949); get λ_{1c}, λ_{1s} by replacing λ with λ_0.

Let $S = \rho ac\,(\Omega R)^2$. Integrating $dF_{xi}{}^a$, $dF_{yi}{}^a$, $dF_{zi}{}^a$ along the blade leads to:

$$F_{xi}{}^a = S\int_e^R \left\{-\frac{\beta}{2}\left[\left[\frac{r}{R}+\mu\mathrm{sen}\psi_i+\mu\delta\cos\psi_i\right]^2\left[\theta_{con}+\frac{r}{R}\theta_{tw}\right]-\left[\frac{r}{R}+\mu\mathrm{sen}\psi_i+\mu\delta\cos\psi_i\right]\right.\right.$$
$$\left.\left.\left[\lambda_0+\lambda_{1c}\frac{r}{R}\cos\psi_i+\lambda_{1s}\frac{r}{R}\mathrm{sen}\psi_i+\frac{r-e}{R}\beta+\beta\mu\cos\psi_i\right]\right]+\frac{C_{d0}}{2a}\delta\left(\frac{r}{R}+\mu\mathrm{sen}\psi_i+\mu\delta\cos\psi_i\right)^2\right\}dr$$
$$F_{yi}{}^a = S\int_e^R\left[-\frac{1}{2}\left[\frac{r}{R}+\mu\mathrm{sen}\psi_i+\mu\delta\cos\psi_i\right]\left[\theta_{con}+\frac{r}{R}\theta_{tw}\right]\chi 2+\right.$$
$$\chi\left[\lambda_0+\lambda_{1c}\frac{r}{R}\cos\psi_i+\lambda_{1s}\frac{r}{R}\mathrm{sen}\psi_i+\frac{r-e}{R}\beta+\beta\mu\cos\psi_i\right]+\frac{1}{2}\left[\lambda_0+\lambda_{1c}\frac{r}{R}\cos\psi_i+\lambda_{1s}\frac{r}{R}\mathrm{sen}\psi_i+\ldots\right]^2 \tag{19}$$
$$\left.\left[\ldots+\frac{r-e}{R}\beta+\beta\mu\cos\psi_i\right]^2\left[\theta_{con}+\frac{r}{R}\theta_{tw}\right]^2-\frac{C_{d0}}{2a}\left[\frac{r}{R}+\mu\mathrm{sen}\psi_i+\mu\delta\cos\psi_i\right]^2\right]dr$$
$$F_{zi}{}^a = \frac{S}{2}\int_e^R\left[\left[\frac{r}{R}+\mu\mathrm{sen}\psi_i+\mu\delta\cos\psi_i\right]^2\left[\theta_{con}+\frac{r}{R}\theta_{tw}\right]-\left[\frac{r}{R}+\mu\mathrm{sen}\psi_i+\mu\delta\cos\psi_i\right]\right.$$
$$\left.\left[\lambda_0+\lambda_{1c}\frac{r}{R}\cos\psi_i+\lambda_{1s}\frac{r}{R}\mathrm{sen}\psi_i+\frac{r-e}{R}\beta+\beta\mu\cos\psi_i\right]\right]dr$$

After integration leads to:

$$\frac{F_{xi}{}^a}{S} = \frac{1}{3}\left[\frac{R^3-e^3}{R^2}+3(R-e)\mu^2(\sin\psi_i+\delta\cos\psi_i)^2\right.$$
$$\left.+3\frac{R^3-e^3}{R}\mu(\sin\psi_i+\delta\cos\psi_i)\right]\left(-\theta_{con}\frac{\beta}{2}+\frac{C_{d0}}{2a}\delta\right)$$
$$-\frac{\beta}{2}\left[\frac{R^4-e^4}{4R^3}+2\mu\frac{R^3-e^3}{3R^2}(\sin\psi_i+\delta\cos\psi_i)\right.$$
$$\left.+\mu^2\frac{R^2-e^2}{R^2}(\sin\psi_i+\delta\cos\psi_i)^2\right]\theta_{tw}$$
$$+\frac{\beta}{2}\left[\frac{R^2-e^2}{2R}+\mu(R-e)(\sin\psi_i+\delta\cos\psi_i)\right](\lambda_0+\mu\delta\cos\psi_i)$$
$$+\frac{\beta}{2}\left[\frac{R^3-e^3}{3R^2}+\mu\frac{R^2-e^2}{2R}(\sin\psi_i+\delta\cos\psi_i)\right]\left(\lambda_{1c}\cos\psi_i+\lambda_{1s}\sin\psi_i+\dot{\beta}\right)$$
$$-e\dot{\beta}\frac{\beta}{2}\left[\frac{R^2-e^2}{2R}+\frac{R-e}{R}\mu(\sin\psi_i+\delta\cos\psi_i)\right]$$
$$\frac{F_{yi}{}^a}{S} = -\left\{(R-e)\left(\lambda_0-\frac{e}{R}\dot{\beta}+\mu\beta\cos\psi_i\right)\mu\,(\sin\psi_i+\delta\cos\psi_i)\theta_{con}\right.$$
$$\left.+\frac{R^2-e^2}{2R}\left(\lambda_{1c}\cos\psi_i+\lambda_{1s}\sin\psi_i+\dot{\beta}\right)\mu(\sin\psi_i+\delta\cos\psi_i)\theta_{con}\right\}$$

$$
\begin{aligned}
&+\left[\frac{{\theta_{con}}^2}{2}-\frac{C_{d0}}{2a}\right]\left[\frac{R^3-e^3}{3R^2}+\mu\frac{R^2-e^2}{2R}(\sin\psi_i+\delta\cos\psi_i)\right.\\
&\qquad\left.+\mu^2(R-e)\mu^2(\sin\psi_i+\delta\cos\psi_i)^2\right]\\
&+\frac{(R-e)}{2}\left({\lambda_0}^2+\beta^2\mu^2\cos^2\psi_i+2\lambda_0\beta\mu\cos\psi_i-2\frac{e}{R}\dot{\beta}(\lambda_0+\beta\mu\cos\psi_i)\right.\\
&\qquad\left.+\frac{e^2}{R^2}\dot{\beta}^2\right)\\
&+\frac{R^2-e^2}{2R}\left[-\left(\lambda_0-\frac{e}{R}\dot{\beta}+\mu\beta\cos\psi_i\right)(\mu(\sin\psi_i+\delta\cos\psi_i)\theta_{tw}+\theta_{con})\right.\\
&\qquad\left.+\left(\lambda_{1c}\cos\psi_i+\lambda_{1s}\sin\psi_i+\dot{\beta}\right)\left(\lambda_0+\beta\mu\cos\psi_i-\frac{e}{R}\dot{\beta}\right)\right]\\
&+\frac{R^3-e^3}{3R^2}\left[-\left(\lambda_0-\frac{e}{R}\dot{\beta}+\mu\beta\cos\psi_i\right)\theta_{tw}-\left(\lambda_{1c}\cos\psi_i+\lambda_{1s}\sin\psi_i+\dot{\beta}\right)\right.\\
&\qquad(\mu(\sin\psi_i+\delta\cos\psi_i)\theta_{tw}+\theta_{con})+\frac{{\lambda_{1c}}^2}{2}\cos^2\psi_i+\frac{{\lambda_{1s}}^2}{2}\sin^2\psi_i+\frac{\dot{\beta}^2}{2}\\
&\qquad\left.+\lambda_{1c}\lambda_{1s}\cos\psi_i\sin\psi_i+\dot{\beta}(\lambda_{1c}\cos\psi_i+\lambda_{1s}\sin\psi_i)\right]\\
&-\frac{R^4-e^4}{4R^3}\theta_{tw}\left(\lambda_{1c}\cos\psi_i+\lambda_{1s}\sin\psi_i+\dot{\beta}\right)\\
&+\left[\frac{R^4-e^4}{4R^3}+2\mu\frac{R^3-e^3}{3R^2}(\sin\psi_i+\delta\cos\psi_i)\right.\\
&\qquad\left.+\mu^2\frac{R^2-e^2}{2R}(\sin\psi_i+\delta\cos\psi_i)^2\right]\theta_{tw}\theta_{con}\\
&+\frac{{\theta_{tw}}^2}{2R^2}\left[\frac{R^5-e^5}{5R^2}+\frac{\mu(\sin\psi_i+\delta\cos\psi_i)}{2R}(R^4-e^4)\right.\\
&\qquad\left.+\frac{\mu^2(\sin\psi_i+\delta\cos\psi_i)^2}{3}(R^3-e^3)\right]
\end{aligned}
$$

$$
\begin{aligned}
\frac{{F_{zi}}^a}{S}=\frac{1}{2}\Bigg\{&\left[\frac{R^3-e^3}{3R^2}+(R-e)\mu^2(\sin\psi_i+\delta\cos\psi_i)^2\right.\\
&\qquad\left.+\frac{R^2-e^2}{R}\mu(\sin\psi_i+\delta\cos\psi_i)\right]\theta_{con}\\
&+\left[\frac{R^4-e^4}{4R^3}+2\mu\frac{R^3-e^3}{3R^2}(\sin\psi_i+\delta\cos\psi_i)\right.\\
&\qquad\left.+\mu^2\frac{R^2-e^2}{R^2}(\sin\psi_i+\delta\cos\psi_i)^2\right]\theta_{tw}\\
&-\left[\frac{R^2-e^2}{2R}+\mu(R-e)(\sin\psi_i+\delta\cos\psi_i)\right](\lambda_0+\mu\delta\cos\psi_i)\\
&-\left[\frac{R^3-e^3}{3R^2}+\mu\frac{R^2-e^2}{2R}(\sin\psi_i+\delta\cos\psi_i)\right]\left(\lambda_{1c}\cos\psi_i+\lambda_{1s}\sin\psi_i+\dot{\beta}\right)\\
&+e\dot{\beta}\frac{\beta}{2}\left[\frac{R^2-e^2}{2R}+\frac{R-e}{R}\mu(\sin\psi_i+\delta\cos\psi_i)\right]\Bigg\}
\end{aligned}
$$

In general, the ratio e/R is very small. In the case of the Super Puma main rotor, one has R = 7.80 m and e = 0.27 m, which gives e/R = 0.035. Simplifying assumptions considered: $R^2 - e^2 \approx R^2$; $R^3 - e^3 \approx R^3$; $R^4 - e^4 \approx R^4$; $R^5 - e^5 \approx R^5$ (the only simplifying assumptions that will not be made is $R - e \approx R$), which will lead us to an error of 0.15% in the efforts calculations, which will be disregarded.

Thus, one obtains:

$$
\begin{aligned}
\frac{F_{xi}{}^{a}}{S} = & \left[\frac{R}{3}+(R-e)\mu^2(\sin\psi_i+\delta\cos\psi_i)^2+R\mu(\sin\psi_i+\delta\cos\psi_i)\right]\left[\theta_{con}-\frac{\beta}{2}+\frac{C_{d0}}{2a}\right] \\
& -\frac{\beta}{2}\left[\frac{R}{4}+2\mu\frac{R}{3}(\sin\psi_i+\delta\cos\psi_i)+\mu^2\frac{R}{2}(\sin\psi_i+\delta\cos\psi_i)^2\right]\theta_{tw} \\
& +\frac{\beta}{2}\left[\frac{R}{2}+\mu(R-e)(\sin\psi_i+\delta\cos\psi_i)\right]\left(\lambda_0+\mu\beta\cos\psi_i-\frac{e}{R}\dot{\beta}\right) \\
& +\frac{\beta}{2}\left[\frac{R}{3}+\mu\frac{R}{2}(\sin\psi_i+\delta\cos\psi_i)\right]\left(\lambda_{1c}\cos\psi_i+\lambda_{1s}\sin\psi_i+\dot{\beta}\right)
\end{aligned}
$$

$$
\begin{aligned}
\frac{F_{yi}{}^{a}}{S} = & \left(\lambda_0+\mu\beta\cos\psi_i-\frac{e}{R}\dot{\beta}\right) \\
& -\Bigg[(R-e)\mu(\sin\psi_i+\delta\cos\psi_i)+\frac{R}{2}\theta_{con}-\frac{R}{2}\mu(\sin\psi_i+\delta\cos\psi_i) \\
& \quad +\frac{R}{3}\theta_{tw}+\frac{R}{2}\left(\lambda_{1c}\cos\psi_i+\lambda_{1s}\sin\psi_i+\dot{\beta}\right)\Bigg] \\
& -\left(\lambda_{1c}\cos\psi_i+\lambda_{1s}\sin\psi_i+\dot{\beta}\right) \\
& \quad \left[\frac{R}{2}\mu(\sin\psi_i+\delta\cos\psi_i)+\frac{R}{3}\theta_{con}+\frac{R}{3}\mu(\sin\psi_i+\delta\cos\psi_i)+\frac{R}{4}\theta_{tw}\right] \\
& +\left[\frac{\theta_{con}{}^2}{2}-\frac{C_{d0}}{2a}\right]\left[\frac{R}{3}+\mu R(\sin\psi_i+\delta\cos\psi_i)+\mu^2(R-e)(\sin\psi_i+\delta\cos\psi_i)^2\right] \\
& +\theta_{tw}\theta_{con}\left[\frac{R}{4}+2\mu\frac{R}{3}(\sin\psi_i+\delta\cos\psi_i)+\mu^2(\sin\psi_i+\delta\cos\psi_i)^2\frac{R}{2}\right] \\
& +\frac{\theta_{tw}{}^2}{2}\left[\frac{R}{5}+\mu(\sin\psi_i+\delta\cos\psi_i)\frac{R}{2}+\mu^2(\sin\psi_i+\delta\cos\psi_i)^2\frac{R}{3}\right] \\
& +\frac{(R-e)}{2}\left(\lambda_0+\mu\beta\cos\psi_i-\frac{e}{R}\dot{\beta}\right)^2+\frac{R}{6}\left(\lambda_{1c}\cos\psi_i+\lambda_{1s}\sin\psi_i+\dot{\beta}\right)^2
\end{aligned}
$$

$$
\begin{aligned}
\frac{F_{zi}{}^{a}}{S} = & \frac{1}{2}\left[\frac{R}{3}+(R-e)\mu^2(\sin\psi_i+\delta\cos\psi_i)^2+R\mu(\sin\psi_i+\delta\cos\psi_i)\right]\theta_{con} \\
& +\frac{1}{2}\left[\frac{R}{4}+2\mu\frac{R}{3}(\sin\psi_i+\delta\cos\psi_i)+\mu^2\frac{R}{2}(\sin\psi_i+\delta\cos\psi_i)^2\right]\theta_{tw} \\
& -\frac{1}{2}\left[\frac{R}{2}+\mu(R-e)(\sin\psi_i+\delta\cos\psi_i)\right]\left(\lambda_0+\mu\beta\cos\psi_i-\frac{e}{R}\dot{\beta}\right) \\
& +\frac{1}{2}\left[\frac{R}{3}+\mu\frac{R}{2}(\sin\psi_i+\delta\cos\psi_i)\right]\left(\lambda_{1c}\cos\psi_i+\lambda_{1s}\sin\psi_i+\dot{\beta}\right)
\end{aligned}
$$

Calculation of the resultant effort in the rotor head

The resultant is obtained by applying the above relationship. The reference frame for the aerodynamic forces (calculated in the rotating rotor reference frame) is changed, as:

$$
\begin{cases}
F_x = F_{xi}{}^{a}\cos\psi_i - F_{yi}{}^{a}\sin\psi_i - m_{i\gamma x} \\
F_y = F_{xi}{}^{a}\sin\psi_i - F_{yi}{}^{a}\cos\psi_i - m_{i\gamma y} \\
F_z = F_{zi}{}^{a} - m_{i\gamma z}
\end{cases}
\tag{20}
$$

With $m_{i\gamma x}$, $m_{i\gamma y}$, $m_{i\gamma z}$, F_{xi}, F_{yi}, F_{zi}: components as previously calculated. What gives:

$$\frac{{F_{xi}}^{a}}{S} = \left[\frac{R}{3} + (R-e)\mu^2(\sin\psi_i + \delta\cos\psi_i)^2 + R\mu(\sin\psi_i + \delta\cos\psi_i)\right]$$
$$\left[\left(-\frac{\beta}{2}\theta_{con} + \frac{C_{d0}}{2a}\right)\cos\psi_i - \sin\psi_i\left(\frac{{\theta_{con}}^2}{2} - \frac{C_{d0}}{2a}\right)\right]$$
$$+\left[\frac{R}{4} + 2\mu\frac{R}{3}(\sin\psi_i + \delta\cos\psi_i) + \mu^2\frac{R}{2}(\sin\psi_i + \delta\cos\psi_i)^2\right]$$
$$\left[-\frac{\beta}{2}\theta_{tw}\cos\psi_i - \sin\psi_i\,\theta_{tw}\theta_{con}\right]$$
$$+\left(\lambda_0 + \mu\beta\cos\psi_i - \frac{e}{R}\dot{\beta}\right)$$
$$\left[\frac{\beta}{2}\cos\psi_i\left(\frac{R}{2} + \mu\frac{R}{2}(R-e)(\sin\psi_i + \delta\cos\psi_i)\right)\right.$$
$$+\sin\psi_i\left[\left(\mu(R-e)(\sin\psi_i + \delta\cos\psi_i) + \frac{R}{2}\theta_{con}\right)\right.$$
$$+\left(\frac{R}{3} + \mu\frac{R}{2}(\sin\psi_i + \delta\cos\psi_i)\right)\theta_{tw}$$
$$\left.\left.-\frac{R}{2}\left(\lambda_{1c}\cos\psi_i + \lambda_{1s}\sin\psi_i + \dot{\beta}\right)\right]\right]$$
$$+\left(\lambda_{1c}\cos\psi_i + \lambda_{1s}\sin\psi_i + \dot{\beta}\right)$$
$$\left[\frac{\beta}{2}\cos\psi_i\left(\frac{R}{3} + \mu\frac{R}{2}(\sin\psi_i + \delta\cos\psi_i)\right)\right.$$
$$+\sin\psi_i\left[\left(\frac{R}{2}\mu(\sin\psi_i + \delta\cos\psi_i) + \frac{R}{3}\right)\theta_{con}\right.$$
$$\left.\left.+\left(\frac{R}{3} + \mu(\sin\psi_i + \delta\cos\psi_i) + \frac{R}{4}\right)\right]\right]$$
$$-\sin\psi_i\frac{{\theta_{tw}}^2}{2}\left[\frac{R}{5} + \mu\frac{R}{2}(\sin\psi_i + \delta\cos\psi_i) + \mu^2(\sin\psi_i + \delta\cos\psi_i)^2\frac{R}{3}\right]$$
$$-\sin\psi_i\frac{(R-e)}{2}\left(\lambda_0 + \mu\beta\cos\psi_i - \frac{e}{R}\dot{\beta}\right)^2$$
$$-\sin\psi_i\frac{R}{6}\left(\lambda_{1c}\cos\psi_i + \lambda_{1s}\sin\psi_i + \dot{\beta}\right)$$
$$+\frac{m_i}{S}e\Omega^2\cos\psi_i$$
$$-\frac{m_{si}}{S}\left[2\beta\dot{\beta}_t\Omega\sin\psi_i - \dot{\beta}^2\left(1 - \frac{\beta^2}{2}\right)\cos\psi_i - \beta\ddot{\beta}_{t.t}\cos\psi_i\right.$$
$$\left.-\Omega^2\left(1 - \frac{\beta^2}{2}\right)\cos\psi_i\right]$$
$$-\frac{m_{si}}{S}\left[2\Omega\dot{\delta}_t\delta\sin\psi_i - \dot{\delta}_t^{\,2}\cos\psi_i - \ddot{\delta}_{t.t}\delta\cos\psi_i + \dot{\delta}_t^{\,2}\delta\sin\psi_i\right.$$
$$\left.-\ddot{\delta}_{t.t}\sin\psi_i - 2\dot{\delta}_t^{\,2}\Omega\cos\psi_i + \Omega^2\delta\sin\psi_i\right]$$

And:

$$\begin{aligned}
\frac{F_{yi}{}^{a}}{S} &= \left[\frac{R}{3}+(R-e)\mu^{2}(\sin\psi_i+\delta\cos\psi_i)^{2}+R\mu(\sin\psi_i+\delta\cos\psi_i)\right] \\
&\quad \left[-\frac{\beta}{2}\theta_{con}+\frac{C_{d0}\delta}{2a}\sin\psi_i+\cos\psi_i\left(\frac{\theta_{con}{}^{2}}{2}-\frac{C_{d0}}{2a}\right)\right] \\
&+\left[\frac{R}{4}+2\mu\frac{R}{3}(\sin\psi_i+\delta\cos\psi_i)+\mu^{2}(\sin\psi_i+\delta\cos\psi_i)^{2}\frac{R}{2}\right] \\
&\quad \left[-\frac{\beta}{2}\theta_{tw}\sin\psi_i+\cos\psi_i\theta_{tw}\theta_{con}\right] \\
&+\left(\lambda_0+\mu\beta\cos\psi_i-\frac{e}{R}\dot{\beta}\right) \\
&\quad \left[\frac{\beta}{2}\sin\psi_i\left(\frac{R}{2}+\mu(R-e)(\sin\psi_i+\delta\cos\psi_i)\right)\right. \\
&\quad -\cos\psi_i\left[\left(\mu(R-e)(\sin\psi_i+\delta\cos\psi_i)+\frac{R}{2}\right)\theta_{con}\right. \\
&\quad \left.\left.+\left(\frac{R}{2}(\sin\psi_i+\delta\cos\psi_i)+\frac{R}{3}\right)\theta_{tw}-\frac{R}{2}\left(\lambda_{1c}\cos\psi_i+\lambda_{1s}\sin\psi_i+\dot{\beta}\right)\right]\right] \\
&+\left(\lambda_{1c}\cos\psi_i+\lambda_{1s}\sin\psi_i+\dot{\beta}\right)\left[\frac{\beta}{2}\sin\psi_i\left(\frac{R}{3}+\mu\frac{R}{2}(\sin\psi_i+\delta\cos\psi_i)\right)\right. \\
&\quad \left.-\cos\psi_i\left[\left(\frac{R}{2}\mu(\sin\psi_i+\delta\cos\psi_i)+\frac{R}{3}\right)\theta_{con}+\left(\frac{R}{3}\mu(\sin\psi_i+\delta\cos\psi_i)+\frac{R}{4}\right)\theta_{tw}\right]\right] \\
&+\cos\psi_i\frac{\theta_{tw}{}^{2}}{2}\left[\frac{R}{5}+\mu(\sin\psi_i+\delta\cos\psi_i)\frac{R}{2}+\mu^{2}(\sin\psi_i+\delta\cos\psi_i)^{2}\frac{R}{3}\right] \\
&+\cos\psi_i\frac{(R-e)}{2}\left(\lambda_0+\mu\beta\cos\psi_i-\frac{e}{R}\dot{\beta}\right)^{2}+\cos\psi_i\frac{R}{6}\left(\lambda_{1c}\cos\psi_i+\lambda_{1s}\sin\psi_i+\dot{\beta}\right)^{2} \\
&+\frac{m_i}{S}e\Omega^{2}\sin\psi_i \\
&+\frac{m_{si}}{S}\left[-2\beta\dot{\beta}_t\Omega\cos\psi_i-\dot{\beta}_t{}^{2}\left(1-\frac{\beta^{2}}{2}\right)\sin\psi_i-\beta\dot{\beta}_{t.t}\sin\psi_i-\Omega^{2}\left(1-\frac{\beta^{2}}{2}\right)\sin\psi_i\right] \\
&-\frac{m_{si}}{S}\left[-2\dot{\delta}_t{}^{2}\Omega\delta\cos\psi_i-\dot{\delta}_t{}^{2}\sin\psi_i-\ddot{\delta}_{t.t}{}^{2}\delta\sin\psi_i-\dot{\delta}_t{}^{2}\delta\cos\psi_i\right. \\
&\quad \left.-\ddot{\delta}_{t.t}\cos\psi_i-2\dot{\delta}_t{}^{2}\Omega\sin\psi_i-\Omega^{2}\delta\cos\psi_i\right]
\end{aligned}$$

$$\begin{aligned}
\frac{F_{zi}{}^{a}}{S} &= \left[\frac{R}{3}+(R-e)\mu^{2}(\sin\psi_i+\delta\cos\psi_i)^{2}+R\mu(\sin\psi_i+\delta\cos\psi_i)\right]\theta_{con} \\
&+\left[\frac{R}{4}+2\mu\frac{R}{3}(\sin\psi_i+\delta\cos\psi_i)+\mu^{2}\frac{R}{2}(\sin\psi_i+\delta\cos\psi_i)^{2}\right]\theta_{tw} \\
&-\left[\frac{R}{2}+(R-e)\mu(\sin\psi_i+\delta\cos\psi_i)\right]\left(\lambda_0+\mu\beta\cos\psi_i-\frac{e}{R}\dot{\beta}\right) \\
&-\left[\frac{R}{3}+\mu\frac{R}{2}(\sin\psi_i+\delta\cos\psi_i)\right]\left(\lambda_{1c}\cos\psi_i+\lambda_{1s}\sin\psi_i+\dot{\beta}\right) \\
&-2\frac{m_{si}}{S}\left[\ddot{\beta}_{t.t}\left(1-\frac{\beta^{2}}{2}\right)-\beta\dot{\beta}_t{}^{2}\right]-2\frac{m_{si}}{S}\left[-2\dot{\delta}_t\dot{\beta}_t\delta-\dot{\delta}_t{}^{2}\beta\right]
\end{aligned}$$

Calculation of the resultant moment in the rotor head

As seen above, by isolating the rotor hub we will be able to determine the rotor head moment M $_{blade \rightarrow hub}$., as indicated in Figure 10.

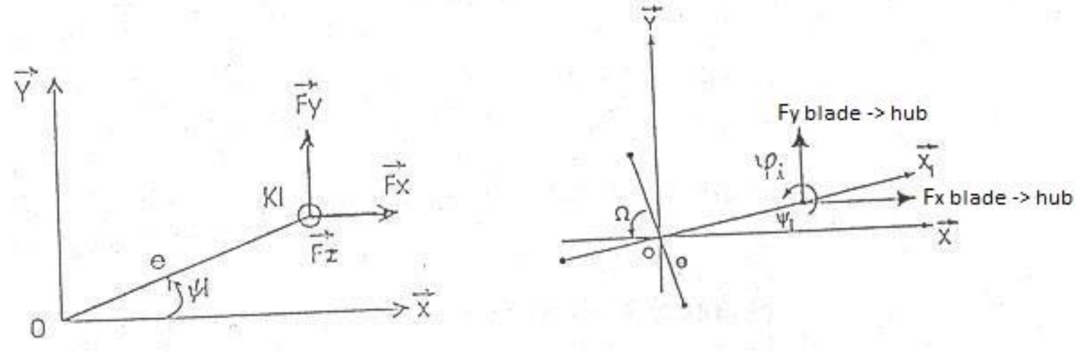

Figure 10: Resulting moment at the rotor head – adapted from (Jorge, 1992)

$\phi_i = K_{i\delta}.\delta_i + C_{i\delta}\,\dot{\delta}_{it}$ (Torsional moment due to drag adapter)

$$
\begin{aligned}
M_x &= \left[\overrightarrow{OK_i}\Lambda\vec{F}_{blade\rightarrow hub}\right].\vec{X} \\
&= e\sin\psi_i.F_z \\
M_y &= \left[\overrightarrow{OK_i}\Lambda\vec{F}_{blade\rightarrow hub}\right].\vec{Y} \\
&= e\cos\psi_i.F_z \\
M_z &= \left[\overrightarrow{OK_i}\Lambda\vec{F}_{blade\rightarrow hub}\right].\vec{Z} \\
&= e\cos\psi_i.F_y - e\sin\psi_i.F_x + K_{i\delta} + C_{i\delta}\,\dot{\delta}_t
\end{aligned}
$$

It is obtained directly:

$$
\begin{aligned}
M_x = \frac{S}{2}e\Bigg\{ & \left[\frac{R}{3} + (R-e)\mu^2(\sin\psi_i + \delta\cos\psi_i)^2 + R\mu(\sin\psi_i + \delta\cos\psi_i)\right]\theta_{con}\sin\psi_i \\
& + \left[\frac{R}{4} + \frac{2}{3}\mu R(\sin\psi_i + \delta\cos\psi_i) + \frac{R}{2}\mu^2(\sin\psi_i + \delta\cos\psi_i)^2\right]\theta_{tw}\sin\psi_i \\
& - \left[\frac{R}{2} + (R-e)\mu(\sin\psi_i + \delta\cos\psi_i)\right]\left(\lambda_0 + \mu\beta\cos\psi_i - \frac{e}{R}\dot{\beta}\right)\sin\psi_i \\
& - \left[\frac{R}{3} + \frac{R}{2}\mu(\sin\psi_i + \delta\cos\psi_i)\right]\left(\lambda_{1c}\cos\psi_i + \lambda_{1s}\sin\psi_i + \dot{\beta}\right)\sin\psi_i \Bigg\} \\
& - m_{si}e\sin\psi_i\left[\ddot{\beta}_{t.t}\left(1 - \frac{b^2}{2}\right) - \beta\dot{\beta}_t^{\,2} - 2\dot{\delta}_t\dot{\beta}_t\delta - \dot{\delta}_t^{\,2}\beta\right]
\end{aligned}
$$

$$
\begin{aligned}
M_y = \frac{S}{2}e\Bigg\{ & \left[\frac{R}{3} + (R-e)\mu^2(\sin\psi_i + \delta\cos\psi_i)^2 + R\mu(\sin\psi_i + \delta\cos\psi_i)\right]\theta_{con}\sin\psi_i \\
& + \left[\frac{R}{4} + \frac{2}{3}\mu R(\sin\psi_i + \delta\cos\psi_i) + \frac{R}{2}\mu^2(\sin\psi_i + \delta\cos\psi_i)^2\right]\theta_{tw}\sin\psi_i \\
& - \left[\frac{R}{2} + (R-e)\mu(\sin\psi_i + \delta\cos\psi_i)\right]\left(\lambda_0 + \mu\beta\cos\psi_i - \frac{e}{R}\beta\right)\cos\psi_i \\
& - \left[\frac{R}{3} + \frac{R}{2}\mu(\sin\psi_i + \delta\cos\psi_i)\right]\left(\lambda_{1c}\cos\psi_i + \lambda_{1s}\sin\psi_i + \beta\right)\cos\psi_i \Bigg\} \\
& - m_{si}e\cos\psi_i\left[\ddot{\beta}_{t.t}\left(1 - \frac{b^2}{2}\right) - \beta\dot{\beta}_t^{\,2} - 2\dot{\delta}_t\dot{\beta}_t\delta - \dot{\delta}_t^{\,2}\beta\right]
\end{aligned}
$$

$$
\begin{aligned}
M_z = Se\left[\frac{R}{3} + (R-e)\mu^2(\sin\psi_i + \delta\cos\psi_i)^2 + R\mu(\sin\psi_i + \delta\cos\psi_i)\right]&\left(\frac{{\theta_{con}}^2}{2}\right. \\
&\left. - \frac{C_{d0}}{2a}\right) \\
+ \left[\frac{R}{4} + 2\mu\frac{R}{3}(\sin\psi_i + \delta\cos\psi_i) + \frac{R}{2}\mu^2(\sin\psi_i + \delta\cos\psi_i)^2\right]&\theta_{tw}\theta_{con} \\
- \left(\lambda_0 + \mu\beta\cos\psi_i - \frac{e}{R}\dot{\beta}\right)\left[\left(\frac{R}{2} + (R-e)\mu(\sin\psi_i + \delta\cos\psi_i)\right)\right.& \\
\left. + -\frac{R}{2}\left(\lambda_{1c}\cos\psi_i + \lambda_{1s}\sin\psi_i + \dot{\beta}\right)\right]& \\
- \left(\lambda_{1c}\cos\psi_i + \lambda_{1s}\sin\psi_i + \dot{\beta}\right)\left[\left(\frac{R}{3} + \frac{R}{2}\mu(\sin\psi_i + \delta\cos\psi_i)\right)\theta_{con}\right.& \\
\left. + \left(\frac{R}{3}\mu(\sin\psi_i + \delta\cos\psi_i) + \frac{R}{4}\right)\theta_{tw}\right]& \\
+ \left[\frac{R}{5} + \frac{R}{2}\mu(\sin\psi_i + \delta\cos\psi_i) + \frac{R}{3}\mu^2(\sin\psi_i + \delta\cos\psi_i)^2\right]\frac{{\theta_{tw}}^2}{2}& \\
+ \left(\lambda_0 + \mu\beta\cos\psi_i - \frac{e}{R}\dot{\beta}\right)^2\frac{(R-e)}{2} + \frac{R}{6}\left(\lambda_{1c}\cos\psi_i + \lambda_{1s}\sin\psi_i + \dot{\beta}\right)^2& \\
+ m_{si}e\left(2\beta\dot{\beta}_t\Omega + 2\dot{\delta}_t\Omega\delta + {\dot{\delta}_t}^2\delta - \ddot{\delta}_{t.t} + \Omega^2\delta\right) + K_{i\delta}.\delta + C_{i\delta}\dot{\delta}_t&
\end{aligned}
$$

Application to a rotor with N blades

The expressions we have just established are valid for each of the blades which compose the rotor. To get the overall effort wrench, it is needed to make a sum of the components for the total number of blades, as shown below.

$$
\begin{aligned}
&[F_x]_{rotor} = \sum_{i=1}^{N}[F_x]_{blade\ i} \qquad &&[M_x]_{rotor} = \sum_{i=1}^{N}[M_x]_{blade\ i} \\
&[F_y]_{rotor} = \sum_{i=1}^{N}[F_y]_{blade\ i} \qquad &&[M_y]_{rotor} = \sum_{i=1}^{N}[M_y]_{blade\ i} \\
&[F_z]_{rotor} = \sum_{i=1}^{N}[F_z]_{blade\ i} \qquad &&[M_z]_{rotor} = \sum_{i=1}^{N}[M_z]_{blade\ i}
\end{aligned}
\tag{21}
$$

Equilibrium equations

The blade is simply articulated in flapping and drag, one can apply the dynamic moment theorem, as indicated in Figure 11.

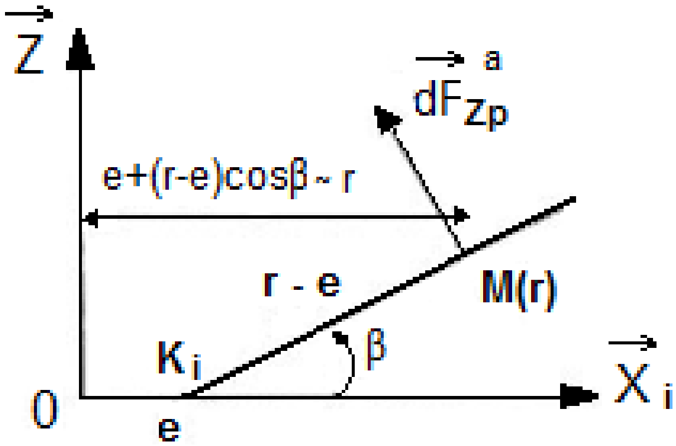

Figure 11: Application of the dynamic moment theorem – adapted from (Jorge, 1992)

$$\vec{\delta}^{K_i}_{blade/Rg} = \vec{M}^{K_i}_{Forces\ \mathrm{ext}\to blade}$$
$$Or$$
$$\vec{\delta}^{K_i}_{blade/Rg} = \int_e^R \overrightarrow{K_i M}\,\Lambda \overrightarrow{\gamma_M} dm_i$$

with $\overrightarrow{\gamma M}$ t be calculated in what follows.

$$\left[\overrightarrow{K_i M}\Lambda\overrightarrow{\gamma_M}\right]_{R_f} = \begin{bmatrix} (r-e)\cos\delta\cos\beta\cos\psi_i - (r-e)\sin\delta\sin\psi_i \\ (r-e)\cos\delta\cos\beta\sin\psi_i - (r-e)\sin\delta\cos\psi_i \\ (r-e)\cos\delta\sin\beta \end{bmatrix} \Lambda \begin{bmatrix} \ddot{\gamma}_x \\ \ddot{\gamma}_y \\ \ddot{\gamma}_z \end{bmatrix} \quad (22)$$

$$\left[\overrightarrow{K_i M}\Lambda\overrightarrow{\gamma_M}\right]_{R_f} = \begin{bmatrix} [(r-e)\cos\delta\cos\beta\sin\psi_i + (r-e)\sin\delta\cos\psi_i]\ddot{\gamma}_z - (r-e)\cos\delta\sin\beta\,\ddot{\gamma}_y \\ -[(r-e)\cos\delta\cos\beta\cos\psi_i - (r-e)\sin\delta\sin\psi_i]\ddot{\gamma}_z + (r-e)\cos\delta\sin\beta\,\ddot{\gamma}_x \\ [(r-e)\cos\delta\cos\beta\cos\psi_i - (r-e)\sin\delta\sin\psi]\ddot{\gamma}_y \\ \quad - [(r-e)\cos\delta\cos\beta\sin\psi_i + (r-e)\sin\delta\cos\psi_i]\ddot{\gamma}_x \end{bmatrix}$$

One can pass to the rotating rotor reference frame through a rotation of (- ψ_i)

$$\left[\overrightarrow{K_i M}\Lambda\overrightarrow{\gamma_M}\right]_{R_f} = \begin{bmatrix} \ddot{\gamma}_z(r-e)\sin\delta + (r-e)\cos\delta\sin\beta\left(\ddot{\gamma}_x\sin\psi_i - \ddot{\gamma}_y\cos\psi_i\right) \\ -\ddot{\gamma}_z(r-e)\cos\delta\cos\beta + (r-e)\cos\delta\sin\beta\left(\ddot{\gamma}\cos\psi_i - \ddot{\gamma}_y\sin\psi_i\right) \\ [(r-e)\cos\delta\cos\beta\cos\psi_i - (r-e)\sin\delta\sin\psi]\ddot{\gamma}_y \\ \quad - [(r-e)\cos\delta\cos\beta\sin\psi_i + (r-e)\sin\delta\cos\psi_i]\ddot{\gamma}_x \end{bmatrix}$$

This gives us, for small angles:

$$\left[\overrightarrow{K_i M}\Lambda\overrightarrow{\gamma_M}\right]_{R_f} = \begin{bmatrix} (r-e)^2\left\{\delta\left[\ddot{\beta}_{t.t}\left(1-\frac{\beta^2}{2}\right) - \dot{\beta}_t^{\,2}\beta - 2\dot{\delta}_t\dot{\beta}_t\delta - \delta_t^{\,2}\beta\right]\right. \\ \left. +\beta\left[2\Omega\dot{\beta}_t\beta + 2\Omega\dot{\delta}_t\delta + \delta_t^{\,2}\delta - \ddot{\delta}_{t.t} + \Omega^2\delta\right]\right\} \\ (r-e)^2\left\{\left(1-\frac{\beta^2}{2}\right)\left[-\ddot{\beta}_{t.t}\left(1-\frac{\beta^2}{2}\right) + \dot{\beta}_t^{\,2}\beta + 2\delta_t\dot{\beta}_t\delta + \dot{\delta}_t^{\,2}\beta\right] + \beta\left[-\ddot{\beta}_{t.t}\beta - \right]\right\} \\ -(r-e)e\beta\Omega^2 \\ (r-e)^2\left[\left(1-\frac{\beta^2}{2}\right)\left(2\Omega\dot{\beta}_t\beta + 2\Omega\dot{\delta}_t\delta + \dot{\delta}_t^{\,2}\delta - \ddot{\delta}_{t.t} + \Omega^2\delta\right)\right. \\ \left. +\delta\left(-\ddot{\beta}_{t.t}\beta - \dot{\beta}_t^{\,2}\left(1-\frac{\beta^2}{2}\right) - \Omega^2\left(1-\frac{\beta^2}{2}\right) - \dot{\delta}_t^{\,2} - \ddot{\delta}_{t.t}\delta - 2\dot{\delta}_t\Omega\right)\right] + (r-e)e\delta\Omega^2 \end{bmatrix}$$

$$\left[\overrightarrow{K_tM}\Lambda\overrightarrow{\gamma_M}\right]_{R_f} = \begin{bmatrix} (r-e)^2\left\{\delta\left[\ddot{\beta}_{t.t}\left(1-\frac{\beta^2}{2}\right)-\dot{\beta}_t^{\,2}\beta-2\dot{\delta}_t\dot{\beta}_t\delta\right]+\beta\left[2\Omega\dot{\beta}_t\beta+2\Omega\dot{\delta}_t\delta-\ddot{\delta}_{t.t}+\Omega^2\delta\right]\right\} \\ \\ (r-e)^2\left[-\ddot{\beta}_{t.t}\left(1-\frac{\beta^4}{4}\right)+2\left(1-\frac{\beta^2}{2}\right)\delta_t\dot{\beta}_t\delta+\dot{\delta}_t^{\,2}\frac{\beta^3}{2}-\ddot{\delta}_{t.t}\delta\beta-2\dot{\delta}_t\beta\Omega\right] \\ -(r-e)\beta\Omega^2\left(e+(r-e)\left(1-\frac{\beta^2}{2}\right)\right) \\ \\ (r-e)^2\left[-2\Omega\dot{\beta}_t\beta\left(1-\frac{\beta^2}{2}\right)+\Omega\dot{\delta}_t\delta\beta^2+\dot{\delta}_t^{\,2}\delta\frac{\beta^2}{2}+\ddot{\delta}_{t.t}\left(1-\frac{\beta^2}{2}+\delta^2\right)\right. \\ \left.+\ddot{\beta}_{t.t}\beta\delta+\dot{\beta}_t^{\,2}\delta\left(1-\frac{\beta^2}{2}\right)\right]+(r-e)e\delta\Omega^2 \end{bmatrix}$$

Where one can assume: $1+\beta^4/4 \approx 1$ and $e+(r-e)\cos\beta \approx e+(r-e)(1-\beta^2/2) \approx r$. We will also disregard the triple products of angles about the double products, since β, δ and δ are small angles, what finally gives:

$$\left[\overrightarrow{K_tM}\ \Lambda\ \overrightarrow{\gamma_M}\right]_{R_t} = \begin{bmatrix} (r\text{-}e)^2\left[\delta\ddot{\beta}_{t.t}+\beta\left(-\ddot{\delta}_{t.t}+\Omega^2\delta\right)\right] \\ (r\text{-}e)^2\left[-\ddot{\beta}_{t.t}\text{-}2\dot{\delta}_t\beta\Omega r\right]-(r\text{-}e)\beta\Omega^2 r \\ (r\text{-}e)^2\left[\text{-}e\Omega\dot{\beta}_t\beta+\ddot{\delta}_{t.t}\right]-(r\text{-}e)\delta\Omega^2 e \end{bmatrix} \tag{23}$$

With $\ddot{\beta}_{t.t}=\Omega^2\ddot{\beta};\ \dot{\beta}_t=\Omega^2\dot{\beta};\ \ddot{\delta}_{t.t}=\Omega^2\ddot{\delta};\ \dot{\delta}_{t.t}=\Omega^2\dot{\delta}$

Flapping motion equations

The dynamic momentum theorem gives us a projection on the y_i axis:

$$\begin{aligned}&\int_e^R (r-e)^2\Omega^2\ddot{\beta}\,mdr+\int_e^R 2(r-e)^2\Omega^2\dot{\delta}\beta\,mdr+\int_e^R (r-e)r\Omega^2\beta\,mdr\\&=\int_e^R (r-e)\,dF_{zp^a}\simeq\int_e^R (r-e)\,dF_{zi^a}\end{aligned} \tag{24}$$

$$\text{with: } dm_i = mdr$$

The static moment of the blade is: $ms_i=\int_e^R (r-e)mdr$ .The flapping inertia of the blade is: $I_\beta=\int_e^R (r-e)^2 mdr$.

Writing: $(r\text{-}e)\ r = r^2 - re = (r\text{-}e)^2 + e\ (r\text{-}e)$, we obtain

$$\dot{\beta}+\left[1+2\dot{\delta}+\frac{e.ms_i}{I_\beta}\right]\beta=\frac{1}{\Omega^2 I_\beta}\int_e^R (r-e)dF_{zi^a} \tag{25}$$

Introducing the previously obtained expression for dF_{zi}^{a}, we have

$$\ddot{\beta} + \left[1 + 2\dot{\delta} + \frac{e.ms_i}{I_\beta}\right]\beta = \frac{\rho acR^2}{2I_\beta}\int_e^R (r-e)\left[\theta\left(\frac{r}{R} + \mu(\sin\psi_i + \delta\cos\psi_i)\right) - \left(\frac{r}{R} + \mu(\sin\psi_i + \delta\cos\psi_i)\right)\left(\lambda + \frac{r\dot{\beta}}{R} - \frac{e}{R}\dot{\beta} + \beta\mu\cos\psi_i\right)\right]dr$$

$$= \frac{\rho ac\,R^2}{2I_\beta}\int_e^R (r-e)\left[\left(\theta_{\text{con}} + \frac{r}{R}\theta_{\text{tw}}\right)\left(\frac{r}{R} + \mu(\sin\psi_i + \delta\cos\psi_i)\right)^2 - \left(\frac{r}{R} + \mu(\sin\psi_i + \delta\cos\psi_i)\right)\left(\lambda_0 + \lambda_{1c}\frac{r}{R}\cos\psi_i + \lambda_{1s}\frac{r}{R}\sin\psi_i + \frac{r\dot{\beta}}{R} - \frac{e\dot{\beta}}{R} + \beta\mu\cos\psi_i\right)\right]dr$$

And, after calculating the integral:

$$\begin{aligned}
\ddot{\beta} + \left[1 + 2\dot{\delta} + \frac{e.ms_i}{I_\beta}\right]\beta = \frac{\rho ace}{2I_\beta}R^2\Bigg\{&\left[\frac{R^3-e^3}{3R^2} + (R-e)\mu^2(\sin\psi_i + \delta\cos\psi_i)^2 + \frac{R^2-e^2}{R}\mu(\sin\psi_i + \delta\cos\psi_i)\right]\theta_{\text{con}} \\
&+ \left[\frac{R^4-e^4}{4R^3} + \frac{2}{3}\mu\frac{R^3-e^3}{R^2}(\sin\psi_i + \delta\cos\psi_i) + \frac{R^2-e^2}{2R}\mu^2(\sin\psi_i + \delta\cos\psi_i)^2\right]\theta_{\text{tw}} \\
&- \left[\frac{R^2-e^2}{2R} + (R-e)\mu(\sin\psi_i + \delta\cos\psi_i)\right]\left(\lambda_0 + \mu\beta\cos\psi_i - \frac{e}{R}\dot{\beta}\right) \\
&- \left[\frac{R^3-e^3}{3R^2} + \frac{R^2-e^2}{2R}\mu(\sin\psi_i + \delta\cos\psi_i)\right]\left(\lambda_0 + \lambda_{1c}\cos\psi_i + \lambda_{1s}\sin\psi_i + \dot{\beta}\right)\Bigg\} \\
+ \frac{\rho ac}{2I_\beta}R^2\Bigg\{&\left[\frac{R^4-e^4}{4R^3} + \frac{R^2-e^2}{2}\mu^2(\sin\psi_i + \delta\cos\psi_i)^2 + \frac{2(R^3-e^3)}{3R}\mu(\sin\psi_i + \delta\cos\psi_i)\right]\theta_{\text{con}} \\
&+ \left[\frac{R^5-e^5}{5R^3} + \frac{R^3-e^3}{3R^2}\mu^2(\sin\psi_i + \delta\cos\psi_i)^2 + \frac{R^4-e^4}{2R^2}\mu(\sin\psi_i + \delta\cos\psi_i)\right]\theta_{\text{tw}} \\
&- \left[\frac{R^3-e^3}{3R^2} + \frac{R^2-e^2}{2}\mu(\sin\psi_i + \delta\cos\psi_i)\right]\left(\lambda_0 + \mu\beta\cos\psi_i - \frac{e}{R}\beta\right) \\
&- \left[\frac{R^4-e^4}{4R^2} + \frac{R^3-e^3}{3R^2}\mu(\sin\psi_i + \delta\cos\psi_i)\right]\left(\lambda_0 + \lambda_{1c}\cos\psi_i + \lambda_{1s}\sin\psi_i + \dot{\beta}\right)\Bigg\}
\end{aligned}$$

Using the simplifications $R^2 - e^2 \approx R^2$; $R^3 - e^3 \approx R^3$; $R^4 - e^4 \approx R^4$; $R^5 - e^5 \approx R^5$ and the Coleman Transformation (Coleman & Feingold, 1957) ($\theta_{con} = \theta_0 + \theta_{1c}\cos\psi_i + \theta_{1s}\sin\psi_i$, $\beta = \beta_0 + \beta_{1c}\cos\psi_i + \beta_{1s}\sin\psi_i$, and $\delta = \delta_0 + \delta_{1c}\cos\psi_i + \delta_{1s}\sin\psi_i$), leads to:

$$
\begin{aligned}
\ddot{\beta} + \left[1 + 2\dot{\delta} + \frac{e.ms_i}{I_\beta}\right]\beta = \frac{\rho ace}{2I_\beta}R^2 \Bigg\{ & \Bigg[\frac{R}{3} + (R-e)\mu^2\left(\sin\psi_i + \delta\cos\psi_i\right)^2 \\
& + R\mu\left(\sin\psi_i + \delta\cos\psi_i\right)\Bigg]\left(\theta_0 + \theta_{1c}\cos\psi_i + \theta_{1s}\sin\psi_i\right) \\
& + \left[\frac{R}{4} + 2\mu\frac{R}{3}\left(\sin\psi_i + \delta\cos\psi_i\right) + \frac{R}{2}\mu^2\left(\sin\psi_i + \delta\cos\psi_i\right)^2\right]\theta_{tw} \\
& - \left[\frac{R}{2} + (R-e)\mu\left(\sin\psi_i + \delta\cos\psi_i\right)\right]\left(\lambda_0 + \mu\beta\cos\psi_i - \frac{e}{R}\dot{\beta}\right) \\
& - \left[\frac{R}{3} + \frac{R}{2}\mu\left(\sin\psi_i + \delta\cos\psi_i\right)\right]\left(\lambda_0 + \lambda_{1c}\cos\psi_i + \lambda_{1s}\sin\psi_i + \dot{\beta}\right)\Bigg\} \qquad (26) \\
+ \frac{\rho ac}{2I_\beta}R^2 \Bigg\{ & \left[\frac{R^2}{4} + \frac{R^2}{2}\mu^2\left(\sin\psi_i + \delta\cos\psi_i\right)^2 + \frac{2}{3}R^2\mu\left(\sin\psi_i + \delta\cos\psi_i\right)\right]\left(\theta_0 + \theta_{1c}\cos\psi_i + \theta_{1s}\sin\psi_i\right) \\
& + \left[\frac{R^2}{5} + \frac{R^2}{3}\mu^2\left(\sin\psi_i + \delta\cos\psi_i\right)^2 + \frac{R^2}{2}\mu\left(\sin\psi_i + \delta\cos\psi_i\right)\right]\theta_{tw} \\
& - \left[\frac{R^2}{3} + \frac{R^2}{2}\mu\left(\sin\psi_i + \delta\cos\psi_i\right)\right]\left(\lambda_0 + \mu\beta\cos\psi_i - \frac{e}{R}\dot{\beta}\right) \\
& - \left[\frac{R^2}{4} + \frac{R^2}{3}\mu\left(\sin\psi_i + \delta\cos\psi_i\right)\right]\left(\lambda_0 + \lambda_{1c}\cos\psi_i + \lambda_{1s}\sin\psi_i + \dot{\beta}\right)\Bigg\}
\end{aligned}
$$

To decouple the different parameters involved in this equation, the following operators will be applied to the flapping equation: $\frac{1}{2\pi}\int_0^{2\pi}(\ldots)d\psi$, $\frac{1}{2\pi}\int_0^{2\pi}(\ldots)cos\psi d\psi$ and $\frac{1}{2\pi}\int_0^{2\pi}(\ldots)sin\psi d\psi$. Disregarding the double products of angles concerning the angles themselves, the influence of the drag angle on the flapping motion will be disregarded. After some transformations and intermediate calculations, the following three equations are then obtained:

$$
\begin{aligned}
* \left[1 + \frac{e.m_{si}}{I_\beta}\right]\beta_0 = \frac{\rho ace}{2I_\beta}R^2 \Bigg[& -e\Bigg\{\frac{R-e}{2}\mu^2\theta_0 + \frac{R}{3}\theta_0 + \frac{R}{4}\theta_{tw} + \frac{R}{2}\left[\mu\theta_{1s} + \frac{\mu^2}{2}\theta_{tw} - \lambda_0 + \frac{\mu}{2}\beta_{1c} - \frac{\mu}{2}\lambda_{1s}\right] \\
& - \frac{\mu(r-e)^e}{2R}\beta_{1c}\Bigg\} + \frac{R^2}{4}\theta_0 + \frac{R^2}{4}\mu^2\theta_0 + \frac{R^2}{3}\mu\theta_{1s} + \frac{R^2}{5}\theta_{tw} + \frac{R^2}{6}\mu^2\theta_{tw} \\
& - \frac{R^2}{3}\lambda_0 - \frac{R^2}{6}\mu\lambda_{1s}\Bigg]
\end{aligned}
$$

$$
\begin{aligned}
* \frac{e.m_{si}}{I_\beta}\beta_{1c} = \frac{\rho ac}{2I_\beta}R^2 \Bigg[& -e\left\{\frac{R}{3}\theta_{1c} + \frac{R}{2}\mu\beta_0 + \frac{R-e}{4}\mu^2\beta_{1s} + \frac{R-e}{4}\mu^2\theta_{1c} - \frac{R}{3}\lambda_{1c} - \frac{R}{3}\beta_{1s} + \frac{e\beta_{1s}}{2}\right\} \\
& - \frac{R^2}{3}\mu\beta_0 + \frac{R^2}{8}\mu^2\theta_{1c} - \frac{R^2}{4}\lambda_{1c} + \frac{Re}{3}\beta_{1s} + \frac{R^2}{4}\theta_{1c} - \frac{R^2}{4}\beta_{1s} - \frac{R^2}{8}\mu^2\beta_{1s}\Bigg]
\end{aligned}
$$

$$* \frac{e.m_{si}}{I_\beta}\beta_{si} = \frac{\rho ac}{2I_\beta}R^2\Bigg[-e\left\{\frac{R}{3}\theta_{1s} + \frac{3(R-e)}{4}\mu^2\theta_{1s} + R\mu\theta_0 + \frac{2R}{3}\mu\theta_{tw} - (R-e)\mu\lambda_0 - \frac{R-e}{4}\mu^2\beta_{1c} - \frac{e\beta_{1c}}{2} - \frac{R}{3}\lambda_{1s} + \frac{R}{3}\beta_{1c}\right\} + \frac{R^2}{4}\theta_{1s} + \frac{3R^2}{8}\mu^2\theta_{1s} + \frac{2R^2}{3}\mu\theta_0 + \frac{R^2}{2}\mu\theta_{tw} + \frac{R^2}{2}\mu\lambda_0 - \frac{R^2}{8}\mu^2\beta_{1c} - \frac{Re}{3}\beta_{1c} - \frac{R^2}{4}\lambda_{1s} + \frac{R^2}{4}\beta_{1c}\Bigg]$$

Introducing the Lock Number: $\gamma = \rho ac\dfrac{R^4}{I_\beta}$, one obtains:

$$* \left[1 + \frac{e.m_{si}}{I_\beta}\right]\beta_0 = \frac{\gamma}{R^2}\left[\theta_{tw}\left[\frac{4R^2 - 5eR}{40}\right] - \left[\frac{R^2 - 2e(R-e)}{8R}e\mu\right]\beta_{1c} + \left(\mu^2\theta_{tw} + 2\mu\theta_{1s} - 2\lambda_0 - \mu\lambda_{1s}\right)\left\{\frac{2R^2 - 3eR}{24}\right\} + \theta_0\left\{\frac{R^2 - 2e(R-e)}{8}\mu^2 + \frac{3R^2 - 4eR}{24}\right\}\right]$$

$$* \frac{e.m_{si}}{I_\beta}\beta_{1c} = \frac{\gamma}{R^2}\left[\left(\theta_{1c} - \beta_{1s}\right)\left\{\frac{R^2 - 2e(R-e)}{16}\mu^2\right\} + \beta_{1s}\left(\frac{4eR - 6e^2}{24}\right) + \beta_0\left\{\frac{-2R^2 + 3eR}{12}\mu\right\} + \left(\theta_{1c} - \beta_{1s} - \lambda_{1c}\right)\left\{\frac{3R^2 - 4eR}{24}\right\}\right] \quad (27)$$

$$* \frac{e.m_{si}}{I_\beta}\beta_{si} = \frac{\gamma}{R^2}\left[\left(2\mu\theta_{tw} + \theta_{1s} + \beta_{1c} - \lambda_{1s}\right)\left\{\frac{3R^2 - 4eR}{24}\right\} + \theta_0\left\{\frac{2R^2 - 3eR}{6}\mu\right\} + \beta_{1c}\left[\frac{6e^2 - 4eR}{24}\right] + \left(3\mu\theta_{1s} - \mu\beta_{1c} - 4\lambda_0\right)\left\{\frac{R^2 - 4e(R-e)}{16}\mu\right\}\right]$$

Drag motion equations

The motion of interest is now around the drag axis, that is, $\vec{Z}_p \equiv \vec{Z'}_p$. But to have the reference frame, without changing it, one must apply the theorem in the reference frame R_t, for the component around Z_i (given that K_i is a joint, so it is articulate), assuming that the restitution moment due to the frequency adapter is also along the Z_i axis, as it was done previously for the calculation of M_z. The dynamic momentum theorem gives us, in projection onto the Z_i axis:

$$\int_e^R (r-e)^2\left(-2\Omega\dot{\beta}_t\,\beta + \ddot{\delta}_{t.t}\right)mdr + \int_e^R (r-e)\delta\Omega^2 e\, mdr$$
$$= \int_e^R (r-e)dF_{yi^a}\cos\beta - K_\delta\delta - C_\delta\dot{\delta}_t \simeq \int_e^R (r-e)dF_{yi^a} - K_\delta\delta - C_\delta\dot{\delta}_t \quad (28)$$

And as $I_\beta = I_\delta = \int_e^R (r-e)^2 mdr$, we have, then:

$$\ddot{\delta} + \frac{C_\delta}{\Omega I_\beta}\dot{\delta} + \left(\frac{e.m_{si}}{I_\beta} + \frac{K_\delta}{\Omega^2 I_\beta}\right)\delta = 2\beta\dot{\beta} + \frac{1}{\Omega^2 I_\beta}\int_e^R (r-e)dF_{yi^a}$$

Introducing the previously obtained expression of dF_{yi}^{a} , we have:

$$\ddot{\delta}+\frac{C_\delta}{\Omega I_\beta}\dot{\delta}+\left(\frac{e.m_{si}}{I_\beta}+\frac{K_\delta}{\Omega^2 I_\beta}\right)\delta=2\beta\dot{\beta}+\frac{\rho ac(\Omega R)^2}{\Omega^2 I_\beta}\int_e^R(R-e)\left\{\frac{1}{2}\left[2\theta\left(x-\mu(\sin\psi_i+\delta)\right)\right.\right.$$
$$\left(\lambda+(x-xe)\dot{\beta}+\beta\mu\cos\psi_i\right)-\left(x-\mu(\sin\psi_i+\delta)\right)^2\theta^2 \tag{29}$$
$$\left.\left.-\left(\lambda+(x-xe)\dot{\beta}+\beta\mu\cos\psi_i\right)^2\right]-\frac{C_{d0}}{2a}\left(x-\mu(\sin\psi_i+\delta)\right)^2\right\}dr$$

After calculating the integral, we have:

$$\ddot{\delta}+\frac{C\delta}{\Omega I_\beta}\dot{\delta}+\left(\frac{e.m_{si}}{I_\beta}+\frac{K_\delta}{\Omega^2 I_\beta}\right)\delta$$
$$=2\beta\dot{\beta}+\frac{\rho acR^2}{I_\beta}\left[\left(\lambda_0+\mu\beta\cos\psi_i-\frac{e}{R}\dot{\beta}\right)\left[\mu(\sin\psi_i+\delta\cos\psi_i)\theta_{con}\left(-\frac{R^2-e^2}{2}+e(R-e)\right)\right.\right.$$
$$+\left(\mu(\sin\psi_i+\delta\cos\psi_i)\theta_{tw}+\theta_{con}\right)\left(-\frac{R^3-e^3}{3R}+e\frac{R^2-e^2}{2R}\right)+\left(\lambda_{1c}\cos\psi_i+\lambda_{1s}\sin\psi_i+\dot{\beta}\right)$$
$$\left.\left(-\frac{R^3-e^3}{3R}+e\frac{R^2-e^2}{2R}\right)-\theta_{tw}\left(\frac{R^4-e^4}{4R^2}+e\frac{R^3-e^3}{3R^2}\right)\right]\Bigg]+\left(\lambda_{1c}\cos\psi_i+\lambda_{1s}\sin\psi_i+\dot{\beta}\right)$$
$$\left[\mu(\sin\psi_i+\delta\cos\psi_i)\theta_{con}\left(-\frac{R^3-e^3}{3R}+e\frac{R^2-e^2}{2R}\right)+\left(\mu(\sin\psi_i+\delta\cos\psi_i)\theta_{tw}+\theta_{con}\right)\right.$$
$$\left.\left(\frac{R^4-e^4}{4R^2}+e\frac{R^3-e^3}{3R^2}\right)-\theta_{tw}\left(\frac{R^5-e^5}{5R^3}-e\frac{R^4-e^4}{4R^3}\right)\right]+\left[\frac{\theta_{con}{}^2}{2}-\frac{C_{d0}}{2a}\right]\left[\left(\frac{R^4-e^4}{4R^2}-e\frac{R^3-e^3}{3R^2}\right)\right.$$
$$\left.+\mu(\sin\psi_i+\delta\cos\psi_i)\left(\frac{2(R^3-e^3)}{3R}-e\frac{R^2-e^2}{R}\right)+\mu^2(\sin\psi_i+\delta\cos\psi_i)^2\left(\frac{R^2-e^2}{2}-e(R-e)\right)\right]$$
$$+\theta_{tw}\theta_{con}\left[\left(\frac{R^5-e^5}{5R^3}-e\frac{R^4-e^4}{4R^3}\right)+\mu(\sin\psi_i+\delta\cos\psi_i)\left(\frac{R^4-e^4}{2R^2}+e\frac{2(R^3-e^3)}{3R^2}\right)\right.$$
$$\left.+\mu^2(\sin\psi_i+\delta\cos\psi_i)^2\left(\frac{R^3-e^3}{3R}-e\frac{R^2-e^2}{2R}\right)\right]+\frac{\theta_{tw}{}^2}{2}\left[\left(\frac{R^6-e^6}{6R^4}-e\frac{R^5-e^5}{5R^4}\right)\right.$$
$$\left.+\mu(\sin\psi_i+\delta\cos\psi_i)\left(\frac{2(R^5-e^5)}{5R^3}-e\frac{R^4-e^4}{2R^3}\right)+\mu^2(\sin\psi_i+\delta\cos\psi_i)^2\left(\frac{R^4-e^4}{4R^2}-e\frac{R^3-e^3}{3R^2}\right)\right]$$
$$+\left(\lambda_0+\beta\mu\cos\psi_i-\frac{e}{R}\dot{\beta}\right)^2\left(\frac{R^2-e^2}{4}-e\frac{(R-e)}{2}\right)+\frac{1}{2}\left(\lambda_{1c}\cos\psi_i+\lambda_{1s}\sin\psi_i+\dot{\beta}\right)^2$$
$$\left.\left(\frac{R^4-e^4}{4R^2}-e\frac{R^3-e^3}{3R^2}\right)\right]$$

Making the assumptions: $R^2 - e^2 \approx R^2$; $R^3 - e^3 \approx R^3$; $R^4 - e^4 \approx R^4$; $R^5 - e^5 \approx R^5$; $R^6 - e^6 \approx R^6$; $R-2eR+2e^2 \approx R-2eR = R(1-2e)$, leads to:

$$
\begin{aligned}
&\ddot{\delta}+\frac{C\delta}{\Omega I_\beta}\dot{\delta}+\left(\frac{e.m_{si}}{I_\beta}+\frac{K_\delta}{\Omega^2 I_\beta}\right)\delta \\
&=2\beta\dot{\beta}+\frac{\rho acR^2}{I_\beta}\left[\left(\lambda_0+\mu\beta\cos\psi_i-\frac{e}{R}\dot{\beta}\right)\left[\mu\left(\sin\psi_i+\delta\cos\psi_i\right)\theta_{con}\frac{R}{2}\left(R-2e\right)\right.\right. \\
&-\left(\mu\left(\sin\psi_i+\delta\cos\psi_i\right)\theta_{tw}+\theta_{con}\right)\frac{R}{6}\left(2R-3e\right)+\left(\lambda_{1c}\cos\psi_i+\lambda_{1s}\sin\psi_i+\dot{\beta}\right)\frac{R}{6}\left(2R-3e\right) \\
&\left.-\theta_{tw}\frac{R}{12}\left(3R-4e\right)\right]+\left(\lambda_{1c}\cos\psi_i+\lambda_{1s}\sin\psi_i+\dot{\beta}\right)\left[\mu\left(\sin\psi_i+\delta\cos\psi_i\right)\theta_{con}\frac{R}{6}\left(2R-3e\right)\right. \\
&\left.-\left(\mu\left(\sin\psi_i+\delta\cos\psi_i\right)\theta_{tw}+\theta_{con}\right)\frac{R}{12}\left(3R-4e\right)-\theta_{tw}\frac{R}{20}\left(4R-5e\right)\right] \\
&+\left[\frac{\theta_{con}{}^2}{2}-\frac{C_{d0}}{2a}\right]\left[\frac{R}{12}\left(3R-4e\right)+\mu\left(\sin\psi_i+\delta\cos\psi_i\right)\frac{R}{3}\left(2R-3e\right)\right. \\
&\left.+\mu^2\left(\sin\psi_i+\delta\cos\psi_i\right)^2\frac{R}{2}\left(2R-3e\right)\right]+\theta_{tw}\theta_{con}\left[\frac{R}{20}\left(4R-5e\right)+\mu\left(\sin\psi_i+\delta\cos\psi_i\right)\frac{R}{6}\left(3R-4e\right)\right. \\
&\left.+\mu^2\left(\sin\psi_i+\delta\cos\psi_i\right)^2\frac{R}{6}\left(2R-3e\right)\right]+\frac{\theta_{tw}{}^2}{2}\left[\frac{R}{30}\left(5R-6e\right)+\mu\left(\sin\psi_i+\delta\cos\psi_i\right)\frac{R}{10}\left(4R-5e\right)\right. \\
&\left.+\mu^2\left(\sin\psi_i+\delta\cos\psi_i\right)^2\frac{R}{12}\left(3R-4e\right)\right]+\left(\lambda_0+\beta\mu\cos\psi_i-\frac{e}{R}\dot{\beta}\right)^2\frac{R}{2}\left(R-2e\right) \\
&\left.+\frac{1}{2}\left(\lambda_{1c}\cos\psi_i+\lambda_{1s}\sin\psi_i+\dot{\beta}\right)^2\frac{R}{12}\left(3R-4e\right)\right]
\end{aligned}
$$

with

$$
\begin{aligned}
\theta_{con} &= \theta_0 + \theta_{1c}\cos\psi_i + \theta_{1s}\sin\psi_i \\
\beta &= \beta_0 + \beta_{1c}\cos\psi_i + \beta_{1s}\sin\psi_i \\
\dot{\beta} &= -\beta_{1c}\sin\psi_i + \beta_{1s}\cos\psi_i \\
\delta &= \delta_0 + \delta_{1c}\cos\psi_i + \delta_{1s}\sin\psi_i \\
\dot{\delta} &= -\delta_{1c}\sin\psi_i + \delta_{1s}\cos\psi_i \\
\ddot{\delta} &= -\delta_{1c}\cos\psi_i - \delta_{1s}\sin\psi_i
\end{aligned}
\tag{30}
$$

Next, we will disregard the terms, of triple products of angles (eg: $\theta_0\ \beta_{1c}\ \delta_{1s} = 0$, etc.) concerning the double products, since θ, β and δ are small angles.

Applying the operators: $\frac{1}{2\pi}\int_0^{2\pi}(\dots)d\psi$, $\frac{1}{2\pi}\int_0^{2\pi}(\dots)\cos\psi d\psi$ and $\frac{1}{2\pi}\int_0^{2\pi}(\dots)\sin\psi d\psi$ leads to (after some intermediate calculations):

$$
\begin{aligned}
&\left(\frac{e.m_{si}}{I_\beta}+\frac{K\delta}{\Omega^2 I_\beta}\right)\delta_0\\
&=\frac{\rho acR^2}{I_\beta}\Bigg[\frac{R}{2}(R-2e)\Bigg[\lambda_0{}^2-\frac{\mu\theta_0}{2}\frac{e}{R}\beta_{1c}\frac{\mu^2}{2}\left(\frac{\theta_0{}^2}{2}-\frac{C_{d0}}{2a}\right)+\frac{e^2}{2R^2}\left(\beta_{1c}{}^2+\beta_{1s}{}^2\right)+\frac{\mu\theta_{1s}}{2}\lambda_0+\lambda_0\beta_{1c}\mu\\
&+\mu\frac{e}{R}\beta_0\beta_{1s}+\frac{\mu^2}{2}\beta_0{}^2+\frac{\theta_{1c}{}^2\mu^2}{16}+\frac{\mu^2\beta_{1s}{}^2}{8}+\frac{3\theta_{1s}{}^2\mu^2}{16}+\frac{3\mu^2\beta_{1c}{}^2}{8}-\frac{\mu^2}{8}\left(\beta_{1c}\theta_{1s}+\beta_{1s}\theta_{1c}\right)+\frac{R}{6}(2R-3e)\\
&-\lambda_0\theta_0+\frac{e}{R}\frac{\beta_{1c}}{2}\left(-\mu\theta_{tw}-\theta_{1s}+\lambda_{1s}-\beta_{1c}\right)-\frac{\mu\theta_0}{2}\left(\lambda_{1s}-\beta_{1c}\right)+\mu\theta_0\theta_{1s}+\frac{\mu^2}{2}\theta_{tw}\theta_0\\
&+\frac{\mu\beta_0-\frac{e}{R}\beta_{1s}}{2}\left(-\theta_{1c}+\lambda_{1c}+\beta_{1s}\right)-\frac{\mu}{2}\theta_0\beta_{1c}\Bigg]+\frac{R}{12}(3R-4e)\Bigg[-\lambda_0\theta_{tw}+\left(\frac{\theta_0{}^2}{2}-\frac{C_{d0}}{2a}\right)\\
&+\frac{\left(\lambda_{1s}-\beta_{1c}\right)}{2}\left(\mu\theta_{tw}+\theta_{1s}\right)+\frac{\theta_{1s}{}^2}{4}+\mu\theta_{tw}\theta_{1s}+\frac{\mu^2\theta_{tw}{}^2}{4}+\frac{\lambda_{1s}{}^2}{4}-\frac{\lambda_{1s}\beta_{1c}}{2}+\frac{\beta_{1c}{}^2}{4}-\frac{\theta_{1c}}{2}\left(\lambda_{1c}-\beta_{1c}\right)+\frac{\theta_{1c}{}^2}{4}\\
&+\frac{\lambda_{1c}{}^2}{4}+\frac{\lambda_{1c}\beta_{1s}}{2}+\frac{\beta_{1s}{}^2}{4}-\mu\frac{\theta_{tw}}{2}\beta_{1c}\Bigg]+\frac{R}{20}(4R-5e)\theta_{tw}\theta_0+\frac{R}{30}(5R-6e)\frac{\theta_{tw}{}^2}{2}\Bigg]
\end{aligned}
\tag{31}
$$

$$
\begin{aligned}
&\frac{1}{2}\left[-\delta_{1c}+\frac{C_\delta}{\Omega I_\beta}\delta_{1s}+\left(\frac{e.m_{si}}{I_\beta}+\frac{K_\delta}{\Omega^2 I_\beta}\right)\delta_{1c}-2\beta_0\beta_{1s}\right]\\
&=\frac{\rho acR^2}{I_\beta}\Bigg[\frac{R}{2}(R-2e)\Bigg[\mu\lambda_0\beta_0-\frac{e}{R}\lambda_0\beta_{1s}-\frac{\mu\theta_{1c}}{8}\frac{e}{R}\beta_{1c}-\frac{\mu\theta_{1s}}{8}\left(\mu\beta_0-\frac{e}{R}\beta_{1s}\right)+\frac{\mu^2}{8}\theta_0\theta_{1c}\\
&+\frac{\mu}{4}\frac{e}{R}\beta_{1s}\beta_{1c}-\frac{3}{4}\mu\frac{e}{R}\beta_{1c}\beta_{1s}+\frac{3}{4}\mu^2\beta_0\beta_{1c}-\frac{\mu^2}{8}\theta_0\beta_{1s}\Bigg]+\frac{R}{6}(2R-3e)\Bigg[-\frac{\theta_0}{2}\left(\mu\beta_0-\frac{e}{R}\beta_{1s}\right)\\
&+\frac{\lambda_0}{2}\left(-\theta_{1c}+\lambda_{1c}+\beta_{1s}\right)-\frac{\mu\theta_{1c}}{8}\left(\lambda_{1s}-\beta_{1c}\right)-\frac{\mu\theta_{1s}}{8}\left(\lambda_{1c}+\beta_{1s}\right)+\frac{\mu}{4}\theta_{1c}\theta_{1s}+\frac{\mu^2}{8}\theta_{tw}\theta_{1c}\\
&+\frac{3}{4}\mu\beta_{1c}\left(-\theta_{1c}+\lambda_{1c}+\beta_{1s}\right)+\mu\frac{\beta_{1s}}{8}\left(-\mu\theta_{tw}-\theta_{1s}+\lambda_{1s}+\beta_{1c}\right)\Bigg]+\frac{R}{12}(3R-4e)\Bigg[-\frac{\theta_{tw}}{2}\left(\mu\beta_0-\frac{e}{R}\beta_{1s}\right)\\
&-\frac{\theta_0}{2}\left(\lambda_{1c}+\beta_{1s}\right)+\frac{\theta_0\theta_{1c}}{2}\Bigg]+\frac{R}{20}(4R-5e)\Bigg[-\frac{\theta_{tw}}{2}\left(\lambda_{1s}+\beta_{1s}\right)+\frac{\theta_{tw}\theta_{1c}}{2}\Bigg]\Bigg]
\end{aligned}
\tag{32}
$$

$$
\begin{aligned}
&\frac{1}{2}\left[-\delta_{1s}+\frac{C_\delta}{\Omega I_\beta}\delta_{1c}+\left(\frac{e.m_{si}}{I_\beta}+\frac{K_\delta}{\Omega^2 I_\beta}\right)\delta_{1s}-2\beta_0\beta_{1c}\right]\\
&=\frac{\rho acR^2}{I_\beta}\Bigg[\frac{R}{2}(R-2e)\Bigg[\frac{\mu\theta_0}{2}\lambda_0+\frac{e}{R}\lambda_0\beta_{1c}-\frac{3\mu\theta_{1s}}{8}\frac{e}{R}\beta_{1c}-\frac{3\mu^2}{8}\theta_0\theta_{1s}-\frac{\mu^2}{8}\theta_0\beta_{1c}\\
&-\frac{\mu\theta_{1c}}{8}\left(\mu\beta_0-\frac{e}{R}\beta_{1s}\right)+\frac{\mu}{4}\frac{e}{R}\beta_{1c}{}^2-\frac{\mu}{4}\frac{e}{R}\beta_{1s}{}^2+\frac{\mu^2}{4}\beta_0\beta_{1s}\Bigg]+\frac{R}{6}(2R-3e)\Bigg[-\frac{\theta_0}{2}\frac{e}{R}\beta_{1c}\\
&+\frac{\lambda_0}{2}\left(-\mu\theta_{tw}-\theta_{1s}+\lambda_{1s}+\beta_{1c}\right)+\mu\left(\frac{\theta_0{}^2}{2}-\frac{C_{d0}}{2a}\right)-\frac{3\mu\theta_{1s}}{8}\left(\lambda_{1s}-\beta_{1c}\right)+\frac{3\mu\theta_{1s}{}^2}{8}+\frac{3\mu^2\theta_{tw}}{8}\theta_{1s}\\
&-\frac{\mu\theta_{1c}}{8}\left(\lambda_{1c}+\beta_{1s}\right)+\frac{\mu\theta_{1c}{}^2}{8}+\frac{\mu\beta_{1c}}{8}\left(-\mu\theta_{tw}-\theta_{1s}+\lambda_{1s}-\beta_{1c}\right)+\frac{\mu\beta_{1s}}{8}\left(-\theta_{1c}+\lambda_{1c}+\beta_{1s}\right)\Bigg]\\
&+\frac{R}{12}(3R-4e)\Bigg[-\frac{\theta_{tw}}{2}\frac{e}{R}\beta_{1c}-\frac{\theta_0}{2}\left(\lambda_{1s}+\beta_{1c}\right)+\frac{\theta_0\theta_{1s}}{2}+\mu\theta_{tw}\theta_0\Bigg]\\
&+\frac{R}{20}(4R-5e)\Bigg[-\frac{\theta_{tw}}{2}\left(\lambda_{1s}-\beta_{1c}\right)+\frac{\theta_{tw}\theta_{1s}}{2}+\frac{\mu\theta_{tw}{}^2}{2}\Bigg]\Bigg]
\end{aligned}
\tag{33}
$$

There are, therefore, three equations that give us $\delta(\delta_0,\delta_{1c}\text{ e }\delta_{1s})$ a function of the setting of the pitch $\theta(\theta_0,\theta_{1c}\text{ e }\theta_{1s})$ and the flapping $\beta(\beta_0,\beta_{1c}\text{ e }\beta_{1s})$.

Calculation of Fuselage Balance and Pitch Setting for the Isotropic Rotor Case

We will return to the expressions of the wrench of the external forces calculated previously, and then apply them to the case of a rotor composed of N strictly identical blades. In this hypothesis, we can apply the Coleman Transformation to our expressions. Thus, we will obtain a linear formulation: in effect, each component will be written in the form of a linear combination of the flight parameters. Next, let's disregard: (i) the triple products of angles concerning the double products in the expressions of Fx, Fy, Mz; and (ii) the double products of angles about the angles themselves in the expressions of Fz, Mx, My.

Application of the Coleman Transformation

The set of coefficients necessary for the calculations is explained in the reference (Coleman & Feingold, 1957). After some intermediate calculations, the components of the wrench of efforts are then obtained as:

$$\begin{aligned}\frac{\{F_x\}_{rotor}}{NS} &= \frac{R-e}{16}\left[-8\frac{e}{R}\lambda_0\beta_{1c}+\mu\left(\frac{e}{R}\left(-\beta_{1c}{}^2-2\beta_{1s}\theta_{1c}+6\beta_{1c}\theta_{1s}+\beta_{1s}{}^2\right)+8\lambda_0\theta_0\right)\right.\\
&\left.+\mu^2\left(\beta_0\theta_{1c}-6\theta_0\theta_{1s}+\beta_{1c}\theta_0+\frac{C_{d0}}{a}\delta_{1c}\right)\right]+\frac{R}{8}\left[2\frac{e}{R}\beta_{1c}\theta_0+\lambda_0\left(3\beta_{1c}-2\lambda_{1s}+2\theta_{1s}\right)\right.\\
&\left.-\beta_0\beta_{1s}\frac{e}{R}+\theta_{tw}\left(-\theta_{1s}+\lambda_{1s}-\beta_{1c}\right)+\mu\left(2\frac{C_{d0}}{a}-2\theta_0{}^2+\beta_0{}^2-\theta_{tw}{}^2+2\lambda_0\theta_{tw}\right)\right]\\
&+\frac{R}{12}\left[-\beta_0\theta_{1c}+\frac{C_{d0}}{a}\delta_{1c}+2\frac{e}{R}\beta_{1c}\theta_{tw}+\theta_0\left(-3\beta_{1c}-4\mu\theta_{tw}+2\lambda_{1s}-2\theta_{1s}\right)+\beta_0\left(\lambda_{1c}+\beta_{1s}\right)\right]\\
&+\frac{R}{32}\left[-2\beta_{1c}\theta_{tw}+\mu\left(-\beta_{1c}\lambda_{1s}-2\theta_{1c}{}^2+4\beta_{1c}{}^2-\beta_{1s}\lambda_{1c}+6\theta_{1s}\left(\lambda_{1s}-\beta_{1c}\right)-6\theta_{1s}{}^2+2\theta_{1c}\left(\lambda_{1c}-\beta_{1s}\right)\right)\right.\\
&\left.+\mu^2\theta_{tw}\left(\beta_{1c}-6\theta_{1s}\right)\right]+\frac{m_{si}\Omega^2}{S}\frac{\delta_{1s}\delta_0}{2}\end{aligned}$$

$$\begin{aligned}\frac{\{F_y\}_{rotor}}{NS} &= \frac{R-e}{16}\left[-8\frac{e}{R}\lambda_0\beta_{1s}+\mu\left(\frac{e}{R}\left(-2\beta_{1c}\beta_{1s}+2\theta_{1s}\beta_{1s}-2\theta_{1c}\beta_{1c}\right)+12\lambda_0\beta_0\right)\right.\\
&\left.+\mu^2\left(\beta_0\left(5\theta_{1s}+8\beta_{1c}\right)+3\frac{C_{d0}}{a}\delta_{1s}+\theta_0\left(-5\beta_{1s}+2\theta_{1c}\right)\right)\right]+\frac{R}{8}\left[2\frac{e}{R}\beta_{1s}\theta_0+\frac{e}{R}\beta_{1c}\beta_0\right.\\
&\left.+\lambda_0\left(3\beta_{1s}-2\theta_{1c}+2\lambda_{1c}\right)+\theta_{tw}\left(\theta_{1c}-\lambda_{1c}-\beta_{1s}\right)+\mu\left(-4\beta_0\theta_0+\theta_{1c}\theta_{1s}+2\frac{C_{d0}}{a}\delta_0\right)\right]\\
&+\frac{R}{12}\left[\beta_0\left(-\theta_{1s}+\lambda_{1s}-\beta_{1c}\right)+\theta_0\left(2\theta_{1c}-3\beta_{1s}-2\lambda_{1c}\right)+\frac{C_{d0}}{a}\delta_{1s}+2\frac{e}{R}\theta_{tw}\beta_{1s}-4\mu\beta_0\theta_{tw}\right]\\
&+\frac{R}{32}\left[-2\beta_{1s}\theta_{tw}+\mu\left(-10\beta_{1s}\theta_{1s}+4\beta_{1c}\beta_{1s}-6\beta_{1c}\theta_{1s}+7\beta_{1c}\lambda_{1c}+5\beta_{1s}\lambda_{1s}-2\theta_{1s}\lambda_{1c}-2\theta_{1c}\lambda_{1s}\right)\right.\\
&\left.+\mu^2\theta_{tw}\left(5\beta_{1s}+2\theta_{1c}\right)\right]-\frac{m_{si}\Omega^2}{S}\frac{\delta_{1s}\delta_0}{2}\end{aligned}$$

$$\frac{\{F_z\}_{rotor}}{NS}=\frac{1}{2}\left\{\frac{R-e}{2}\mu^2\theta_0+\frac{R}{3}\theta_0+\frac{R}{4}\theta_{tw}-\frac{R-e}{2}\mu\frac{e}{R}\beta_{1c}+\frac{R}{2}\left(\mu\theta_{1s}+\frac{\mu^2}{2}\theta_{tw}-\lambda_0-\frac{\mu}{2}\lambda_{1s}\right)\right\}$$

$$\frac{\{M_x\}_{rotor}}{N.S.e}=\frac{R-e}{4}\left[\frac{\mu^2}{4}\left(3\theta_{1s}-\beta_{1c}\right)-\mu\lambda_0\right]+\frac{R}{4}\left[\mu\theta_0-\frac{e}{R}\frac{\beta_{1c}}{2}\right]+\frac{R}{6}\left[\frac{\theta_{1s}}{2}+\mu\theta_{tw}-\frac{\lambda_{1s}}{2}+\frac{\beta_{1c}}{2}\right]+\frac{m_{si}}{2.S}\Omega^2\beta_{1s}$$

$$\frac{\{M_y\}_{rotor}}{N.S.e} = \frac{1}{2}\left[\frac{R-e}{8}\mu^2(\theta_{1c}-\beta_{1s}) + \frac{R}{4}\left[\mu\beta_0 - \frac{e}{R}\beta_{1s}\right] + \frac{R}{6}(\lambda_{1c}+\beta_{1s}-\theta_{1c})\right] - \frac{m_{si}}{2.S}\Omega^2\beta_{1c}$$

$$\begin{aligned}\frac{\{M_z\}_{rotor}}{N.S.e} = \frac{R-e}{16}\Bigg[&8\lambda_0{}^2 + \frac{4e^2}{R^2}\left(\beta_{1s}{}^2+\beta_{1c}{}^2\right) \\ &+ 8\mu\left(\lambda_0(\beta_{1c}-\theta_{1s}) - \frac{e}{R}(\beta_{1c}\theta_0+\beta_{1s}\beta_0)\right) \\ &+ \mu^2\left(4\theta_0{}^2+\theta_{1c}{}^2+3\theta_{1s}{}^2 - \frac{4C_{d0}}{a} - 2\beta_{1c}\theta_{1s} - \beta_{1s}\theta_{1c} + 4\beta_0{}^2 + 3\beta_{1c}{}^2 + \beta_{1s}{}^2\right)\Bigg] \\ &+ \frac{R}{8}\Bigg[\theta_0(2\theta_{tw}-4\lambda_0) + 2\frac{e}{R}\beta_{1s}(\theta_{1c}-\lambda_{1c}-\beta_{1s}) - \frac{2e}{R}\beta_{1c}(\theta_{1s}-\lambda_{1s}+\beta_{1c}) \\ &+ \mu\left(2\theta_0(2\theta_{1s}-\lambda_{1s}) + 2\beta_0(\lambda_{1c}+\beta_{1s}-\theta_{1c}) - \frac{2e}{R}\beta_{1c}\theta_{tw}\right) + 2\mu^2\theta_{tw}\theta_0\Bigg] \\ &+ \frac{R}{10}\theta_{tw}{}^2 \\ &+ \frac{R}{12}\Bigg[2\theta_0{}^2+\theta_{1c}{}^2+\theta_{1s}{}^2 - 2\frac{C_{d0}}{a} - 4\lambda_0\theta_{tw} - 2\theta_{1c}(\lambda_{1c}+\beta_{1s}) + 2\theta_{1s}(\beta_{1c}-\lambda_{1s}) \\ &+ \lambda_{1c}{}^2+\lambda_{1s}{}^2+\beta_{1s}{}^2+\beta_{1c}{}^2+\lambda_{1c}\beta_{1s} - 2\lambda_{1s}\beta_{1c} + 2\mu\theta_{tw}(2\theta_{1s}-\lambda_{1s}) + \mu^2\theta_{tw}{}^2\Bigg] \\ &+ \left[m_{si}\frac{\Omega^2}{.S} + \frac{K_{i\delta}}{Se}\right]\delta_0\end{aligned}$$

Therefore, the rotor head forces are expressed as a function of the different flight parameters, where: (i) the induced velocity coefficients (λ_0, λ_{1c}, λ_{1s}) are determined by the Drees formulation (Meijer Drees, 1949); (ii) the twist θ_{tw} is given; (iii) the coefficients of the flapping motion (β_0, β_{1c}, β_{1s}) are calculated, using the previously obtained equilibrium equations, as a function of (θ_0, θ_{1c}, θ_{1s}) (and also of other parameters already known or calculated); and (iv) the drag coefficients (δ_0, δ_{1c}, δ_{1s}) are calculated, using previously obtained equilibrium equations, as functions of (θ_0, θ_{1c}, θ_{1s}) and (β_0, β_{1c}, β_{1s}). The six equations for the rotor head efforts are, therefore, functions of just three parameters: (θ_0, θ_{1c}, θ_{1s}).

Fuselage balance equations

The known parameters are the dimensions and the limits (of mass and mass center) of the helicopter (in this study, the AS 332L-Super Puma – elongated version):

- the total mass of the helicopter: M (minimum and maximum mass limits).
- the centering (position of the helicopter's CG, about the rotor head) (forward and rearward limits).
  $X_{CG} = X_{CG} - X_{Rp} = X_{CG} - 4.67\text{m}$ (> 0 for aft CG; < 0 for forward CG);

  Y_{CG} (> 0 to the right; < 0 to the left); $-Z_{CG} = 4p = 2.45\text{m}$
- The air density (ρ).
- The forward flight speed (V) is limited by the V_{ne} of the helicopter.

- The inclination of the main rotor mast of the helicopter ($\alpha_m = 5°$).
  The position of the helicopter tail rotor (relative to the rotor head): $X_{Ra} = 9.4m$; $Y_{Ra} = 0$; $-Z_{Ra} = 4p - 4a = 2.45 - 2.1 = 0.35m$
- The position of the fuselage drag center (A), assumed to be independent of the longitudinal base (angle of attack relative to horizontal axis): (relative to the rotor head). $X_A = 0$; $Y_A = 0$; $-Z_A = 0.1m$
- The C_xS of the fuselage assumed independent of the base of the helicopter: $(C_xS)_f = 2{,}35$ m2
- The position of the center of the horizontal empennage (stabilizer), is assumed independent of the fuselage base: (relative to the rotor head).
  $X_{eh} = 9.4 - 0.1 = 9.3m$;
  $Y_{eh} = -2.113/3 \approx -0.7m$ (assuming the empennage center at 1/3 of its wing span);
  $-Z_{eh} = 2.45 - 2.1 + 0.4 = 0.75m$ (approx. value, taken directly from the figure)
- the negative lift effect of the horizontal tail, assumed equal to $T_{eh} = 1/2\ \rho V^2\ (C_zS)_{eh}$ where $(C_zS)_{eh}$ is assumed constant and equal to: $(C_zS)_{eh} = 0.135\ m^2$ (independent of the helicopter base), which gives us, for V = 280 km/h, a negative lift of $T_{eh} = 500$ N. In the helicopter reference frame, we have:

$$\left(T_{eh}\right)_{Rh} = \begin{cases} 0 \\ 0 \\ -T_{eh} \end{cases}$$

- the anti-torque rotor thrust (T_{AR}) is what is needed to balance the main rotor reaction couple on the fuselage. The T_{AR} value is obtained to give a zero base rotation (ψ_f), that is, no skidding of the fuselage in forward flight. We have, in the helicopter reference frame:

$$\left(T_{Ra}\right)_{Rh} = \begin{cases} 0 \\ -T_{Ra} \\ 0 \end{cases}$$

One has, as unknowns: (i) the rotor head efforts, which are a function of only three parameters: (θ_0, θ_{1c}, θ_{1s}); (ii) The angular inclinations (tilts) of the fuselage: longitudinal (pitch) (α_f), lateral (roll) (γ_f); and (iii) The anti-couple rotor thrust (T_{Ra}) (obtained by assuming the rotation in yaw (ψ_f) is zero). The nose-tail balance (pitch) is illustrated in Figure 12.

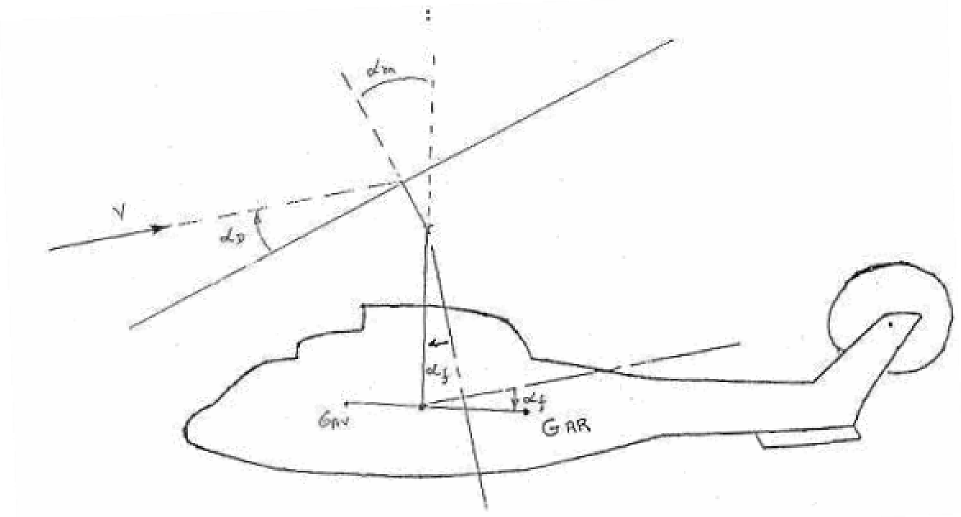

Figure 12: nose-tail balance (pitch) – adapted from (Jorge, 1992)

with: $\alpha_f = \alpha_D - \alpha_m$; rotor plane and CG limits (forward and aft) are indicated in Figure 13.

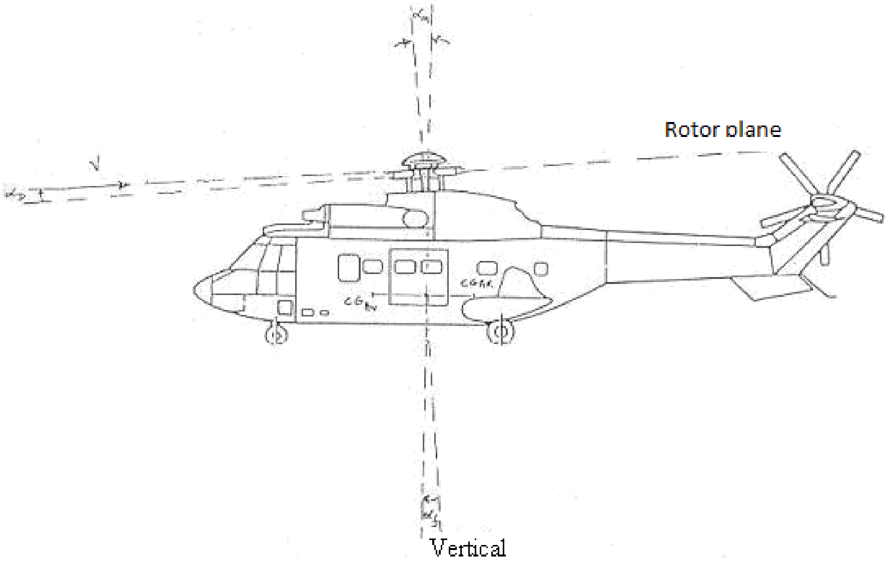

Figure 13: nose-tail balance (pitch): rotor plane; CG limits – adapted from (Jorge, 1992)

The rolling balance (roll) is illustrated in Figure 14, as seen from the front of the helicopter.

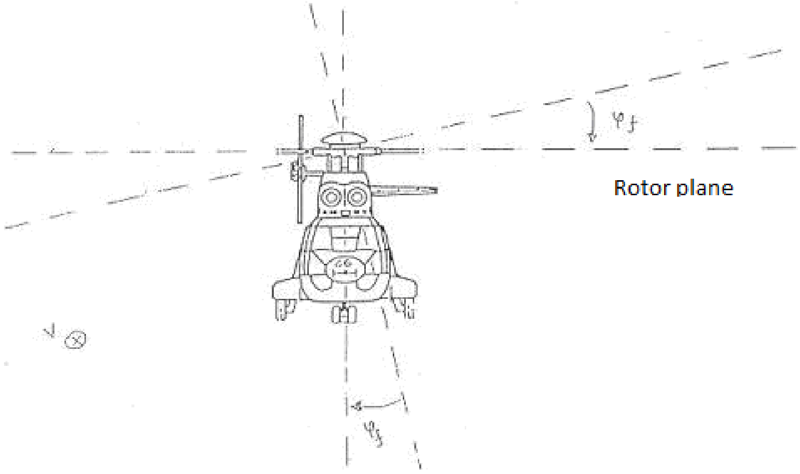

Figure 14: rolling balance (roll): rotor plane (front view) – adapted from (Jorge, 1992)

The rolling balance (roll) is illustrated in Figure 15, as seen from the rear of the helicopter.

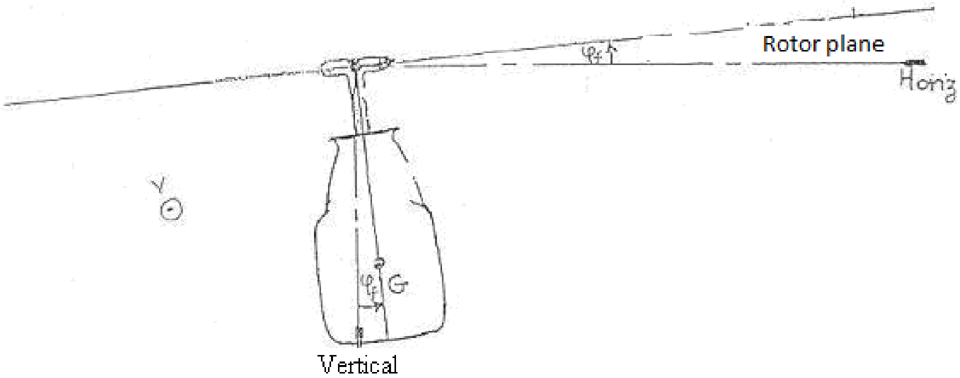

Figure 15: rolling balance (roll): rotor plane (rear view) – adapted from (Jorge, 1992)

The directional balance (yaw) is illustrated in Figure 16.

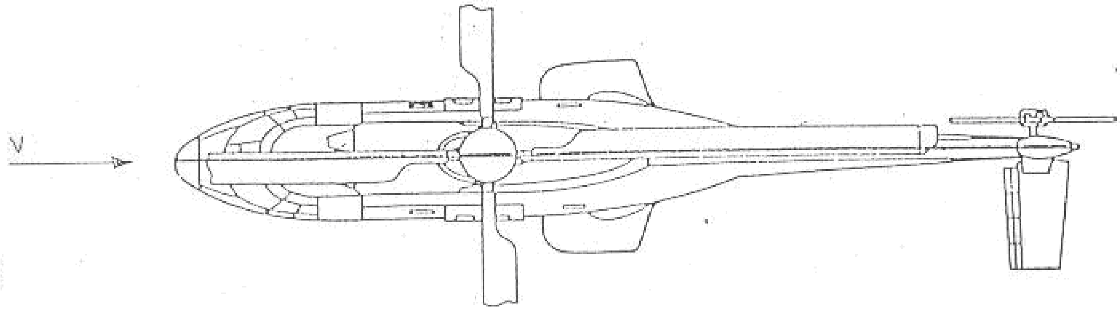

Figure 16: directional balance (yaw) – adapted from (Jorge, 1992)

A rotation of (- α_m) leads from the fixed rotor reference frame to the helicopter frame.

$$\begin{bmatrix} \{F_{x_h}\}_{rotor} \\ \{F_{y_h}\}_{rotor} \\ \{F_{z_h}\}_{rotor} \end{bmatrix}_{R_h} = \begin{bmatrix} \cos\alpha_m & 0 & -\sin\alpha_m \\ 0 & 1 & 0 \\ \sin\alpha_m & 0 & \cos\alpha_m \end{bmatrix} \begin{bmatrix} \{F_x\}_{rotor} \\ \{F_y\}_{rotor} \\ \{F_z\}_{rotor} \end{bmatrix}_{R_h} = \begin{bmatrix} \{F_x\}_{rotor}\cos\alpha_m - \{F_z\}_{rotor}\sin\alpha_m \\ \{F_y\}_{rotor} \\ \{F_x\}_{rotor}\sin\alpha_m + \{F_z\}_{rotor}\cos\alpha_m \end{bmatrix}$$

$$\begin{bmatrix} \{M_{x_h}\}_{rotor} \\ \{M_{y_h}\}_{rotor} \\ \{M_{z_h}\}_{rotor} \end{bmatrix}_{R_h} = \begin{bmatrix} \cos\alpha_m & 0 & -\sin\alpha_m \\ 0 & 1 & 0 \\ \sin\alpha_m & 0 & \cos\alpha_m \end{bmatrix} \begin{bmatrix} \{M_x\}_{rotor} \\ \{M_y\}_{rotor} \\ \{M_z\}_{rotor} \end{bmatrix}_{R_h} = \begin{bmatrix} \{M_x\}_{rotor}\cos\alpha_m - \{M_z\}_{rotor}\sin\alpha_m \\ \{M_y\}_{rotor} \\ \{M_x\}_{rotor}\sin\alpha_m + \{M_z\}_{rotor}\cos\alpha_m \end{bmatrix} \tag{34}$$

The forward speed (and therefore the relative wind (V)) was expressed in the aerodynamic reference frame. We pass from the aerodynamic reference frame to the helicopter frame by a rotation of $\alpha_f = \alpha_D - \alpha_m$:

$$\{\vec{V}\}_{Rh} = \begin{bmatrix} \cos\alpha_f & 0 & \sin\alpha_f \\ 0 & 1 & 0 \\ -\sin\alpha_f & 0 & \cos\alpha_f \end{bmatrix} \begin{bmatrix} V \\ 0 \\ 0 \end{bmatrix}_{Ra} = \begin{bmatrix} V\cos\alpha_f \\ 0 \\ -V\sin\alpha_f \end{bmatrix} \tag{35}$$

In the case considered here (horizontal forward flight, stabilized, with constant speed), the aerodynamic reference frame and the Galilean reference frame are confounded. The helicopter's net weight (Mg) is passed from this Galilean reference frame to the helicopter reference frame by a rotation of (-α_f) around $Y_g = Y_h$, and then a rotation of (-γ_f) around X_h.

$$\{M_{\vec{g}}\}_{Rh} = \begin{bmatrix} \cos\alpha_f & 0 & -\sin\alpha_f \\ 0 & 1 & 0 \\ \sin\alpha_f & 0 & \cos\alpha_f \end{bmatrix} \begin{bmatrix} 0 \\ 0 \\ -M_g \end{bmatrix}_{Rg} = \begin{bmatrix} M_g\sin\alpha_f \\ 0 \\ -M_g\cos\alpha_f \end{bmatrix} \tag{36}$$

$$\{M_{\vec{g}}\}_{Rh} = \begin{bmatrix} 1 & 0 & 0 \\ 0 & \cos\alpha_f & \sin\alpha_f \\ 0 & -\sin\alpha_f & \cos\alpha_f \end{bmatrix} \begin{bmatrix} M_g\sin\alpha_f \\ 0 \\ -M_g\cos\alpha_f \end{bmatrix}_{Rg} = \begin{bmatrix} M_g\sin\alpha_f \\ -M_g\sin\alpha_f\cos\alpha_f \\ -M_g\cos\alpha_f\cos\alpha_f \end{bmatrix} \tag{37}$$

The equilibrium, in the helicopter reference frame, gives us:

$$
\begin{aligned}
&\sum F_{x_h} = 0 \\
&\left\{F_{x_h}\right\}_{rotor} + M_g \sin\alpha_f + \frac{1}{2}\rho\left(C_x S\right)_f V^2 = 0 \\
&\sum F_{y_h} = 0 \\
&\left\{F_{y_h}\right\}_{rotor} + M_g \sin\gamma_f \cos\alpha_f - T_{Ra} = 0 \\
&\sum F_{z_h} = 0 \\
&\left\{F_{z_h}\right\}_{rotor} + M_g \cos\gamma_f \cos\alpha_f + \frac{1}{2}\rho\left(C_z S\right)_{eh} V^2 = 0
\end{aligned}
\tag{38}
$$

Taking the balance of moments around the rotor hub: $\sum \overrightarrow{M_0} = 0$

$$
\begin{bmatrix} M_{x_h} \\ M_{y_h} \\ M_{z_h} \end{bmatrix}_{rotor} + \begin{bmatrix} x_{CG} \\ y_{CG} \\ z_{CG} \end{bmatrix} \Lambda \begin{bmatrix} M_g \sin\alpha_f \\ -M_g \sin\gamma_f \cos\alpha_f \\ -M_g \cos\gamma_f \cos\alpha_f \end{bmatrix} + \begin{bmatrix} x_A \\ y_A \\ z_A \end{bmatrix} \Lambda \begin{bmatrix} \frac{1}{2}\rho\left(C_x S\right)_f V^2 \\ 0 \\ 0 \end{bmatrix}
$$

$$
+ \begin{bmatrix} x_{eh} \\ y_{eh} \\ z_{eh} \end{bmatrix} \Lambda \begin{bmatrix} 0 \\ 0 \\ \frac{1}{2}\rho\left(C_z S\right)_{eh} V^2 \end{bmatrix} + \begin{bmatrix} x_{Ra} \\ y_{Ra} \\ z_{Ra} \end{bmatrix} \Lambda \begin{bmatrix} 0 \\ -T_{Ra} \\ 0 \end{bmatrix} = \begin{bmatrix} 0 \\ 0 \\ 0 \end{bmatrix}
$$

$$
\text{with}: y_{Ra} = x_A = y_A = 0
$$

What gives us:

$$
\begin{aligned}
&\left\{M_{x_h}\right\}_{rotor} + \left[-y_{CG} M_g \cos\varphi_f \cos\alpha_f + z_{CG} M_g \sin\varphi_f \cos\alpha_f\right] - y_{eh}\frac{1}{2}\rho V^2\left(C_z S\right)_{eh} + z_{Ra} T_{Ra} = 0 \\
&\left\{M_{y_h}\right\}_{rotor} + \left[-x_{CG} M_g \cos\varphi_f \cos\alpha_f + z_{CG} M_g \sin\alpha_f\right] - z_A\frac{1}{2}\rho V^2\left(C_x S\right)_f + x_{eh}\frac{1}{2}\rho V^2\left(C_z S\right)_{eh} = 0 \\
&\left\{M_{z_h}\right\}_{rotor} + \left[-x_{CG} M_g \sin\varphi_f \cos\alpha_f + y_{CG} M_g \sin\alpha_f\right] - x_{Ra} T_{Ra} = 0
\end{aligned}
\tag{39}
$$

And we arrive at the six fuselage equilibrium equations:

$$
\begin{aligned}
&\left\{F_x\right\}_{rotor} \cos\alpha_m - \left\{F_z\right\}_{rotor} \sin\alpha_m + M_g \sin\alpha_f + \frac{1}{2}\rho\left(C_x S\right)_f V^2 = 0 \\
&\left\{F_y\right\}_{rotor} - M_g \sin\varphi_f \cos\alpha_f - T_{Ra} = 0 \\
&\left\{F_x\right\}_{rotor} \sin\alpha_m + \left\{F_z\right\}_{rotor} \cos\alpha_m - M_g \cos\varphi_f \cos\alpha_f - \frac{1}{2}\rho V^2\left(C_z S\right)_{eh} = 0 \\
&\left\{M_x\right\}_{rotor} \cos\alpha_m - \left\{M_z\right\}_{rotor} \sin\alpha_m - y_{CG} M_g \cos\varphi_f \cos\alpha_f + z_{CG} M_g \sin\alpha_f \cos\alpha_f \\
&-y_{eh}\frac{1}{2}\rho V^2\left(C_z S\right)_{eh} + z_{Ra} T_{Ra} = 0 \\
&\left\{M_y\right\}_{rotor} + x_{CG} M_g \cos\varphi_f \cos\alpha_f - z_{CG} M_g \sin\alpha_f + z_A\frac{1}{2}\rho\left(C_x S\right)_f V^2 + xeh\frac{1}{2}\rho V^2\left(C_z S\right)_{eh} = 0 \\
&\left\{M_x\right\}_{rotor} \sin\alpha_m + \left\{M_z\right\}_{rotor} \cos\alpha_m - x_{CG} M_g \sin\varphi_f \cos\alpha_f - y_{CG} M_g \sin\alpha_f - x_{Ra} T_{Ra} = 0
\end{aligned}
\tag{40}
$$

The hypothesis of small angles: $\cos\alpha_m \approx \cos\alpha_f \approx \cos\varphi_f \approx 1$; $\sin\alpha_m \approx \alpha_m$; $\sin\alpha_f \approx \alpha_f$; $\sin\varphi_f \approx \varphi_f$ leads to:

$$\begin{gathered}
\{F_x\}_{rotor} - \{F_z\}_{rotor}\alpha_m + M_g\alpha_f + \frac{1}{2}\rho(C_xS)_f V^2 = 0 \\
\{F_y\}_{rotor} - M_g\varphi_f - T_{Ra} = 0 \\
\{F_x\}_{rotor}\alpha_m + \{F_z\}_{rotor} - M_g - \frac{1}{2}\rho V^2(C_zS)_{eh} = 0 \\
\{M_x\}_{rotor} - \{M_z\}_{rotor}\alpha_m - y_{CG}M_g + z_{CG}M_g\varphi_f - y_{eh}\frac{1}{2}\rho V^2(C_zS)_{eh} + z_{Ra}T_{Ra} = 0 \\
\{M_y\}_{rotor} + x_{CG}M_g - z_{CG}M_g\alpha_f + z_A\frac{1}{2}\rho(C_xS)_f V^2 + xeh\frac{1}{2}\rho V^2(C_zS)_{eh} = 0 \\
\{M_x\}_{rotor}\alpha_m + \{M_z\}_{rotor} - x_{CG}M_g\varphi_f - y_{CG}M_g\alpha_f - x_{Ra}T_{Ra} = 0
\end{gathered} \tag{41}$$

With the wrench of the rotor head efforts (in the fixed rotor reference frame) previously obtained, with the rotor incidence equal to $\alpha_0 = \alpha_f + \alpha_m$ and with:

$C_T = \dfrac{\{F_z\}_{rotor}}{\rho A(\Omega R)^2} = \dfrac{\{F_z\}_{rotor}}{NS}.\dfrac{\sigma a}{R}$, where the rotor rigidity is defined as: $\sigma = \dfrac{Nc}{\pi R}$. With the flapping and drag equations, therefore, we have a system of twelve nonlinear equations with twelve unknowns ($\theta_0, \theta_{1c}, \theta_{1s}, \alpha_f, \varphi_f, T_{Ra}, \beta_0, \beta_{1c}, \beta_{1s}, \delta_0, \delta_{1c}, \delta_{1s}$).

3.3 Study of the effect of the introduction of defects in the main rotor

Analysis of Influential Parameters

To calculate the wrench of the forces on the rotor head, in any azimuthal position (ψ_i) (corresponding to a certain time: $t = \psi_i/\Omega$, after passing the blades through the reference position, $\psi_i = 0$, which corresponds to the synchronism signal given by the magnetic sensor in the rotor head), it is necessary and sufficient to know $\lambda(\psi_i), \theta_i(\psi_i), \beta_i(\psi_i), \delta_i(\psi_i)$, the parameters of the blades (R, e, c), and their profile (Cd_0, a), the advance rate μ, the air density (ρ), the mass of the blades (m_i), the static moment of the blades (m_{si}) and the inertia of the blades ($I_{\beta i}$). Analyzing each of the variables:

- A static moment of the blades (m_{si}): $m_{si} = \int_e^R r dm_i = \int_e^R rmdr$, where m is the mass per unit of the linear length of blade *i*. (m_{si} may be different for each blade, because of anisotropies).
- Blade masses (m_i): $m_i = \int_e^R dm_i = \int_e^R mdr$.
- The inertia of the blades ($I_{\beta i}$): $I\beta_i = \int_e^R r^2 dm_i = \int_e^R r^2 mdr$ (m_i and $I_{\beta i}$ may also be different for each blade, due to anisotropies).

The three parameters: m_i, m_{si}, and $I_{\beta i}$ are interdependent. A change in m_i leads to a corresponding change in the values of m_{si} and $I_{\beta i}$. One can distinguish in the rotor:

- rotor hub, or rotor cube, is integral with the rotating mast, which supports the forces from the blades through four spherical joints made of laminated rubber (spherical abutments).
- the flapping part, consisting of a metal sleeve and a composite blade.

The rotor parts are illustrated in Figure 17, for the helicopter in the study

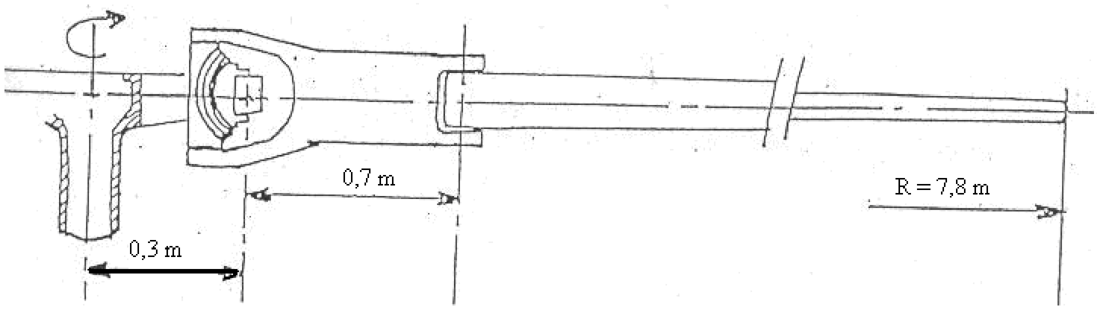

Figure 17: rotor parts: hub, sleeve, and blade – adapted from (Jorge, 1992)

- The balance masses (shot spheres), between 0 and 1 kg, can be inserted at the end of the sleeve, i.e., r = 1.0 m.
- The insertion of an equilibrium mass (Δm_i) leads us to changes in the parameters of blade *i*, from the isotropic values of m_{si} and of $I_{\beta i}$.:
  $m_{\rho i} = m_{\rho\ iso} + \Delta m_i$, where $m_{\rho\ iso} = 88.2$kg
  $m_{s\rho i} = m_{s\rho\ iso} + \Delta m_i(0.7)$, where $m_{s\rho\ iso} = 331.7$kg.m
  $I_{\beta i} = I_{\beta\ iso} + \Delta m_i(0.7)^2$, where $I_{\beta\ iso} = 1675$kg.m^2
- Air density (ρ): depends on pressure altitude and temperature. It is a parameter given, for example, from the standard atmosphere tables.
- Advance ratio (μ): depends on the speed of the helicopter relative to the air (V) and the pitch of the rotor disk (α_D). Note: The longitudinal attitude of the fuselage (α_f) depends on α_D and the tilt of the rotor mast (α_m) so that: $\alpha_f = \alpha_D - \alpha_m$ (α_f is smaller than α_D).
- The parameters of the blades (R, e, c) and their profile (Cd_0, a) can cause anisotropies but, within the scope of this study, they will be considered as constants, independent of the blades. All blade anisotropies will be considered to be "equivalent" anisotropies at the blade adjustment positions. In this way, an anisotropy in m_i (and, consequently, in m_{si} and $I_{\beta i}$) can be considered as an "equivalent" mass change in the radial position where the equilibrium mass can be added (in the Super Puma case, r = 1.0 m, i.e. at the end of the sleeve).
  In the same way, anisotropies to the lift of the profiles can be considered as "equivalent" variations of the blade pitch ($\theta_i(\psi_i)$) which can be changed by regulating the length of the blades' pitch rods, or pitch links (which changes the collective pitch θ_o of blade *i*) and the deflection of the tabs (which gives a moment around the axis $\overrightarrow{X_i}$, introducing efforts on the rods (which will be transmitted to the fuselage) and, at the same time, giving a variation of the blade lift, which is supposed to be proportional to the speed of forward flight (i.e., assuming that the bracketing of the tabs does not affect the taper (conicity) (β_0) of the rotor in stationary flight, that its effect increases with μ and that it is more important on the advancing blade side, and less important on the retreating blade side. Thus, we will be simulating the deflection of tabs as anisotropy in θ_{is}.
  In this way, if $\theta_{is} \neq 0$ (all the other parameters equal to zero) in the flapping motion equations, for stationary flight ($\mu = 0$), one obtains: $\beta_0 = 0$; $\beta_{1c} \approx - \theta_{1s}$; $\beta_{1s} \approx 0$. And for the forward flight, we will have: $\beta_0 =$ constant $\mu - \theta_{1s}$, which shows that there will be an increase in the taper (conicity) (β_0) that will be proportional to θ_{is} and μ, as we want to simulate.
- The induced velocity: depends on the advance rate (μ), the rotor disc inclination (α_D), the lift coefficient (C_T) (which expresses the lift (thrust) of the helicopter (F_z) and considers the air density (ρ)) and the azimuthal position (ψi). We will assume that there is no anisotropy on the induced velocity and, therefore, that λ does not depend on blade *i*.

- The blade pitch: θ_i (ψ_i): It depends on the azimuthal position (ψ_i) and the balance of the helicopter (that is, of the fuselage), exposed to external forces and considered in stationary flight or forward flight with a constant speed. For the balance of the fuselage, one has assumed, as external efforts: (i) rotor head efforts; (ii) the net weight of the helicopter (the mass and the balance, i.e. the position of the fuselage center of gravity); (iii) the drag of the fuselage (assumed as applied a fixed point (A) and as independent of the longitudinal base of the fuselage); (iv) the negative lift effect of the horizontal empennage (assumed to be applied at a fixed point, and independent of the longitudinal attitude (tilt) of the fuselage); (v) the thrust of the anti-torque rotor, necessary to balance the torque applied on the main rotor.

  The calculation of θ_i (ψ_i) is divided into two steps: 1°) assuming that there is no anisotropy on the rotor, we will have the blade pitch (θ_0, θ_{1c}, θ_{is}) from the isotropic rotor equilibrium equations, as seen in the previous section; and 2°) the anisotropies are introduced on a blade (θ_{0i}, θ_{1si}) assuming that the fixation of the other blades will not change.

- The flapping movement β_i (ψ_i): As previously seen, β_i depends on the azimuthal position (ψ_i), the fixation of the pitch θ_i (ψ_i), the induced velocity λ (ψ_i), the air density (ρ), on the blade parameters (R, e, c, a, m_{si}, $I_{\beta i}$), on the advance rate (μ). We will divide the calculation of β_i (ψ_i) into two steps:

  1°) We will assume that there is no anisotropy on the rotor. All blades have the same: mass (m), static moment (m_s), the moment of inertia (I_β), the value of pitch (θ), and the pitch angle is calculated from the balance of the helicopter, as previously seen. We will have an expression of $\beta(\psi_i)$ which is valid for all blades;

  2°) The anisotropies to be studied on the blade (i) are introduced: (i) equilibrium mass on the sleeve (change of m_i, m_{si}, $I_{\beta i}$); (ii) adjustment of the blade control rod (change of θ_i); (iii) deflection of the tab (change of θ_{1si}).
  The flapping of this blade (β_i (ψ_i)) is calculated again, assuming that it will not influence the flapping movements of the other blades.

- The drag motion $\delta i(\psi i)$: We've seen above that δ_i depends on ψ_i, θ_i, λ_i, β_i, the air density (ρ), the advance rate (μ), and the blade parameters (R, e, c, a, m_{si} , $I_{\beta i}$). Like what was done for θ_i and β_i, we will split the calculation into two steps: 1°) assuming that there is no anisotropy on the rotor, the drag (δ_0, δ_{1c}, δ_{1s}) will be obtained from the isotropic rotor equilibrium equations, as seen previously; and 2°) anisotropies are introduced on the blade (*i*) if this blade not influence the dragging motion of the other blades.

Apart from the change in δ due to the already mentioned variations in θ and β, one can also have a variation in the angle δ due to anisotropy in a frequency adapter (either in its stiffness $K_{\delta i}$, or in its damping $C_{\delta i}$). In the case of the isotropic rotor, the rotor head forces are constant (for a certain equilibrium position). These efforts are applied to a fuselage, assumed rigid, in equilibrium, either in stationary flight, or in forward flight at a constant speed, where, consequently, all the fuselage accelerations are null (the linear accelerations of the center of gravity of the fuselage and the angular accelerations around this center of gravity), and the balance, previously calculated as a static equilibrium, gave us the values of the attitudes of the fuselage, longitudinal (α_f), lateral (φ_f) and in rotation (ψ_f), which are all constant.

The introduction of anisotropies and the calculation of the new angles θ, β, and δ leads us to new rotor head forces, which will no longer be constant but will be functions of ψ_i, that is, they will be forces at the frequency 1Ω (one-per-revolution of the rotor). Assuming the fuselage attitudes are constant functions plus the functions in 1Ω. The constant part of these attitudes is the one previously calculated, which is assumed to be unchanged after the introduction of anisotropies on the rotor. This means that the introduction of anisotropy will not change the stationary attitudes of the fuselage but will introduce variations of these attitudes around the equilibrium position and that these variations will be functions of 1Ω, which will lead us to accelerations of the fuselage which will also be functions of the 1Ω frequency.

Incorporation of defects into the formulation

Introduction

The wrench of the rotor head efforts, and the flight parameters (θ, β, δ, α_f, ψ_f, T_{Ra}) are calculated, for an isotropic rotor. With the application of the Coleman Transformation (Coleman & Feingold, 1957), the rotor head efforts, as well as the flight parameters, are constant concerning time.

When a defect is introduced, the rotor head efforts will be functions of ψ_i (and therefore functions of time, since $t = \psi_i/\Omega$), which will be introduced in the fuselage balance equations which, at this moment, will no longer be homogeneous (right-hand term equal to zero), as previously calculated, since there will be accelerations transmitted to the fuselage, due to the variable efforts in the rotor head. Whenever a defect is introduced on a blade, the flapping (β) and drag (δ) of the other blades are assumed to be unchanged, and we will recalculate, for a blade (i), the flapping (β_{0i}, β_{1ci}, β_{1si}) and the drag (δ_{0i}, δ_{1ci}, δ_{1si}) with the correspondent previously derived equations, since the defect to be introduced is known a priori: (i) Mass defects: change in m_i, m_{si} and $I_{\beta i}$; (ii) Rod defects: change in θ_{0i}; (iii) Tab defects: change in θ_{1si}.

We will assume that the introduction of defects does not lead to average attitude changes of the fuselage and, therefore, that the accelerations that we will have on the fuselage will not have constant terms, but only terms in 1Ω. In this way, for the center of gravity of the fuselage, we will have the accelerations:

$$
\begin{aligned}
\ddot{x}_{t.t} &= \Omega^2 \ddot{x} = \Omega^2 \left(-x_{ic}\cos\psi - x_{is}\sin\psi\right) \\
\ddot{y}_{t.t} &= \Omega^2 \ddot{y} = \Omega^2 \left(-y_{ic}\cos\psi - y_{is}\sin\psi\right) \\
\ddot{z}_{t.t} &= \Omega^2 \ddot{z} = \Omega^2 \left(-z_{ic}\cos\psi - z_{is}\sin\psi\right) \\
\ddot{\alpha}_{f_{t.t}} &= \Omega^2 \ddot{\alpha}_f = \Omega^2 \left(-\alpha_{f_{1c}}\cos\psi - \alpha_{f_{1s}}\sin\psi\right) \qquad (\text{pitch}) \\
\ddot{\varphi}_{f_{t.t}} &= \Omega^2 \ddot{\varphi}_f = \Omega^2 \left(-\varphi_{f_{1c}}\cos\psi - \varphi_{f_{1s}}\sin\psi\right) \qquad (\text{row}) \\
\ddot{\psi}_{f_{t.t}} &= \Omega^2 \ddot{\psi}_f = \Omega^2 \left(-\psi_{f_{1c}}\cos\psi - \psi_{f_{1s}}\sin\psi\right) \qquad (\text{yaw})
\end{aligned}
\tag{42}
$$

Efforts on the rotor head after the introduction of defects

The efforts on the rotor head will have, after the introduction of the defects, a constant component (the one previously calculated, with the isotropic rotor equilibrium) plus the cyclic components, that is, in 1Ω. Therefore, we will have:

$$\begin{aligned}
\left\{F_x\right\}_{rotor} &= \left\{F_{x_0}\right\}_{rotor} + \left\{F_{x_{1c}}\right\}_{rotor}\cos\psi + \left\{F_{x_{1s}}\right\}_{rotor}\sin\psi \\
\left\{F_y\right\}_{rotor} &= \left\{F_{y_0}\right\}_{rotor} + \left\{F_{y_{1c}}\right\}_{rotor}\cos\psi + \left\{F_{y_{1s}}\right\}_{rotor}\sin\psi \\
\left\{F_z\right\}_{rotor} &= \left\{F_{z_0}\right\}_{rotor} + \left\{F_{z_{1c}}\right\}_{rotor}\cos\psi + \left\{F_{z_{1s}}\right\}_{rotor}\sin\psi \\
\left\{M_x\right\}_{rotor} &= \left\{M_{x_0}\right\}_{rotor} + \left\{M_{x_{1c}}\right\}_{rotor}\cos\psi + \left\{M_{x_{1s}}\right\}_{rotor}\sin\psi \\
\left\{M_y\right\}_{rotor} &= \left\{M_{y_0}\right\}_{rotor} + \left\{M_{y_{1c}}\right\}_{rotor}\cos\psi + \left\{M_{y_{1s}}\right\}_{rotor}\sin\psi \\
\left\{M_z\right\}_{rotor} &= \left\{M_{z_0}\right\}_{rotor} + \left\{M_{z_{1c}}\right\}_{rotor}\cos\psi + \left\{M_{z_{1s}}\right\}_{rotor}\sin\psi
\end{aligned} \tag{43}$$

where the index "0" indicates the constant efforts, calculated assuming the isotropic rotor. These efforts are obtained from a sum, according to the number of blades, of the efforts due to each blade, as previously derived. For blade *i*, the new angles of pitch (θ_i), flapping (β_i), and drag (δ_i), were calculated as previously derived. The rotor head forces, for blade *i*, will be the ones due to these new angles, by using the previously derived expressions for forces and moments, knowing that these efforts and their resultant have cyclic components in $\sin\psi$ and $\cos\psi$, in addition to the constant component.

To make the components, in $\sin\psi$ and $\cos\psi$, for blade *i*, appear explicitly, we will apply to the expression of efforts the operators: $\frac{1}{2\pi}\int_0^{2\pi}(\ldots)\sin\psi d\psi$ and $\frac{1}{2\pi}\int_0^{2\pi}(\ldots)\cos\psi d\psi$, which leads to the twelve expressions below, where the index "*i*" of the angles (pitch, flapping, and drag) was suppressed for simplicity of the notation.

$$\begin{aligned}
\frac{F_{x_{1si}}}{2S} = {} & \frac{R-e}{32}\left[-8\lambda_0{}^2 - 2\frac{e^2}{R^2}\beta_{1s}{}^2 - 6\frac{e^2}{R^2}\beta_{1c}{}^2 + \mu\left(2\lambda_0\beta_{1c} + 12\lambda_0\theta_{1s} - 6\frac{e}{R}\beta_{1s}\beta_0 + 12\frac{e}{R}\beta_{1c}\theta_0 - 4\lambda_0\beta_{1c}\right)\right. \\
& \left. + \mu^2\left(\beta_{1c}\theta_{1s} + \beta_{1s}\theta_{1c} - 6\theta_0{}^2 + 6\frac{Cd_0}{a} - \theta_{1c}{}^2 - 5\theta_{1s}{}^2\right)\right] \\
& + \frac{R}{8}\left[-\theta_{tw}\theta_0 + 2\lambda_0\theta_0 + \lambda_{1s}\theta_{1s} - \beta_{1c}\theta_{1s} + \beta_{1c}\lambda_{1s} + \mu\left(-3\theta_0\theta_{1s} - 2\theta_{tw}\theta_{1s} + \theta_{tw}\lambda_{1s} - \theta_{tw}\beta_{1c}\right)\right] \\
& + \frac{R}{48}\left[-\beta_{1c}\theta_{1s} + \beta_{1s}\theta_{1c} - 4\theta_0{}^2 - 4\frac{Cd_0}{a} - \theta_{1c}{}^2 + 8\lambda_0\theta_{tw} - \beta_{1s}\lambda_{1c} + 2\theta_{1c}\lambda_{1c} + \lambda_{1s}\beta_{1c} - \beta_{1c}{}^2 - \lambda_{1c}{}^2\right] \\
& + \frac{R}{32} - \left[2\theta_{1s}{}^2 - \frac{e}{R}\beta_{1s}\left(-\beta_{1s} + 2\theta_{1c} - 2\lambda_{1c}\right) + \frac{e}{R}\beta_{1c}\left(7\beta_{1c} + 6\theta_{1s} - 6\lambda_{1s}\right) - 2\lambda_{1s}{}^2 - 2\beta_{1c}{}^2\right. \\
& \left. + \mu\left(2\frac{Cd0}{a}\delta_{1c} - \lambda_{1c}\beta_0 + 6\frac{e}{R}\beta_{1c}\theta_{tw} + \beta_{1s}\beta_0 + 6\lambda_{1s}\theta_0 - 6\beta_{1c}\theta_0\right) + \mu^2\left(-6\theta_{tw}\theta_0 - 2\theta_{tw}{}^2\right)\right] \\
& + \frac{R}{20}\left(-\theta_{tw}{}^2\right) + \frac{m_{si}\Omega^2}{8S}\left[-\beta_{1c}\beta_{1s} - 4\delta_0\right]
\end{aligned} \tag{44}$$

$$\begin{aligned}
\frac{F_{x_{1ci}}}{2S} &= \frac{R-e}{32}\left[4\frac{e^2}{R^2}\beta_{1s}\beta_{1c}+\mu\left(-2\lambda_0\beta_{1s}+4\lambda_0\theta_{1c}-4\frac{e}{R}\beta_{1s}\theta_0-2\frac{e}{R}\beta_{1c}\beta_0\right)\right.\\
&\left.+\mu^2\left(2\beta_0\theta_0+\beta_{1c}\theta_{1c}+\beta_{1s}\theta_{1s}+2\frac{Cd_0}{a}\delta_0-2\theta_{1c}\theta_{1s}\right)\right]\\
&+\frac{R}{32}\left[4\lambda_0\beta_0-2\beta_{1c}\theta_{1c}-2\theta_{tw}\beta_0-\frac{e}{R}\beta_{1s}\left(6\beta_{1c}+2\theta_{1s}-2\lambda_{1s}\right)+\frac{e}{R}\beta_{1c}\left(2\theta_{1c}-2\lambda_{1c}\right)+2\beta_{1c}\lambda_{1c}\right.\\
&\left.+2\beta_{1c}\beta_{1s}+\mu\left(-2\frac{e}{R}\beta_{1s}\theta_{tw}+2\frac{Cd_0}{a}\delta_{1s}-4\theta_0\theta_{1c}+7\beta_0\beta_{1c}-\beta_0\lambda_{1s}+2\theta_0\lambda_{1c}+2\theta_0\beta_{1s}\right)+\mu^2\theta_{tw}\beta_0\right]\\
&+\frac{R}{48}\left[-4\beta_0\theta_0+\beta_{1s}\theta_{1s}+4\frac{Cd_0}{a}\delta_0-2\theta_{1c}\theta_{1s}+2\lambda_{1c}\theta_{1s}-\beta_{1s}\lambda_{1s}+\beta_{1c}\beta_{1s}+2\theta_{1c}\lambda_{1s}-2\theta_{1c}\beta_{1c}-2\lambda_{1c}\lambda_{1s}\right.\\
&\left.+2\lambda_{1c}\beta_{1c}+\mu\left(-4\theta_{tw}\theta_{1c}+2\theta_{tw}\lambda_{1c}+2\theta_{tw}\beta_{1s}\right)\right]+\frac{m_i e\Omega^2}{2S}+\frac{m_{si}\Omega^2}{2S}\left[1-\frac{\beta_0{}^2}{2}-\frac{3}{8}\beta_{1c}{}^2-\frac{\beta_{1s}{}^2}{8}\right]
\end{aligned} \tag{45}$$

$$\begin{aligned}
\frac{F_{y_{1si}}}{2S} &= \frac{R-e}{32}\left[-4\frac{e^2}{R^2}\beta_{1s}\beta_{1c}+\mu\left(10\lambda_0\beta_{1s}-4\lambda_0\theta_{1c}+4\frac{e}{R}\beta_{1s}\theta_0+10\frac{e}{R}\beta_{1c}\beta_0\right)\right.\\
&\left.+\mu^2\left(-10\beta_0\theta_0-3\beta_{1c}\theta_{1c}-7\beta_{1s}\theta_{1s}+6\frac{Cd_0}{a}\delta_0+2\theta_{1c}\theta_{1s}+4\beta_{1c}\beta_{1s}\right)\right]\\
&+\frac{R}{32}\left[4\lambda_0\beta_0-2\beta_{1s}\theta_{1s}-2\theta_{tw}\beta_0-\frac{e}{R}\beta_{1s}\left(-6\beta_{1c}-2\theta_{1s}+2\lambda_{1s}\right)-\beta_{1s}\beta_{1c}+\frac{e}{R}\beta_{1c}\left(-2\theta_{1c}+2\lambda_{1c}\right)\right.\\
&+2\beta_{1s}\lambda_{1s}+\mu\left(-2\beta_{1s}\theta_0+2\mu\frac{e}{R}\beta_{1s}\theta_{tw}-8\beta_0\theta_{1s}-8\beta_{1s}\theta_0+6\frac{Cd_0}{a}\delta_{1s}+4\theta_0\theta_{1c}-3\beta_0\beta_{1c}+5\beta_0\lambda_{1s}\right.\\
&\left.\left.-22\theta_0\lambda_{1c}-4\theta_{tw}\beta_{1s}\right)-5\mu^2\beta_0\theta_{tw}\right]\\
&+\frac{R}{48}\left[-4\beta_0\theta_0+\beta_{1c}\theta_{1c}+4\frac{Cd_0}{a}\delta_0+2\theta_{1c}\theta_{1s}-\beta_{1c}\lambda_{1c}-\beta_{1c}\beta_{1s}-2\theta_{1s}\lambda_{1c}-2\theta_{1s}\beta_{1s}-2\theta_{1c}\lambda_{1s}+2\lambda_{1c}\lambda_{1s}\right.\\
&\left.+2\lambda_{1s}\beta_{1s}+\mu\left(4\theta_{tw}\theta_{1c}-4\beta_{1s}\theta_{tw}-2\lambda_{1c}\theta_{tw}\right)\right]+\frac{m_i e\Omega^2}{2S}+\frac{m_{si}\Omega^2}{2S}\left[1-\frac{\beta_0{}^2}{2}-\frac{\beta_{1c}{}^2}{8}-\frac{3}{8}\beta_{1s}{}^2\right]
\end{aligned} \tag{46}$$

$$\begin{aligned}
\frac{F_{y_{1ci}}}{2S} &= \frac{R-e}{32}\left[8\lambda_0{}^2+6\frac{e^2}{R^2}\beta_{1s}{}^2+2\frac{e^2}{R^2}\beta_{1c}{}^2+\mu\left(2\lambda_0\beta_{1c}-4\lambda_0\theta_{1s}-14\frac{e}{R}\beta_{1s}\beta_0-4\frac{e}{R}\beta_{1c}\theta_0+12\lambda_0\beta_{1c}\right)\right.\\
&\left.+\mu^2\left(-3\beta_{1c}\theta_{1s}-3\beta_{1s}\theta_{1c}+2\theta_0{}^2-2\frac{Cd_0}{a}+\theta_{1c}{}^2+\theta_{1s}{}^2+8\beta_0{}^2+6\beta_{1c}{}^2+2\beta_{1s}{}^2\right)\right]\\
&+\frac{R}{32}\left[4\theta_{tw}\theta_0-8\lambda_0\theta_0-4\theta_{1c}\lambda_{1c}-4\theta_{1c}\beta_{1s}+2\theta_{1c}{}^2-\frac{e}{R}\beta_{1s}\left(7\beta_{1s}-6\theta_{1c}+6\lambda_{1c}\right)\right.\\
&+\frac{e}{R}\beta_{1c}\left(-\beta_{1c}-2\theta_{1s}+2\lambda_{1s}\right)+2\lambda_{1c}{}^2+2\beta_{1s}{}^2+4\lambda_{1c}\beta_{1s}+\mu\left(-4\beta_{1c}\theta_{tw}-8\beta_0\theta_{1c}-6\beta_{1c}\theta_0\right.\\
&\left.\left.+2\frac{Cd_0}{a}\delta_{1c}+4\theta_0\theta_{1s}+9\beta_0\beta_{1s}+7\beta_0\lambda_{1c}-2\frac{e}{R}\beta_{1c}\theta_{tw}-2\theta_0\lambda_{1s}\right)+2\mu^2\theta_{tw}\theta_0\right]\\
&+\frac{R}{48}\left[\beta_{1c}\theta_{1s}-\beta_{1s}\theta_{1c}+4\theta_0{}^2-4\frac{Cd_0}{a}+\theta_{1s}{}^2-8\lambda_0\theta_{tw}+\beta_{1s}\lambda_{1c}+\beta_{1s}{}^2-\lambda_{1s}\beta_{1c}-2\theta_{1s}\lambda_{1s}+\lambda_{1s}{}^2\right.\\
&\left.+\mu\left(4\theta_{tw}\theta_{1s}-2\lambda_{1s}\theta_{tw}\right)+\mu^2\theta_{tw}{}^2\right]++\frac{R}{20}\theta_{tw}{}^2+\frac{m_{si}\Omega^2}{8S}\left[-\beta_{1c}\beta_{1s}-4\delta_0\right]
\end{aligned} \tag{47}$$

$$\frac{F_{z_{1si}}}{S} = \frac{R-e}{8}\left[3\mu^2\theta_{1s} - 4\mu\lambda_0 - \mu^2\beta_{1c}\right] + \frac{R}{6}\left[\theta_{1s} + 2\mu\theta_{tw} - \lambda_{1s} + \beta_{1c}\right] + \frac{R}{4}\left[2\mu\theta_0 - \frac{e}{R}\beta_{1c}\right] + \frac{m_{si}}{S}\Omega^2\beta_{1s} \tag{48}$$

$$\frac{F_{z_{1ci}}}{S} = \frac{R-e}{8}\left[\mu^2\theta_{1c} - \mu^2\beta_{1s}\right] + \frac{R}{6}\left[\theta_{1c} - \lambda_{1c} - \beta_{1s}\right] + \frac{R}{4}\left[-\mu\beta_0 + \frac{e}{R}\beta_{1s}\right] + \frac{m_{si}}{S}\Omega^2\beta_{1c} \tag{49}$$

$$M_{x_{1si}} = Se\left\{\frac{R-e}{8}\left[3\mu^2\theta_0 - 3\mu\frac{e}{R}\beta_{1c}\right] + \frac{R}{6}\theta_0 + \frac{R}{16}\left[6\mu\theta_{1s} + 2\theta_{tw} + 3\mu^2\theta_{tw} - 4\lambda_0 + 2\mu\beta_{1c} - 3\mu\lambda_{1s}\right]\right\} \tag{50}$$

$$M_{x_{1ci}} = Se\left\{\frac{R-e}{8}\left[-\mu^2\beta_0 + \mu\frac{e}{R}\beta_{1s}\right] + \frac{R}{16}\left[2\mu\theta_{1c} - 2\mu\beta_{1s} - 3\mu\lambda_{1c}\right]\right\} \tag{51}$$

$$M_{y_{1si}} = -Se\left\{\frac{R-e}{8}\left[-\mu^2\beta_0 - \mu\frac{e}{R}\beta_{1s}\right] + \frac{R}{16}\left[2\mu\theta_{1c} - 2\mu\beta_{1s} - \mu\lambda_{1c}\right]\right\} \tag{52}$$

$$M_{y_{1ci}} = -Se\left\{\frac{R-e}{8}\left[\mu^2\theta_0 - \mu\frac{e}{R}\beta_{1c}\right] + \frac{R}{6}\theta_0 + \frac{R}{16}\left[2\mu\theta_{1s} + 2\theta_{tw} + \mu^2\theta_{tw} - 4\lambda_0 + 2\mu\beta_{1c} - \mu\lambda_{1s}\right]\right\} \tag{53}$$

$$\begin{aligned}
\frac{M_{z_{1si}}}{2} = Se\Bigg\{&\frac{R-e}{16}\Bigg[8\frac{e}{R}\lambda_0\beta_{1c} + \mu\left(-8\lambda_0\theta_0 + 2\frac{e}{R}\theta_{1c}\beta_{1s} - 6\frac{e}{R}\beta_{1c}\theta_{1s} + 2\frac{e}{R}\beta_{1c}{}^2 - 2\frac{e}{R}\beta_{1s}{}^2\right) \\
&+\mu^2\left(6\theta_0\theta_{1s} - 2\theta_{1c}\beta_0 - 2\beta_{1c}\theta_0 + 2\beta_0\beta_{1s}\right)\lambda_{1s}\Bigg] + \frac{R}{12}\left[2\theta_0\theta_{1s} - 2\frac{e}{R}\beta_{1c}\theta_{tw} - 2\theta_0\left(\lambda_{1s} - \beta_{1c}\right) + 4\mu\theta_{tw}\theta_0\right] \\
&+\frac{R}{16}\Bigg[2\theta_{tw}\theta_{1s} - 4\lambda_0\left(\theta_{1s} - \lambda_{1s} + \beta_{1c}\right) - 4\frac{e}{R}\beta_{1c}\theta_0 - 2\theta_{tw}\left(\lambda_{1s} - \beta_{1c}\right) + \mu\Bigg(4\theta_0{}^2 - 4\frac{Cd_0}{a} + \theta_{1c}{}^2 + 3\theta_{1s}{}^2 \\
&-4\lambda_0\theta_{tw} - \beta_{1c}\left(-2\theta_{1s} - \lambda_{1s} + \beta_{1c}\right) - \beta_{1s}\left(2\theta_{1c} - \lambda_{1c} - \beta_{1s}\right) - \theta_{1c}\lambda_{1c} - 3\theta_{1s}\lambda_{1s} + 2\theta_{tw}{}^2\Bigg) \\
&+\mu^2\left(3\theta_{tw}\theta_{1s} - \beta_{1c}\theta_{tw}\right)\Bigg]\Bigg\} + m_{si}e\Omega^2\left[-\beta_{1c}\beta_0 - \delta_{1c}\delta_0 + \delta_{1s}\right] + K_{i\delta}\frac{\delta_{1s}}{2} - C_{i\delta}\frac{\delta_{1c}}{2}\Omega
\end{aligned} \tag{54}$$

$$\begin{aligned}
\frac{M_{z1ci}}{2} = Se\Bigg\{&\frac{R-e}{16}\Bigg[-8\frac{e}{R}\lambda_0\beta_{1s} + \mu\left(2\frac{e}{R}\theta_{1s}\beta_{1s} - 2\frac{e}{R}\beta_{1c}\theta_{1c} + 8\lambda_0\beta_0 - 4\frac{e}{R}\beta_{1c}\beta_{1s}\right) \\
&+\mu^2\left(2\theta_0\theta_{1c} - 2\theta_{1s}\beta_0 - 2\beta_{1s}\theta_0 + 6\beta_0\beta_{1c}\right)\Bigg] \\
&+\frac{R}{12}\left[2\theta_0\theta_{1c} + 2\frac{e}{R}\theta_{tw}\beta_{1s} - 2\theta_0\left(\lambda_{1c} + \beta_{1s}\right) - 2\mu\theta_{tw}\beta_0\right] \\
&+\frac{R}{16}\Bigg[2\theta_{tw}\theta_{1c} - 4\lambda_0\left(\theta_{1c} - \lambda_{1c} - \beta_{1s}\right) + 4\frac{e}{R}\theta_0\beta_{1s} - 2\theta_{tw}\left(\lambda_{1c} + \beta_{1s}\right) + \mu\big(2\theta_{1c}\theta_{1s} - 4\theta_0\beta_0 + 3\beta_{1c}\lambda_{1c} \\
&+2\beta_{1c}\beta_{1s} - 2\beta_{1s}\theta_{1s} + \beta_{1s}\lambda_{1s} - \theta_{1s}\lambda_{1c} - \theta_{1c}\lambda_{1s} - 2\theta_{1c}\beta_{1c}\big) + \mu^2\left(\theta_{tw}\theta_{1c} - \beta_{1s}\theta_{tw}\right)\Bigg]\Bigg\} \\
&+m_{si}e\Omega^2\left[\beta_{1s}\beta_0 + \delta_{1s}\delta_0 + \delta_{1c}\right] + K_{i\delta}\frac{\delta_{1c}}{2} + C_{i\delta}\frac{\delta_{1s}}{2}\Omega
\end{aligned} \tag{55}$$

In order to apply the sum according to the number of blades, as previously derived, for the case of this study (rotor with N = 4 blades), we will have: $\varphi_1 = \varphi$ (yellow blade); $\varphi_2 = \varphi + \pi/2$ (blue blade); $\varphi_3 = \varphi + \pi$ (black blade); $\varphi_4 = \varphi + 3\pi/2$ (red blade), what gives:

$$
\begin{aligned}
Fx_1 &= Fx_{01} + Fx_{1c1}\cos\varphi + Fx_{1s1}\sin\varphi \\
Fx_2 &= Fx_{02} + Fx_{1c2}\cos(\varphi+\pi/2) + Fx_{1s2}\sin(\varphi+\pi/2) \\
&= Fx_{02} + Fx_{1s2}\cos\varphi - Fx_{1c2}\sin\varphi \\
Fx_3 &= Fx_{03} + Fx_{1c3}\cos(\varphi+\pi) + Fx_{1s3}\sin(\varphi+\pi) \\
&= Fx_{03} - Fx_{1c3}\cos\varphi - Fx_{1s3}\sin\varphi \\
Fx_4 &= Fx_{04} + Fx_{1c4}\cos(\varphi+3\pi/2) + Fx_{1s4}\sin(\varphi+3\pi/2) \\
&= Fx_{04} - Fx_{1s4}\cos\varphi + Fx_{1c4}\sin\varphi
\end{aligned}
$$

Finally, we will have:

$$
\begin{aligned}
\{Fx_{1c}\}_{rotor} &= Fx_{1c1} + Fx_{1s2} - Fx_{1c3} - Fx_{1s4} \\
\{Fx_{1s}\}_{rotor} &= Fx_{1s1} - Fx_{1c2} - Fx_{1s3} - Fx_{1c4}
\end{aligned}
$$

Likewise, for the other components we will have:

$$
\begin{aligned}
\{Fy_{1c}\}_{rotor} &= Fy_{1c1} + Fy_{1s2} - Fy_{1c3} - Fy_{1s4} \\
\{Fy_{1s}\}_{rotor} &= Fy_{1s1} - Fy_{1c2} - Fy_{1s3} + Fy_{1c4}
\end{aligned}
$$

$$
\begin{aligned}
\{Fz_{1c}\}_{rotor} &= Fz_{1c1} + Fz_{1s2} - Fz_{1c3} - Fz_{1s4} \\
\{Fz_{1s}\}_{rotor} &= Fz_{1s1} - Fz_{1c2} - Fz_{1s3} + Fz_{1c4}
\end{aligned}
$$

$$
\begin{aligned}
\{Mx_{1c}\}_{rotor} &= Mx_{1c1} + \mathrm{M}x_{1s2} - Mx_{1c3} - Mx_{1s4} \\
\{Mx_{1s}\}_{rotor} &= Mx_{1s1} - Mx_{1c2} - Mx_{1s3} - Mx_{1c4}
\end{aligned}
$$

$$
\begin{aligned}
\{My_{1c}\}_{rotor} &= My_{1c1} + \mathrm{M}y_{1s2} - My_{1c3} - My_{1s4} \\
\{My_{1s}\}_{rotor} &= My_{1s1} - My_{1c2} - My_{1s3} + My_{1c4}
\end{aligned}
$$

$$
\begin{aligned}
\{Mz_{1c}\}_{rotor} &= Mz_{1c1} + \mathrm{M}z_{1s2} - Mz_{1c3} - Mz_{1s4} \\
\{Mz_{1s}\}_{rotor} &= FMz_{1s1} - Mz_{1c2} - Mz_{1s3} + Mz_{1c4}
\end{aligned}
$$

Fuselage balance after the introduction of rotor defects

The fuselage balance equations are homogeneous. The balance of external forces gives:

$$
\begin{aligned}
&\{Fx\}_{rotor} - \{Fz\}_{rotor}\,\alpha_m + Mg\alpha_f + 1/2\rho(Cx\ S)_f V^2 = M\,\ddot{x}_{t,t} \\
&\{Fy\}_{rotor} - Mg\ \varphi_f - T_{Ra} = M\,\ddot{y}_{t,t} \qquad (56) \\
&\alpha_m\ \{Fx\}_{rotor} + \{Fz\}_{rotor} - Mg - 1/2\rho V^2 (Cz\ S)_{eh} = M\,\ddot{z}_{t,t}
\end{aligned}
$$

The equations of moments were previously obtained for the equilibrium concerning the rotor head. As we are interested in the movement of the center of gravity of the aircraft, these equations must be rewritten to consider the wrench of the external forces, no longer at the rotor head, but at the center of gravity. In addition, we will need the fuselage moments of inertia about the center of gravity, whose position changes as a function of mass centering: moments of inertia in roll (I_{xx}), pitch (I_{yy}), and yaw (I_{zz}), as well as the inertia product representing the yaw-roll coupling (I_{zx}). The other couplings are assumed to be null. From the moments and products of inertia $I=m\rho^2$, we have the radii of gyration. From the data of an aircraft with mass M and with moments and products of inertia, the radii of gyration will only be a function of the centering. For a helicopter with M = 9,500 kg (AS 332 MK II), the data is presented in Table 1.

Table 1: Data for the helicopter of the study case – adapted from (Jorge, 1992)

	AV centering X_{CG} = 4.48 m	**Zero centering X_{CG} = 4.67 m**	**AR Center X_{CG} = 4.95 m**
I_{xx} (m^2kg)	16 104	14 707	12 650
I_{yy} (m^2kg)	61 163	61 104	61 017
I_{zz} (m^2kg)	54 101	52 684	50 596
I_{zx} (m^2kg)	3 880	2 914	1 491
ρ_{xx} (m)	1.30	1.24	1.15
ρ_{yy} (m)	2.54	2.54	2.53
ρ_{zz} (m)	2.39	2.35	2.31
ρ_{xz} (m)	0.64	0.55	0.40

The inertias for zero centering were interpolated from the given inertias AV (forward) and AR (aft). The radii of gyration for any longitudinal centering can be interpolated from Table 1. The equilibrium of moments about the center of gravity is written as:

$$\begin{bmatrix} Mx_h \\ My_h \\ Mz_h \end{bmatrix}_{rotor} + \begin{bmatrix} -x_{CG} \\ -y_{CG} \\ -z_{CG} \end{bmatrix} \Lambda \begin{bmatrix} Fx_h \\ Fy_h \\ Fz_h \end{bmatrix}_{rotor} + \begin{bmatrix} x_A - x_{CG} \\ y_A - y_{CG} \\ z_A - z_{CG} \end{bmatrix} \Lambda \begin{bmatrix} 1/2\,\rho (CxS)_f V^2 \\ 0 \\ 0 \end{bmatrix}$$

$$+ \begin{bmatrix} x_{eh} - x_{CG} \\ y_{eh} - y_{CG} \\ z_{eh} - z_{CG} \end{bmatrix} \Lambda \begin{bmatrix} 0 \\ 0 \\ -1/2\,\rho (CzS)_{eh} V^2 \end{bmatrix} + \begin{bmatrix} x_{Ra} - x_{CG} \\ y_{Ra} - y_{CG} \\ z_{Ra} - z_{CG} \end{bmatrix} \Lambda \begin{bmatrix} 0 \\ -T_{Ra} \\ 0 \end{bmatrix} =$$

$$= \begin{bmatrix} \rho_{xx}{}^2 & 0 & \rho_{xz}{}^2 \\ 0 & \rho_{yy}{}^2 & 0 \\ \rho_{xz}{}^2 & 0 & \rho_{zz}{}^2 \end{bmatrix} \begin{bmatrix} \ddot{\varphi}\, f_{t.t} \\ \ddot{\alpha}\, f_{t.t} \\ \ddot{\psi}\, f_{t.t} \end{bmatrix} = M \begin{bmatrix} \rho_{xx}{}^2 \ddot{\varphi}\, f_{t.t} + \rho_{xz}{}^2 \ddot{\psi}\, f_{t.t} \\ \rho_{yy}{}^2 \ddot{\alpha}\, f_{t.t} \\ \rho_{xz}{}^2 \ddot{\varphi}\, f_{t.t} + \rho_{zz}{}^2 \ddot{\psi}\, f_{t.t} \end{bmatrix}$$

with $y_{Ra} = x_A = y_A = 0$. Thus, Equation (57) is obtained as:

$$\begin{gathered} \{Mx_h\}_{rotor} - y_{CG}\{Fz_h\}_{rotor} + z_{CG}\{Fy_h\}_{rotor} - (y_{eh} - y_{CG})\frac{1}{2}\rho V^2 (CzS)_{eh} + (z_{Ra} - z_{CG})T_{Ra} \\ = M\left(\rho_{xx}{}^2 \ddot{\varphi}\, f_{t.t} + \rho_{xz}{}^2 \ddot{\psi}\, f_{t.t}\right) \\ \{My_h\}_{rotor} - x_{CG}\{Fz_h\}_{rotor} - z_{CG}\{Fx_h\}_{rotor} + (z_A - z_{CG})\frac{1}{2}\rho V^2 (CxS)_f + (x_{eh} - x_{CG})\frac{1}{2}\rho V^2 (CzS)_{eh} \\ = M\rho_{yy}{}^2 \ddot{\alpha}\, f_{t.t} \end{gathered} \tag{57}$$

$$\left\{Mz_h\right\}_{rotor} - x_{CG}\left\{Fy_h\right\}_{rotor} - y_{CG}\left\{Fx_h\right\}_{rotor} - y_{CG}\frac{1}{2}\rho V^2\left(CxS\right)_f - \left(x_{Ra} - x_{CG}\right)T_{Ra}$$
$$= M\left(\rho_{xz}{}^2\ddot{\varphi}\, f_{t.t} + \rho_{zz}{}^2\ddot{\psi}\, f_{t.t}\right)$$

And finally, Equation (58) is obtained as:

$$\left\{Mx_h\right\}_{rotor} - \left\{Mz_h\right\}_{rotor}\alpha_m - y_{CG}\left(\left\{Fx\right\}_{rotor}\alpha_m + \left\{Fz\right\}_{rotor}\right) + z_{CG}\left\{Fy_h\right\}_{rotor}$$
$$-\left(y_{eh} - y_{CG}\right)\frac{1}{2}\rho V^2\left(CzS\right)_{eh} + \left(z_{Ra} - z_{CG}\right)T_{Ra} = M\left(\rho_{xx}{}^2\ddot{\varphi}\, f_{t.t} + \rho_{xz}{}^2\ddot{\psi}\, f_{t.t}\right)$$

$$\left\{My\right\}_{rotor} + x_{CG}\left(\left\{Fx\right\}_{rotor}\alpha_m + \left\{Fz\right\}_{rotor}\right) - z_{CG}\left(\left\{Fx\right\}_{rotor} - \left\{Fz\right\}_{rotor}\alpha_m\right) + \left(z_A - z_{CG}\right)\frac{1}{2}\rho V^2\left(CxS\right)_f$$
$$+\left(x_{eh} - x_{CG}\right)\frac{1}{2}\rho V^2\left(CzS\right)_{eh} = M\rho_{yy}{}^2\ddot{\alpha}\, f_{t.t} \tag{58}$$

$$\left\{Mx\right\}_{rotor}\alpha_m + \left\{Mz\right\}_{rotor} - x_{CG}\left\{Fy\right\}_{rotor} + y_{CG}\left(\left\{Fx\right\}_{rotor} - \left\{Fz\right\}_{rotor}\alpha_m\right) - y_{CG}\frac{1}{2}\rho V^2\left(CxS\right)_f$$
$$-\left(x_{Ra} - x_{CG}\right)T_{Ra} = M\left(\rho_{xz}{}^2\ddot{\varphi}\, f_{t.t} + \rho_{zz}{}^2\ddot{\psi}\, f_{t.t}\right)$$

with :
ρ_{xx}: radius of gyration of the fuselage concerning the X_h axis (roll)
ρ_{yy}: radius of gyration of the fuselage about the Y_h axis (pitch)
ρ_{zz}: radius of gyration of the fuselage to the Z_h axis (yaw)

$$\alpha_f = \alpha_{f0} + \alpha f_{1c}\cos\psi + \alpha f_{1s}\sin\psi$$

And with: $\varphi_f = \varphi_{f0} + \varphi f_{1c}\cos\psi + \varphi f_{1s}\sin\psi$

$$T_{Ra} = T_{Ra0} + T_{Ra1c}\cos\psi + T_{Ra1s}\sin\psi$$

where α_{f0}, φ_{f0}, and T_{Ra0} were previously obtained from the fuselage equilibrium with the isotropic rotor and T_{Ra1c}, T_{Ra1s} are the components of the tail rotor thrust needed to make the ψ_{f1c} and ψ_{f1s} components of the rotational motion null. Since ψ_{f1c} and ψ_{f1s} are assumed not to be zero in the calculation of $\ddot{\psi}_{ft,t}$, then $TRa_{1c} = TRa_{1s} = 0$ (therefore it is assumed that the tail rotor does not provide the cyclic thrust that could cancel the cyclic motion in yaw). To find the twelve unknowns of the fuselage accelerations: $-\Omega^2\left(x_{1c}, x_{1s}, y_{1c}, y_{1s}, z_{1c}, z_{1s}, \alpha f_{1c}, \alpha f_{1s}, \varphi f_{1c}, \varphi f_{1s}, \psi f_{1c}, \psi f_{1s}\right)$, we will apply, to the equilibrium equations, the operators: $\frac{1}{2\pi}\int_0^{2\pi}(...)\sin\psi d\psi$ and $\frac{1}{2\pi}\int_0^{2\pi}(...)\cos\psi d\psi$.

The rotor head efforts, after intermediate calculations, lead to Equations (59) to (70):

$$\frac{\left[Fx_{1s}\right]_{rotor}}{2} - \frac{\left[Fz_{1s}\right]_{rotor}}{2}.\alpha_m + Mg\frac{\alpha f_{1s}}{2} = -M\Omega^2\frac{x_{1s}}{2} \tag{59}$$

$$\frac{\left[Fx_{1c}\right]_{rotor}}{2} - \frac{\left[Fz_{1c}\right]_{rotor}}{2}.\alpha_m + Mg\frac{\alpha f_{1c}}{2} = -M\Omega^2\frac{x_{1c}}{2} \tag{60}$$

$$\frac{\left[Fy_{1s}\right]_{rotor}}{2} - Mg\frac{\varphi f_{1s}}{2} = -M\Omega^2\frac{y_{1s}}{2} \tag{61}$$

$$\frac{\left[Fy_{1c}\right]_{rotor}}{2} - Mg\frac{\varphi f_{1c}}{2} = -M\Omega^2\frac{y_{1c}}{2} \tag{62}$$

$$\frac{\left[Fx_{1s}\right]_{rotor}}{2}.\alpha_m - \frac{\left[Fz_{1s}\right]_{rotor}}{2} = -M\Omega^2\frac{z_{1s}}{2} \tag{63}$$

$$\frac{\left[Fx_{1c}\right]_{rotor}}{2}.\alpha_m - \frac{\left[Fz_{1c}\right]_{rotor}}{2} = -M\Omega^2\frac{z_{1c}}{2} \tag{64}$$

$$\begin{aligned}&\frac{\left[Mx_{1s}\right]_{rotor}}{2} - \alpha_m\frac{\left[Mz_{1s}\right]_{rotor}}{2} - y_{cg}\alpha_m\frac{\left[Fx_{1s}\right]_{rotor}}{2} - y_{cg}\frac{\left[Fz_{1s}\right]_{rotor}}{2} + z_{cg}\frac{\left[Fy_{1s}\right]_{rotor}}{2} = \\ &= -M\Omega^2\left(\rho_{xx}{}^2\frac{\varphi f_{1s}}{2} + \rho_{xz}{}^2\frac{\varphi f_{1c}}{2}\right)\end{aligned} \tag{65}$$

$$\begin{aligned}&\frac{\left[Mx_{1c}\right]_{rotor}}{2} - \alpha_m\frac{\left[Mz_{1c}\right]_{rotor}}{2} - y_{cg}\alpha_m\frac{\left[Fx_{1c}\right]_{rotor}}{2} - y_{cg}\frac{\left[Fz_{1c}\right]_{rotor}}{2} + z_{cg}\frac{\left[Fy_{1c}\right]_{rotor}}{2} = \\ &= -M\Omega^2\left(\rho_{xx}{}^2\frac{\varphi f_{1c}}{2} + \rho_{xz}{}^2\frac{\varphi f_{1c}}{2}\right)\end{aligned} \tag{66}$$

$$\frac{\left[My_{1s}\right]_{rotor}}{2} + \left(x_{cg}\alpha_m - z_{cg}\right)\frac{\left[Fx_{1s}\right]_{rotor}}{2} + \left(x_{cg} + z_{cg}\alpha_m\right)\frac{\left[Fz_{1s}\right]_{rotor}}{2} = -M\Omega^2\rho_{yy}{}^2\frac{\varphi f_{1s}}{2} \tag{67}$$

$$\frac{\left[My_{1c}\right]_{rotor}}{2} + \left(x_{cg}\alpha_m - z_{cg}\right)\frac{\left[Fx_{1c}\right]_{rotor}}{2} + \left(x_{cg} + z_{cg}\alpha_m\right)\frac{\left[Fz_{1c}\right]_{rotor}}{2} = -M\Omega^2\rho_{yy}{}^2\frac{\varphi f_{1c}}{2} \tag{68}$$

$$\begin{aligned}&\alpha_m\frac{\left[Mx_{1s}\right]_{rotor}}{2} + \frac{\left[Mz_{1s}\right]_{rotor}}{2} - x_{cg}\frac{\left[Fy_{1s}\right]_{rotor}}{2} + y_{cg}\frac{\left[Fx_{1s}\right]_{rotor}}{2} - y_{cg}\alpha_m\frac{\left[Fz_{1s}\right]_{rotor}}{2} \\ &= -M\Omega^2\left(\rho_{xz}{}^2\frac{\varphi f_{1s}}{2} + \rho_{zz}{}^2\frac{\varphi f_{1s}}{2}\right)\end{aligned} \tag{69}$$

$$\begin{aligned}&\alpha_m\frac{\left[Mx_{1c}\right]_{rotor}}{2} + \frac{\left[Mz_{1c}\right]_{rotor}}{2} - x_{cg}\frac{\left[Fy_{1c}\right]_{rotor}}{2} + y_{cg}\frac{\left[Fx_{1c}\right]_{rotor}}{2} - y_{cg}\alpha_m\frac{\left[Fz_{1c}\right]_{rotor}}{2} \\ &= -M\Omega^2\left(\rho_{xz}{}^2\frac{\varphi f_{1c}}{2} + \rho_{zz}{}^2\frac{\varphi f_{1c}}{2}\right)\end{aligned} \tag{70}$$

Passing the accelerations from the fuselage C.G. to the given measurement points

Fuselage helicopter vibration is measured through accelerometers, installed at given measurement points. The position vector of point (M) of the fuselage (assumed rigid) concerning its CG (G) is written in the Galilean reference frame, parallel to the aerodynamic frame, after rotation ($-\psi_f$, $-\alpha_f$, $-\varphi_f$) from the helicopter reference frame R_h.

$$\overrightarrow{GM} = \begin{bmatrix}\cos\psi_f & \sin\psi_f & 0\\ -\sin\psi_f & \cos\psi_f & 0\\ 0 & 0 & 1\end{bmatrix}\begin{bmatrix}\cos\alpha_f & 0 & -\sin\alpha_f\\ 0 & 1 & 0\\ \sin\alpha_f & 0 & \cos\alpha_f\end{bmatrix}\begin{bmatrix}1 & 0 & 0\\ 0 & \cos\varphi_f & \sin\alpha_f\\ 0 & -\sin\alpha_f & \cos\alpha_f\end{bmatrix}\begin{bmatrix}X_M - X_G\\ Y_M - Y_G\\ Z_M - Z_G\end{bmatrix} \tag{71}$$

with: X, Y, Z the coordinates of the points in the frame R_h.

The vector position is:

$$\overrightarrow{GM}=\begin{bmatrix} (X_M-X_G)\cos\psi_f\cos\alpha_f+(Y_M-Y_G)\left(\cos\psi_f\sin\alpha_f\sin\phi_f+\sin\psi_f\cos\phi_f\right) \\ +(Z_M-Z_G)\left(-\cos\psi_f\sin\alpha_f\cos\phi_f+\sin\psi_f\sin\phi_f\right) \\ \\ (X_M-X_G)\left(-\sin\psi_f\cos\alpha_f\right)+(Y_M-Y_G)\left(-\sin\psi_f\sin\alpha_f\sin\phi_f+\cos\psi_f\cos\phi_f\right) \\ +(Z_M-Z_G)\left(\sin\psi_f\sin\alpha_f\cos\phi_f+\cos\psi_f\sin\phi_f\right) \\ \\ (X_M-X_G)\sin\alpha_f+(Y_M-Y_G)\left(-\cos\alpha_f\sin\phi_f\right)+(Z_M-Z_G)\left(\cos\alpha_f\cos\phi_f\right) \end{bmatrix}$$

The first derivative of the vector position is written as:

$$\frac{d\overrightarrow{GM}}{dt}=\begin{bmatrix} (X_M-X_G)\left(-\sin\psi_f\cos\alpha_f\,\dot{\psi}_{ft}-\cos\psi_f\sin\alpha_f\,\dot{\alpha}_{ft}\right) \\ +(Y_M-Y_G)\left(-\sin\psi_f\sin\alpha_f\sin\phi_f\,\dot{\psi}_{ft}+\cos\psi_f\cos\alpha_f\sin\phi_f\,\dot{\alpha}_{ft}+\cos\psi_f\sin\alpha_f\cos\phi_f\,\dot{\phi}_{ft}\right. \\ \left.+\cos\psi_f\cos\phi_f\,\dot{\psi}_{ft}-\sin\psi_f\sin\phi_f\,\dot{\phi}_{ft}\right) \\ +(Z_M-Z_G)\left(\sin\psi_f\sin\alpha_f\cos\phi_f\,\dot{\psi}_{ft}-\cos\psi_f\cos\alpha_f\cos\phi_f\,\dot{\alpha}_{ft}+\cos\psi_f\sin\alpha_f\sin\phi_f\,\dot{\phi}_{ft}\right. \\ \left.+\cos\psi_f\sin\phi_f\,\dot{\psi}_{ft}+\sin\psi_f\cos\phi_f\,\dot{\phi}_{ft}\right) \\ \\ (X_M-X_G)\left(-\cos\psi_f\cos\alpha_f\,\dot{\psi}_{ft}+\sin\psi_f\sin\alpha_f\,\dot{\psi}_{ft}\dot{\alpha}_{ft}\right) \\ +(Y_M-Y_G)\left(-\cos\psi_f\sin\alpha_f\sin\phi_f\,\dot{\psi}_{ft}-\sin\psi_f\cos\alpha_f\sin\phi_f\,\dot{\alpha}_{ft}-\sin\psi_f\sin\alpha_f\cos\phi_f\,\dot{\phi}_{ft}\right. \\ \left.-\sin\psi_f\cos\phi_f\,\dot{\psi}_{ft}-\cos\psi_f\sin\phi_f\,\dot{\phi}_{ft}\right) \\ +(Z_M-Z_G)\left(\cos\psi_f\sin\alpha_f\cos\phi_f\,\dot{\psi}_{ft}+\sin\psi_f\cos\alpha_f\cos\phi_f\,\dot{\alpha}_{ft}-\sin\psi_f\sin\alpha_f\sin\phi_f\,\dot{\phi}_{ft}\right. \\ \left.-\sin\psi_f\sin\phi_f\,\dot{\psi}_{ft}+\cos\psi_f\cos\phi_f\,\dot{\phi}_{ft}\right) \\ \\ (X_M-X_G)\cos\alpha_f\,\dot{\alpha}_{ft}+(Y_M-Y_G)\left(\sin\alpha_f\sin\phi_f\,\dot{\alpha}_{ft}-\cos\alpha_f\cos\phi_f\,\dot{\phi}_{ft}\right) \\ +(Z_M-Z_G)\left(-\sin\alpha_f\cos\phi_f\,\dot{\alpha}_{ft}-\cos\alpha_f\sin\phi_f\,\dot{\phi}_{ft}\right) \end{bmatrix}$$

The second derivative of the vector position is evaluated in R_g. The acceleration of M is:

$$\frac{d^2}{dt^2}\overrightarrow{GM}=\frac{d^2}{dt^2}\overrightarrow{G'G}+\frac{d^2}{dt^2}\overrightarrow{GM} \tag{72}$$

Point G' in Galileo's frame coincides with G at this instant. The acceleration of the CG is:

$$\left.\frac{d^2}{dt^2}\overrightarrow{G'G}\right]_{Rh}=\begin{bmatrix} \ddot{x}_{t.t} \\ \ddot{y}_{t.t} \\ \ddot{z}_{t.t} \end{bmatrix} \tag{73}$$

Thus, in the helicopter reference frame:

$$\left.\frac{d^2}{dt^2}\overrightarrow{GM}\right]_{Rh}=\begin{bmatrix} 1 & 0 & 0 \\ 0 & \cos\varphi_f & -\sin\varphi_f \\ 0 & \sin\varphi_f & \cos\varphi_f \end{bmatrix}\begin{bmatrix} \cos\varphi_f & 0 & \sin\varphi_f \\ 0 & 1 & 0 \\ \sin\varphi_f & 0 & \cos\varphi_f \end{bmatrix}\begin{bmatrix} \cos\varphi_f & -\sin\varphi_f & 0 \\ \sin\varphi_f & \cos\varphi_f & 0 \\ 0 & 0 & 1 \end{bmatrix}\left.\frac{d^2}{dt^2}\overrightarrow{GM}\right]_{Rg}$$

$$\left.\frac{d^2}{dt^2}\overrightarrow{GM}\right]_{Rh}=\left[\begin{array}{l}
(X_M-X_G)\left(\dot\alpha_{ft}^{\,2}-\cos\alpha_f\,\dot\psi_{ft}^{\,2}\right)\\
+(Y_M-Y_G)\left(2\cos\phi_f\,\dot\alpha_{ft}\dot\phi_{ft}+\sin\phi_f\,\ddot\alpha_{ft}+\cos^2\alpha_f\,\ddot\psi_{ft}-\cos\alpha_f\sin\alpha_f\sin\phi_f\,\dot\phi_{ft}^{\,2}\right.\\
\left.-2\cos\alpha_f\sin\alpha_f\,\dot\psi_{ft}\dot\phi_{ft}\right)\\
+(Z_M-Z_G)\left(2\sin\phi_f\,\dot\alpha_{ft}\dot\phi_{ft}-\cos\phi_f\,\ddot\alpha_{ft}+2\cos^2\alpha_f\,\dot\psi_{ft}\dot\phi_{ft}+\cos\alpha_f\sin\alpha_f\,\ddot\psi_{ft}\right.\\
\left.+\cos\alpha_f\sin\alpha_f\cos\phi_f\,\dot\phi_{ft}^{\,2}\right)\\
\\
(X_M-X_G)(\quad\left(2\cos\phi_f\sin\alpha_f\,\dot\psi_{ft}\dot\alpha_{ft}-\cos\phi_f\cos\alpha_f\,\ddot\psi_{ft}-\sin\phi_f\cos\alpha_f\sin\alpha_f\,\dot\psi^2{}_{ft}\right.\\
\left.-\sin\phi_f\,\ddot\alpha_{ft}\right)+(Y_M-Y_G)\left(-\dot\phi_{ft}^{\,2}-2\cos^2\phi_f\sin\alpha_f\,\dot\psi_{ft}\dot\phi_{ft}-\cos^2\phi_f\,\dot\psi_{ft}^{\,2}-sen^2\phi_f\dot\alpha_{ft}^{\,2}\right.\\
\left.-sen^2\alpha_f sen^2\phi_f\dot\psi_{ft}^{\,2}-2\sin\phi_f\,sen^2\alpha_f\dot\psi_{ft}\dot\phi_{ft}-2\cos\alpha_f\cos\phi_f\sin\phi_f\,\dot\psi_{ft}\dot\alpha_{ft}\right)\\
+(Z_M-Z_G)\left(2\cos^2\phi_f\cos\alpha_{ff}\,\dot\psi_{ft}\dot\alpha_{ft}+\cos^2\phi_f\sin\alpha_f\,\ddot\psi_{ft}+\ddot\phi_{ft}\right.\\
-2\cos\phi_f\sin\phi_f\sin\alpha_f\,\dot\psi_{ft}\dot\phi_{ft}-\cos\phi_f\sin\phi_f\,\dot\alpha_{ft}\dot\psi_{ft}^{\,2}+2\sin\phi_f\sin\alpha_f\cos\alpha_f\,\dot\phi_{ft}\dot\psi_{ft}\\
\left.+\sin\phi_f\cos\phi_f\,\dot\alpha_{ft}^{\,2}+\sin\phi_f\sin^2\alpha_f\,\ddot\psi_{ft}+\sin^2\alpha_f\sin\phi_f\cos\phi_f\,\dot\psi_{ft}^{\,2}\right)\\
\\
(X_M-X_G)\left(2\sin\phi_f\sin\alpha_f\,\dot\psi_{ft}\dot\alpha_{ft}-\sin\phi_f\cos\alpha_f\,\ddot\psi_{ft}+\cos\phi_f\cos\alpha_f\sin\alpha_f\,\dot\psi_{ft}^{\,2}\right.\\
\left.+\cos\phi_f\,\ddot\alpha_{ft}\right)+(Y_M-Y_G)\left(-2\sin\alpha_f\sin\phi_f\cos\phi_f\,\dot\phi_{ft}\dot\psi_{ft}-\sin\phi_f\cos\phi_f\,\dot\psi_{ft}^{\,2}\right.\\
+\sin\phi_f\cos\phi_f\,\dot\alpha_{ft}^{\,2}+\sin^2\alpha_f\cos\phi_f\sin\phi_f\,\dot\psi_{ft}^{\,2}+2\cos\phi_f\sin^2\alpha_f\,\dot\psi_{ft}\dot\phi_{ft}\\
\left.-\sin\alpha_f\,\ddot\psi_{ft}+\ddot\phi_{ft}-2\cos\alpha_f\sin^2\phi_f\,\dot\psi_{ft}\dot\alpha_{ft}\right)+(Z_M-Z_G)\left(2\cos\alpha_f\sin\phi_f\cos\phi_f\,\dot\psi_{ft}\dot\alpha_{ft}\right.\\
+\sin\phi_f\cos\phi_f\sin\alpha_f\,\ddot\psi_{ft}-\dot\phi_{ft}^{\,2}+2\sin\alpha_f\sin^2\phi_f\,\dot\psi_{ft}\dot\phi_{ft}-\sin^2\phi_f\,\dot\phi_{ft}^{\,2}\\
\left.-2\cos\phi_f\sin\alpha_f\cos\alpha_f\,\ddot\psi_{ft}\dot\phi_{ft}-\cos^2\phi_f\,\dot\alpha_{ft}^{\,2}-\cos\phi_f\sin^2\alpha_f\,\ddot\psi_{ft}-\sin^2\alpha_f\cos^2\phi_f\,\dot\psi_{ft}^{\,2}\right)
\end{array}\right. \tag{74}$$

Assuming angles: sinφr ≈ φ_f; $\sin\alpha_f \approx \alpha_f$; $\sin\psi_f \approx \psi_f$; $\cos\varphi_f \approx 1$; $\cos\alpha_f \approx 1$; $\cos\psi_f \approx 1$, and disregarding triple products concerning the double products leads to:

$$\left.\frac{d^2}{dt^2}\overrightarrow{GM}\right]_{Rh}=\left[\begin{array}{l}
(X_M-X_G)\left(-\dot\alpha_{ft}^{\,2}-\dot\psi_{ft}^{\,2}\right)+(Y_M-Y_G)\left(2\dot\alpha_{ft}\dot\varphi_{ft}+\varphi_f\ddot\alpha_{ft}+\ddot\psi_{ft}\right)\\
+(Z_M-Z_G)\left(-\ddot\alpha_{ft}+2\dot\psi_{ft}\dot\varphi_{ft}+\alpha_f\ddot\psi_{ft}\right)\\
\\
(X_M-X_G)\left(-\ddot\psi_{ft}-\varphi_f\ddot\alpha_{ft}\right)+(Y_M-Y_G)\left(-\dot\varphi_{ft}^{\,2}-\dot\psi_{ft}^{\,2}\right)\\
+(Z_M-Z_G)\left(2\dot\psi_{ft}\dot\alpha_{ft}+\alpha_f\ddot\psi_{ft}+\ddot\varphi_{ft}\right)\\
\\
(X_M-X_G)\left(-\varphi_f\ddot\psi_{ft}+\ddot\alpha_{ft}\right)+(Y_M-Y_G)\left(-\alpha_f\ddot\psi_{ft}-\ddot\varphi_{ft}\right)\\
+(Z_M-Z_G)\left(-\dot\varphi_{ft}^{\,2}-\dot\alpha_{ft}^{\,2}\right)
\end{array}\right. \tag{75}$$

The acceleration of point M is, therefore: $\left.\frac{d^2}{dt^2}\overrightarrow{G'M}\right]_{Rh} = \begin{bmatrix} \ddot{x}_{Mt.t} \\ \ddot{y}_{Mt.t} \\ \ddot{z}_{Mt.t} \end{bmatrix} = \begin{bmatrix} \ddot{x}_{Mt.t} \\ \ddot{y}_{Mt.t} + \frac{d^2}{dt^2}\overrightarrow{GM} \\ \ddot{z}_{Mt.t} \end{bmatrix}$

With accelerations given by : $\begin{aligned} \ddot{x}_{Mt.t} &= \Omega^2 \ddot{x}_M = \Omega^2\left(-x_{M1c}\cos\psi - x_{M1s}\sin\psi\right) \\ \ddot{y}_{Mt.t} &= \Omega^2 \ddot{y}_M = \Omega^2\left(-y_{M1c}\cos\psi - y_{M1s}\sin\psi\right) \\ \ddot{z}_{Mt.t} &= \Omega^2 \ddot{z}_M = \Omega^2\left(-z_{M1c}\cos\psi - z_{M1s}\sin\psi\right) \end{aligned}$

The six unknowns (accelerations of point M) can be found after applying the operators: $\frac{1}{2\pi}\int_0^{2\pi}(\dots)sin\psi d\psi$ and $\frac{1}{2\pi}\int_0^{2\pi}(\dots)cos\psi d\psi$, what gives, after intermediate calculations:

$$\begin{aligned}
x_{M1s} &= x_{1s} + \left(Y_M - Y_G\right)\left(\varphi_{f0}\alpha_{f1s} + \psi_{f1s}\right) + \left(Z_M - Z_G\right)\left(\alpha_{f0}\psi_{f1s} + \alpha_{f1s}\right) \\
x_{M1c} &= x_{1c} + \left(Y_M - Y_G\right)\left(\varphi_{f0}\alpha_{f1c} + \psi_{f1c}\right) + \left(Z_M - Z_G\right)\left(\alpha_{f0}\psi_{f1c} + \alpha_{f1c}\right) \\
y_{M1s} &= y_{1s} + \left(X_M - X_G\right)\left(-\varphi_{f0}\alpha_{f1s} - \psi_{f1s}\right) + \left(Z_M - Z_G\right)\left(\alpha_{f0}\psi_{f1s} + \varphi_{f1s}\right) \\
y_{M1c} &= y_{1c} + \left(X_M - X_G\right)\left(-\varphi_{f0}\alpha_{f1c} - \psi_{f1c}\right) + \left(Z_M - Z_G\right)\left(\alpha_{f0}\psi_{f1c} + \varphi_{f1c}\right) \\
z_{M1s} &= z_{1s} + \left(X_M - X_G\right)\left(-\varphi_{f0}\psi_{f1s} - \alpha_{f1s}\right) + \left(Y_M - Y_G\right)\left(-\alpha_{f0}\psi_{f1s} - \varphi_{f1s}\right) \\
z_{M1c} &= z_{1c} + \left(X_M - X_G\right)\left(-\varphi_{f0}\psi_{f1c} - \alpha_{f1c}\right) + \left(Y_M - Y_G\right)\left(-\alpha_{f0}\psi_{f1c} - \varphi_{f1c}\right)
\end{aligned} \tag{76}$$

The amplitude and phase of the accelerations

The efforts on the rotor head were expressed as a function of the azimuthal coordinate of blade number 1: $\psi_1 = \psi = \Omega t$, where t represents the time that elapsed from the moment when this blade passed through the origin position ($\psi = 0$) and the magnetic sensor triggered the signal to synchronize the time. From this moment (t = 0) on, the vibration measured in the fuselage is expressed in terms of amplitude and phase, which can be calculated from the different components, as summarized in Tables 2 and 3.

Table 2: Acceleration at the fuselage CG – adapted from (Jorge, 1992)

Entry data	Vibration amplitude	Vibration phase
x_{1s}, x_{1c}	$AX = \Omega^2\sqrt{x_{1s}^2 + x_{1c}^2}$	$\phi X = \arctan\frac{x_{1c}}{x_{1s}}$
y_{1s}, y_{1c}	$AY = \Omega^2\sqrt{y_{1s}^2 + y_{1c}^2}$	$\phi Y = \arctan\frac{y_{1c}}{y_{1s}}$
z_{1s}, z_{1c}	$AZ = \Omega^2\sqrt{z_{1s}^2 + z_{1c}^2}$	$\phi Z = \arctan\frac{z_{1c}}{z_{1s}}$

Table 3: Acceleration of point M at the fuselage – adapted from (Jorge, 1992)

Entry data	Vibration amplitude	Vibration phase
x_{M1s}, x_{M1c}	$AX_M = \Omega^2 \sqrt{{x_{M1s}}^2 + {x_{M1c}}^2}$	$\phi X_M = \arctan \frac{x_{M1c}}{x_{M1s}}$
y_{M1s}, y_{M1c}	$AY_M = \Omega^2 \sqrt{{y_{M1s}}^2 + {y_{M1c}}^2}$	$\phi Y_M = \arctan \frac{y_{M1c}}{y_{M1s}}$
z_{M1s}, z_{M1c}	$AZ_M = \Omega^2 \sqrt{{z_{M1s}}^2 + {z_{M1c}}^2}$	$\phi Z_M = \arctan \frac{z_{M1c}}{z_{M1s}}$

3.4 Validation of the calculation code

The Possibilities

Several procedures for validating the calculation code can be envisaged, not only within the scope of the direct problem but also for the opposite inverse, which will be introduced in a later section.

The first possibility is to validate the codes with accelerometers installed as foreseen in the Maintenance Manual (MET) of the helicopter, to be able to compare the results obtained with the correction maps (which are experimental, obtained in-flight tests) that already exist in MET. We've simulated, in the scope of this work, some flight conditions, to validate the calculation code of the direct problem.

A second possibility is to validate the codes through flight tests, which can give us, the different flight conditions and known corrections introduced in the rotor, the efforts measured in the rotor head, as well as the accelerations at different points of the fuselage. This validation is adapted not only to the direct problem but also to the inverse problem, since it is possible to place the six accelerometers in the fuselage, necessary to find the CG accelerations of the fuselage and the efforts that result in the rotor head, as we will see in the discussion of the inverse problem, in a later section.

A third possibility is to validate the code with the help of a helicopter rotor numerical code, such as R85, HOST, etc. For references on numerical codes for helicopter rotor simulation see (Rabe & Wilke, 2018), (Wilke, 2017), (Johnson, 2013b), (Benoit et al., 2000). To be able to compare the codes, it is necessary to put the isotropy of the blades as a hypothesis, which leads us to the validation of the part of the code related to the isotropic rotor balance. This possibility can lead to a decrease in the workload required in the flight tests (second possibility, above), which will serve, therefore, to validate only the second part of the code (the introduction of defects in the rotor head).

Comparison with the MET

Several possibilities for installing accelerometers are provided in the MET: (i) Accelerometers (lateral and longitudinal) positioned on the electrical panel, to the left of the 3rd man's seat, at the top; (ii) Accelerometers (vertical, lateral, and longitudinal) positioned on the floor to the left, below the co-pilot seat; and (iii) Accelerometer (lateral) positioned below the main gearbox (BTP).

The calculation code, as previously derived, is composed of two parts: the first part corresponds to the calculation of the equilibrium, with the isotropic rotor, while the second part corresponds to the introduction of defects. The calculation of the isotropic rotor equilibrium is done by calculating the solution of a system of 12 nonlinear equations with 12 unknowns. These are the three flapping equations, the three drag equations, and the six fuselage balance equations, as seen before. As the equations are non-linear, a subroutine of the IMSL library was used in a FORTRAN software, which finds the solution of a system of non-linear equations with the Jacobian of this system provided a priori. For that, the Jacobian of the system of non-linear equations of isotropic rotor equilibrium is calculated as a matrix 12 x12, obtained from all the partial derivatives of the twelve equations concerning the twelve unknowns.

$$FJAC(1,1)=\frac{\partial F(1)}{\partial X(1)}=\frac{\partial F(1)}{\partial \theta_0}=\frac{\rho acR^2}{2I_\beta}\left[-e\left\{\frac{R-e}{2}\mu^2+\frac{R}{3}\right\}+\frac{R^2}{4}+\frac{R^2}{4}\mu^2\right]$$

$$\text{.... etc, up to} \tag{77}$$

$$FJAC(12,12)=\frac{\partial F(12)}{\partial X(12)}=\frac{\partial F(12)}{\partial T_{Ra}}=-x_{Ra}$$

The unknowns are angles in radians and, therefore, very small, and a subroutine that works in double precision was used. Even with all the precautions from the numerical point of view, the system was always very sensitive to two parameters:

- The criterion to finish the calculation (a relative error criterion). A root is accepted if the relative error between two successive approximations of this root is less than the relative error criterion. The chosen value of the criterion is very important for the convergence of the subroutine; if the relative error criterion is too large, the subroutine fails to find a solution that can nullify the system of equations before the difference between two successive iterations, for root, be already reached. On the other hand, if the relative error criterion is too small, the subroutine may interrupt the iteration because it hasn't made good progress. The system of equations is extremely sensitive to the knowledge, with good precision, of the unknown parameter values.
- The approximate guess value of θ is used to initialize the subroutine. This value must be provided a priori and slight changes in this value may sometimes prevent the subroutine to find the system solution.

In this way, the simulation of all possibilities in terms of flight conditions, mass, and balance, with the subroutine, becomes a problem since, for each case, it is necessary to effectively evaluate the relative error criterion and the initial pitch θ values, to be supplied to the subroutine. For a more complete simulation, it will be necessary to find a system solution subroutine more adapted to this specific problem. The results of the isotropic rotor equilibrium can be found for different flight conditions (stationary flight, ground level, etc.), with different values for the helicopter mass and centering (mass center location). Limits of mass and centering are shown in Figure 18, for this case.

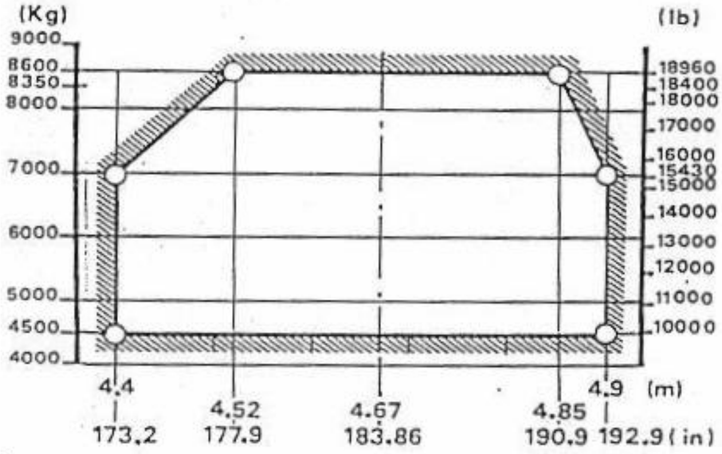

Figure 18: limits of mass and centering: helicopter AS332L – adapted from (Jorge, 1992)

For the second part of the calculation code, there are no numerical problems in terms of convergence to the solution. Figure 19 shows a rotor balance chart, from the MET. Starting from the isotropic rotor, the introduction of an equilibrium mass Δm = 500 g on blade n° 2 leads us to a lateral vibration of 0.25 IPS amplitude, and 270° phase (point X on the chart). Entering the same mass in the software, for the obtained equilibrium, the deviation found (in amplitude and phase) is small (point O on the chart).

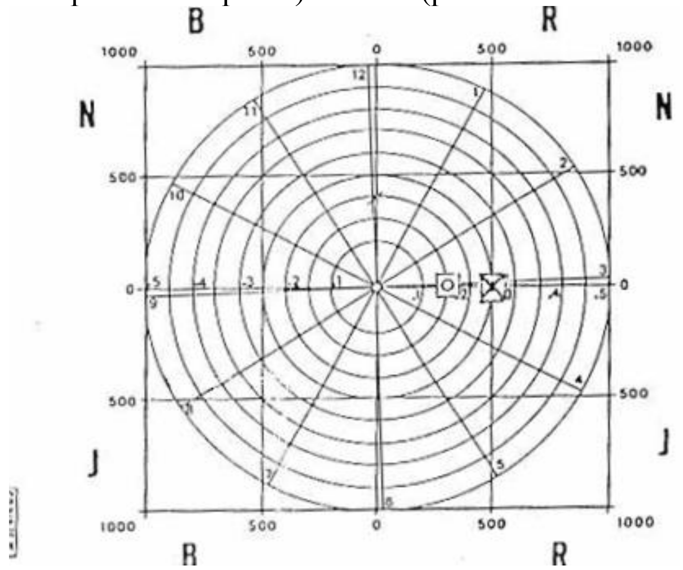

Figure 19: Helicopter Maintenance Manual (MET) chart: simulation and predicted vibration values – adapted from (Jorge, 1992)

This small deviation can be explained by the fact that the balance chart is an average chart, obtained from the user experience of several aircraft whose characteristics were not identical. Furthermore, it is a map that is assumed to be valid throughout the helicopter flight domain, when one can see, in the previously obtained formulations, that the introduction of the same equilibrium mass under different flight conditions or with different configurations (in terms of weight and centering of the aircraft) can lead to different efforts on the rotor head and, consequently, to measured vibrations on the fuselage which are different, too. In this way, the comparison with the MET serves as an initial point of reference, knowing that the complete validation of the system must be done, in principle, by flight tests.

A comment on the results

The subroutine provided by the IMSL library for calculating the isotropic rotor balance is very sensitive to variations in the given parameters and the initial values considered for the unknown parameters (in particular, the initial pitch angle θ). A subroutine more adapted to this specific problem should be sought, to be more robust, that is, less affected by variations of parameters that have nothing to do with the flight condition as such, but with only numerical constraints (in this case, the need, for the subroutine, to know a priori what the maximum permissible error is, and to have initial values of the pitch angle θ, to initialize the subroutine.

It can also be seen that the simple comparison with the MET cannot be taken as a complete validation of the system but must be considered as an initial point of reference for more complete validation, with flight tests, for different flight conditions and aircraft settings.

3.5 The inverse problem for identification of unbalanced and out-of-track blades in a helicopter main rotor system and the optimization of the accelerometer positions– perspectives

Analysis of the Inverse Problem

As in the case of the study of the introduction of defects, the problem can be divided into two stages: (i) the study of the isotropic rotor; (ii) the study of the inverse problem as such from the vibrations measured on the fuselage.

For this second step, the equilibrium with the isotropic rotor (θ, β, δ,α_f, φ_f, T_{Ra}) is, therefore, known a priori. From the installation of accelerometers at different points of the fuselage, it is possible to have, as input data, the amplitude and phase of the accelerations at these locations. It was previously seen the passage of the six accelerations (three linear and three angular) to the three linear accelerations of any point M in the fuselage. To calculate the inverse, it is necessary and sufficient to have six linear accelerations at chosen points on the fuselage (example: the three accelerations in x, y, and z of two points: M_1 and M_2), to find the six accelerations of the CG, the fuselage seen as a rigid body.

From the twelve components (in sines and cosines) of the CG accelerations and the knowledge of the fuselage radii of gyration (which are a function of the centering of the aircraft, which is known from the isotropic rotor equilibrium), the twelve components (in sines and cosines) of the resulting efforts on the rotor head (Fx, Fy, Fz, Mx, My, Mz) are found.

From this point on, the inverse of the previously obtained expressions is no longer possible to be obtained without making additional assumptions, since each of the resulting efforts in the rotor head was obtained from the sum of the efforts generated by each of the four blades. One must note that, at this point, there are twelve equations and forty-eight unknowns. From the practical experience of balancing the rotors, it can be seen that in terms of the measured vibration: (i) the introduction of an equilibrium mass ($+\Delta m$) on a blade *i* is equivalent to the removal of the same mass ($-\Delta m$) on the blade that is diametrically opposite to it (*i + 180°*); (ii) the increase in rod (pitch link) length ($\Delta\theta_0$) on blade *i* is equivalent to the corresponding decrease ($-\Delta\theta_0$) on the opposite blade (*i + 180°).*

In addition, MET maintenance procedures generally prohibit the operator from making adjustments to one blade, called standard. For this blade, the rod length, as well as the adjustment of the tabs and the balance mass at the sleeve will remain unchanged. Thanks to this equivalence between the balance corrections to be introduced either on blade *i*, or on blade *i + 180°,* we will consider only the introduction of corrections for two rotor blades (example: blades *i* and *i + 90°),* the other two will continue to be unchanged. In this way, we now have twelve equations and twenty-four unknowns (the forces generated in the rotor head by these two blades being considered), the forces generated for the two other blades are obtained with the isotropic rotor hypothesis. Maintenance procedures recommend not introducing two simultaneous corrections on two different blades. In this way, the process is iterative: corrections are introduced on a blade, the vibration measurement is re-done, new corrections are introduced on the same blade or another one, the measurements are re-done and so on, in sequence, until obtaining levels of vibrations below a certain value, defined a priori as acceptable, and predicted in the helicopter maintenance manual (MET).

We will solve the passage from the resulting efforts at the rotor head to the efforts in the rotor head due to a blade *i* in the same iterative way: (i) It is assumed that the other three blades are isotropic, and we will have a system of twelve equations with twelve unknowns (the efforts on the rotor head generated by blade *i*). Then, the corrections to be introduced on this blade are calculated (see below); (ii) Next, it is assumed an isotropic blade *i* to calculate the rotor head efforts generated by blade *i* + 90° (in our example) and, thus, the corrections to be introduced on this blade (see below); and (iii) The calculated correction is introduced, and then the accelerometer measurements and also all calculations to obtain new corrections are redone, until the vibration level is below an acceptable value.

For code validation regarding the inverse problem, it is sufficient to take the corrections calculated before for blade *i* and input them in the calculation code of the direct problem, to verify if the introduced corrections cause vibrations at the fuselage measurement points (M_1 and M_2), which are of similar amplitude but in phase opposition concerning the vibrations measured initially (which were the given parameters in the calculation of the inverse problem). Thus, the vibrations caused by the corrections will cancel out those from the beginning. It remains to analyze the corrections to be introduced on a blade *i*. It was obtained, above, the efforts in the head of the rotor generated by blade *i*. It was also seen that these efforts come from the introduction of defects in θ_0, θ_{1s}, and m_p, which generated the new flapping (β) and drag (δ) angles.

The mass effect is more important on "lateral" and "longitudinal" (in the rotor plane) vibrations, while the rod and tab effect is more important on "vertical" (orthogonal to the rotor plane) vibrations. In this way, we will separate the problem into two parts:

- For the efforts in the plane (Fx, Fy, and the moment generated by these two forces: Mz), we will assume that there is no variation due to the pitch (θ). In this way, θ, β and δ are the angles already obtained with the isotropic rotor hypothesis and the unknowns are now: m_p, m_{sp}, and I_β. Finally, these last three parameters have a relationship with the change in blade mass due to the introduction of the equilibrium mass (Δm), which will give us, in the end, the equilibrium mass to be introduced or withdrawn on this blade *i* (Δmi) to obtain the forces Fx, Fy and Mz.

- For the forces orthogonal to the rotor plane, we will assume that m_p, m_{sp}, and I_β are the parameters of the isotropic rotor. We will have six equations (Fz, Mx, My, in sines and cosines) in addition to the flapping and drag equations, to obtain the new pitch angles (θ), as well as the corresponding flapping (β) and drag (δ) angles. This problem can be treated in two parts, too. Current rotor balancing procedures are to perform, in the first step, a steady-state flight ($\mu = 0$) from which corrections are introduced on the pitch rod. Then, a stabilized level flight is carried out, where corrections tab adjustment are introduced since the tabs influences restricts to forward flight.

Thus, for simplicity of calculation, the inverse problem can be calculated:

- In the first step, for $\mu = 0$, with θ_{1c} and θ_{1s} calculated with the isotropic rotor and the only defect is the one in θ_0, with the corresponding changes in β and δ;
- In a second step, for $\mu \neq 0$, we will assume that θ_0 is the one calculated in the first step, and will have, as unknowns: θ_{1s} (equivalent to a change of tab, as seen in the analysis done previously) and the corresponding terms in β and δ.

Optimization of the accelerometer positions

To look for the optimal position of the accelerometers, it is necessary to use the second possibility of validating the calculation code, mentioned above, that is, the flight tests. The intention is to minimize the calculations to be made, and the possible couplings between the different parameters, during the calculation of the inverse problem, and, for that, the most adapted validation method is the flight tests. It is at this stage of the work that we will consider, also, the constraints or limitations of the problem, such as: (i) The maximum permissible balancing mass in the sleeve; (ii) The maximum permissible effort on the rod; (iii) The maximum adjustment of tabs, etc. Several possible positions of accelerometers should be studied. For example:

- Three accelerometers (vertical, lateral, and longitudinal) on the floor to the left, below the co-pilot seat;
- Two accelerometers (vertical and lateral) on the floor on the right, in the strong frame (Z = 6,815 mm) (the end of the floor and the beginning of the tail boom);
- One accelerometer (vertical) on the floor on the left (same frame: Z = 6,815 mm).

The 2nd step of the optimization process, the effect of the tab, as previously analyzed, can be considered as a change in θ_{1s} and, in addition, a change in blade twist, to account for the fact that the tab generates a torsion moment on the blade, which can lead to a twisting of this blade because the blade has a certain torsional flexibility, which can be considered. This can also lead us to calculate the efforts that will be passed to the fuselage through the rods and the chain of command. Non-linearities, such as, for example, the play of a connecting rod, can also be considered, as well as non-linearities in the operation of drag adapters.

4 Model-based parameter identification for unbalanced and out-of-track helicopter rotor blades: a case study of a 3-blade main rotor

This section is based on a Master's Thesis (González, 2012), Post Graduate Program in Mechanical & Aeronautical Engineering at ITA, São José dos Campos, Brazil, 2012.

4.1 Introduction

Case study: 3-blade main rotor: model development & comparison with flight tests

Following the steps of the above study for the 4-blade helicopter case, this Section focuses on the analytical modeling of the relationship between the simplified dynamics of a fuselage-main rotor system and the vibratory level of its response, measured at two points on the fuselage, for the case of a 3-blade helicopter. The mathematical model derived by (Jorge, 1992) was adapted for the peculiarities of a typical small helicopter with three blades. Most of the text from (González, 2012) was retained. Some equations at the beginning of these derivations, before adding the total number of blades, are similar to the ones obtained in the previous section, for the case of the 4-blade study, and thus their Equation numbers are only referenced in the following text, to avoid eventually repeating some previously obtained equations. As before, the response is limited to measurements of amplitude and phase of once-per-rev vibrations at the circular frequency of the main rotor (1-per-rev or 1Ω) on the x, y, and z axes. An additional limitation to this model comes from the approximations assumed for some design parameters, not available in the literature or manuals, thus adopted as representative of the 3-blade helicopter in the study, the AS355 F2 Squirrel model.

As in Section 3, this section presents mathematical modeling for the analytical expression of the wrench of the efforts in the rotor hub, modeled as a set of articulated blades under the degrees of freedom in pitch, flapping, and lead-lag. Three distinct phases make up any type of analysis: analytical modeling, mathematical modeling, and dynamic behavior. In line with good engineering practices to obtain adequate analytical modeling (among several always possible), a set of simplifying hypotheses is adopted to reduce a real dynamic system to another equivalent of the type represented by mass-spring-damper; and the same is represented by a free body diagram that reflects its properties also defined by the analyst, such as inertia (mass), rigidity (spring), energy dissipation (damper), and type of loading (forces). The model needs to be a compromise solution between the sophistication that brings it closer to the complex reality and the simplification that, moving away from it, analyzes the corresponding mathematical model viable, with the resources and deadlines available. Mathematical modeling includes small vibrations around an equilibrium position, and their associated accessory conditions (initial and/or boundary conditions). Among the basic and didactic approach techniques for deducing the differential equations governing the motion, one can group them into Lagrangian Mechanics (according to scalar energy concepts) and Newtonian Mechanics (based on vector quantities). Despite complex structures recommending the first (more systematic), the latter is chosen in this text, given the more intuitive nature of identifying the efforts and their visualization in the free body diagram (necessary in this option), conceived in a relatively simple way, given the simplifications to be discussed. The resolution of these equations, either in the time or frequency domain, then reveals the dynamic behavior resulting from the adopted analytical model, and in this text, it is performed numerically in the frequency domain with computational aid.

THE HYPOTHESES

The analytical modeling of the isotropic fuselage-rotor system begins by opting for the design of the free-body diagram only for the defect-free rotor system (from this point onwards, the term "isotropic" is adopted), or more precisely, of any of its three blades, since it concentrates, within the adopted hypotheses, all the dynamic efforts to be integrated by the rotor hub and then added up and transmitted to the fuselage (supposedly assumed as stationary concerning any other loads). Always looking for a compromise solution between the simplicity of the model and the accuracy of the results, for the necessary definition of the reference flight configuration, despite directly influencing the vibration index, for simplicity, this study adopts:

1. The fixed value of 1.225 kg/m^3 of the air density, which flows through the profiles of the blades and empennages, and this is directly proportional to their lift and drag, also creates resistance to the fuselage advance. This value corresponds to the standard atmosphere ISA (International Standard Atmosphere - model established by the ICAO), without ΔT temperature adjustments (non-varied ISA), and at sea level (troposphere, under standardized conditions of temperature (15ºC) and pressure (101325N/m2))

2. Zero load factor (acceleration of the body dimensionless by the acceleration of gravity g, a result of the ratio between the force applied to it and its weight), that is, stationary, straight, level, and stabilized flight (structure not subjected to any accelerations);

3. In the broad spectrum of frequencies, even when aware of the importance of other harmonics associated with other defects, for simplicity, only vibrations at the fundamental frequency of value 1Ω are considered here, equal to once the rotation of the main rotor, as it is still an important item associated with direct intervention actions in maintenance practice.

4. Articulated rotor according to the following degrees of freedom for each blade, under small-displacement angles to reduce non-linearities: (i) flapping (flexion out of the plane of rotation): as in forward flight it compensates for lift asymmetry; (ii) forward and backward movement or lead-lag (flexion in the plane of rotation): as it is due to the non-linear Coriolis force associated with the flapping motion (although independent of the lead-lag), according to a flap-lag coupling, for which relief is required bay means of a lead-lag joint normal to that plane; and (iii) variation of pitch or incidence in pitch or feathering or torsion (rotation around the elastic axis): as it is the end of the collective and/or cyclical chain of action, and its coupling with each of the above degrees of freedom.

For simplicity of the model to be calculated, the torsional freedom of the blade or twist associated with the tab adjustments (which here is associated with torsion) is disregarded, since it is assumed that it has sufficient stiffness to contain it. There is only the built-in, permanent and linear torsion, as a given intrinsic to the project. Furthermore, all nonlinearities linked to pitch-flap-lag couplings, represented by the triple products of their displacements or associated functions, are disregarded.

5. Rigid blades, for simplicity of calculations. Therefore, the degree of freedom in the flexible mode of torsion of the blade (twist) along its elastic line is disregarded. This positioning eliminates the adjustment through the tabs, which also corrects the tracking by variation of the lift in the respective section of the blade in which they are installed.

6. Blade submitted to aerodynamic loading resulting from two-dimensional flow according to the Blade Element Theory (Johnson, 2013b): adopts a high aspect ratio for the profile) in a steady-state, without gust-type disturbances being considered.

The actual blade is made of composite material and is reasonably flexible in bending and torsion, like most of them, so it is subject to aeroelastic effects related to flap-lag, pitch-flap, pitch-lag, and pitch-flap-lag couplings (only this one is disregarded here in the model). This study disregards the effects of flow on the retreating blade (flow detachments, dynamic stall and reverse flow), and on the forward blade tip (compressibility and associated advances implemented by modern blade tip designs, as well as the effects of tip loss), as well as at its root (offset loss), and large flap deformations of the blades (source of nonlinearities).

Aerodynamic forces are well determined by fundamental modes (rigid body movements), but excitation in elastic torsional and bending modes by high harmonics of these forces can produce large loads on the section, even under small deflections. Hence the natural frequency of the blade in these modes must be kept away from the harmonics of Ω (Johnson, 2013a).

7. It is assumed that the fuselage, assumed to be a semi-rigid body, can be dynamically equivalent to a rigid body with six degrees of freedom (three components of position and three orientation angles). Hence, the configuration of fuselage states can be described in terms of only six degrees of freedom, along with and around each of the three axes X, Y, and Z (the larger arrows shown in Figure 20) for their equilibrium under external forces, such as the aerodynamic forces, which, added to the blade motion equations (at small flapping and lead-lag angles) form twelve non-linear differential equations with twelve unknowns.

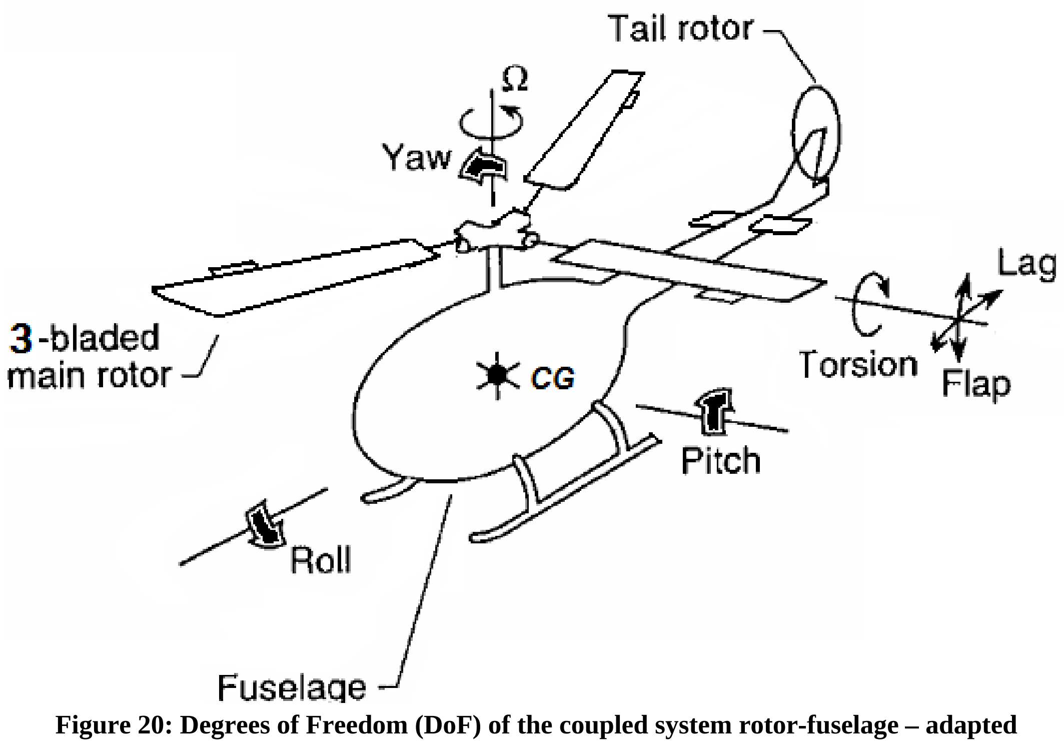

Figure 20: Degrees of Freedom (DoF) of the coupled system rotor-fuselage – adapted from (Friedmann & Hodges, 2003)

8. The loading on the rotor hub is determined from the sum of the three integrations (on each blade) of the efforts considered according to the Blade Element Theory.

In the modeling adopted in this study, despite all the simplifications that even disregard all the flap-torsion, lag-torsion, and flap-lag-torsion couplings, the nature of the system of equations of motion of the rotor-fuselage system, which takes the flap-lag, is still non-linear, and in its numerical resolution process, it is internally linearized by the computational algorithm selected in the MATLAB® software environment.

THE PARAMETERS

It is necessary to adopt some parameters to establish the aircraft object of the simulation and some flight condition(s), where the responses of the isotropic rotor-fuselage system will be investigated, and which later serve as a reference for the evaluations of the effects of the introduced anisotropies. These parameters are:

• system mass: fundamental proportionality factor in the evaluation of accelerations related to the submitted efforts. It is assumed constant, that is, the reduction due to fuel consumption is neglected, when compared to the original mass.

• aircraft centering: responsible for the positioning of its center of gravity (CG) and the definition of the relative moment arms (associated with the fuselage attitude states), as well as for the propagation of the vibration characteristics along the fuselage. Generally, the CG is presented by the manufacturer in the form of Figure 21, within which its "walk" is allowed (in the vicinity of the vertical of the mast and, therefore, of the main rotor traction), to guarantee longitudinal and lateral stability. directional, as well as the flight qualities desirable to the project. Figure 21 shows the relevant data used, such as the forward flight speed. In this study, the cases of null velocity and 222 knots (corresponding to the maximum not-to-exceed speed) were considered).

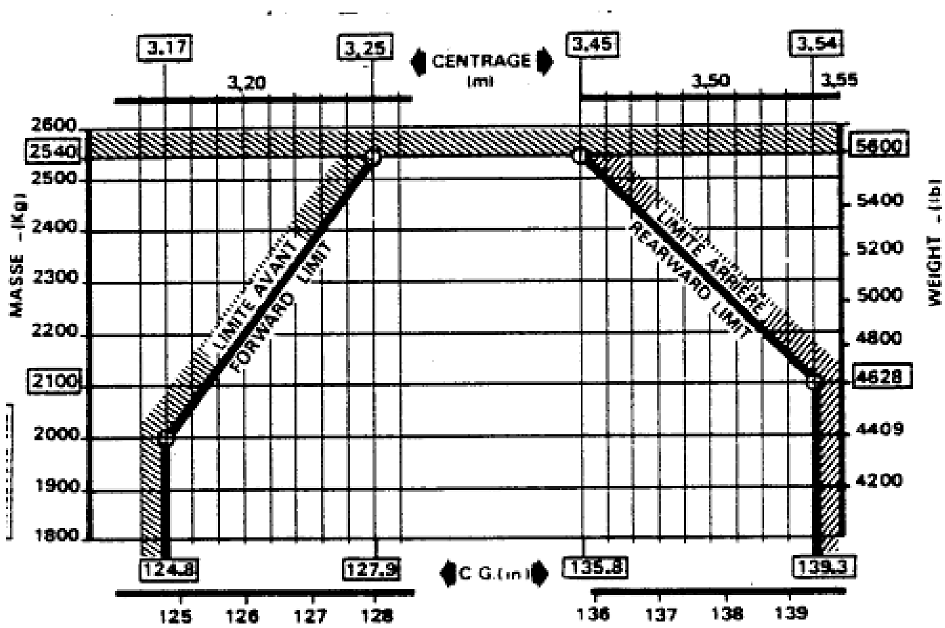

Figure 21: Longitudinal centering diagram for the adopted helicopter (AS355F2 Squirrel) (Note the 9cm maximum CG range) – adapted from (HELIBRAS, 1994)

It is worth mentioning that proprietary confidential information about helicopter design, in this work, some estimated values were assumed for the other parameters necessary for the application of the model. In the future, as the actual parameters are obtained and/or estimated by parameter identification, the model can easily be updated/refined to better represent the aircraft of interest. In the absence of better alternatives, the criterion for estimating these values which could not be obtained consisted of linearly associating, when feasible, the desired parameters with the analogs of the AS 332L Super Puma aircraft, shown in Section 3, and originally presented in (Jorge, 1992).

4.2 Balance study of the system: main rotor plus fuselage

BLADE MOTION EQUATION

In continuity, one evolves to mathematical modeling. A large part of the expressions was established in (Jorge, 1992), and conveniently adapted for this text.

Newton's 2nd Law of Classical Mechanics (Fundamental Principle of Dynamics) is used, chosen to obtain the equations of motion resulting from two phases: the determination of the free-body diagram of the system; followed by the application of this Law in its forms for translations and rotations. In this type of approach, care must be taken not to confuse the directions of efforts and their reactions, which is the most susceptible error when evaluating multibody systems with three-dimensional loads, which is the situation in this model.

BLADE DYNAMIC BALANCE

In the modeling shown in Figure 22, each of the blades that make up the rotor is subject to inertia ($\int_e^R (\frac{d^2\overrightarrow{OM}}{dt^2})dm_i$) and aerodynamic ($\vec{F}_{aerodynamic}$) efforts, respectively, constituting the parts of the equation that follows.

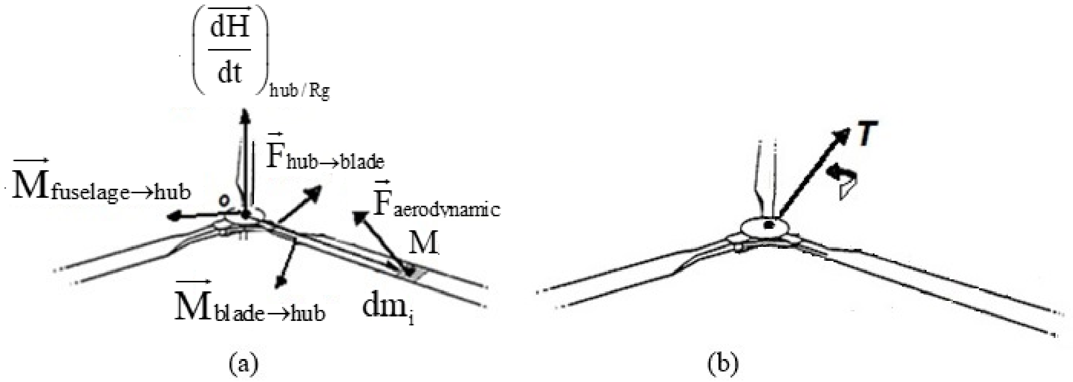

Figure 22: Rotor hub free-body diagram with efforts (forces F and moments M) applied to a blade (a) and their corresponding wrench T (b) – adapted from (González, 2012)

Applying Newton's 2nd Law to an element of mass dm_i of blade *i*, located by the position-vector $\overrightarrow{OM}$, about the Galilean Reference Frame - R_g (fixed to the center of the Earth, and considered non-inertial), one obtains vectorially that: $\int_e^R (\frac{d^2\overrightarrow{OM}}{dt^2})dm_i = \vec{F}_{hub \to blade} + \vec{F}_{aerodynamic}$, where:

R_f: fixed rotor reference frame (O, X, Y, Z)
R_t: rotating reference frame of the rotor (O, X_i, Y_i, Z_i)
R_p: reference frame of the blade beating (O, $X_{p'}$, $Y_{p'}$, $Z_{p'}$)
R_p: blade reference frame in beating followed by lead-lag (O, X_p, Y_p, Z_p)
R_a: aerodynamic reference frame (O, X_a, Y_a, Z_a)
R_h: helicopter reference frame (O, X_h, Y_h, Z_h)

One has that, in R_g, the resultant of the vector of forces $\vec{F}$ of the blade on the hub, applied in the flapping joint, is $\vec{F}_{blade \to hub} = \vec{F}_{aerodynamic} - \int_e^R (\frac{d^2\overrightarrow{OM}}{dt^2})dm_i$. Now by applying Newton's 2nd Law again in terms of angular movements concerning R_g, around the rotor hub by the blade and fuselage, we obtain: $\left(\frac{d\overrightarrow{H}}{dt}\right)_{hub/Rg} = \overrightarrow{M}_{blade \to hub} + \overrightarrow{M}_{fuselage \to hub}$. As the cube is rotating at a constant speed (zero angular acceleration), the time derivative of angular momentum $\left(\frac{d\overrightarrow{H}}{dt}\right)_{hub/Rg}$ is zero. Hence $\overrightarrow{M}_{hub \to fuselage} = \overrightarrow{M}_{blade \to hub}$, that is, the moments applied by the hub to the fuselage, symmetrical to those received by the hub, are equivalent to the action of the moments applied by the blade to the hub. Given the above, it is clear that it is necessary to obtain $\int_e^R (\frac{d^2\overrightarrow{OM}}{dt^2})dm_i$, $\vec{F}_{aerodynamic}$ and $\overrightarrow{M}_{blade \to hub}$. The result of these three calculations gathers the components, in R_g, of the wrench of the efforts in the rotor hub $\{T\}_0$. A wrench, by definition, replaces all forces and moments acting on a rigid body by the representation of a force vector and a moment vector, applied at the same point (Beer et al., 2019). The zero index is justified since it is constant about the azimuth position of the blades (and therefore about time) due to the isotropic rotor hypothesis and that the study was limited to the 1Ω frequency.

$$\{T\}_0 = \begin{Bmatrix} \vec{F}_{blade \to hub} \\ \overrightarrow{M}_{blade \to hub} \end{Bmatrix}_0 = \begin{Bmatrix} F_x \overrightarrow{X} + F_y \overrightarrow{Y} + F_z \overrightarrow{Z} \\ M_x \overrightarrow{X} + M_y \overrightarrow{Y} + M_z \overrightarrow{Z} \end{Bmatrix}_0$$

After this calculation for a blade, the sum is performed according to the number of blades to obtain the wrench of the efforts of the complete rotor applied to its hub.

BLADE ACCELERATIONS

The dynamic resultant, applied to the body of blade *i* is obtained from the integral in space along the blade according to the distance *r* varying from the eccentricity *e* to the radius *R*. Thus, given the blade model as simply articulated in flapping and lead-lag, first, there is the following relationship between the rotor reference frames according to these adopted degrees of freedom. It can be observed that, except for the fixed reference (XYZ) to the hub and originating from it, all origins are established in the flapping joint, here modeled as the blade attachment point. For generality, any point M located on the blade surface at a radial coordinate r is considered, as previously shown in Figure 8. It is necessary to calculate the acceleration $\overrightarrow{\gamma_M}$ of this point M in the fixed rotor frame and then integrate the obtained expressions along the blade. As seen from the fixed rotor reference R_f (O, X, Y, Z), we have the position vector of the point M relative to the origin O as in the previously obtained Equation (1).

The rotor is assumed to rotate at a constant speed $\dot{\psi}_i = \Omega$. The position vector from Equation (1) is derived twice concerning time, and the acceleration vector of the point M concerning reference O is obtained, as previously seen, as Equation (2). As before, a simplifying notation is used for the derivatives of β, and similar simplifications are done, considering β and δ small angles, leading to the three components of the acceleration vector of point M in the fixed frame. Again, the integration $\int_e^R (\frac{d^2\overline{OM}}{dt^2})dm_i$ is required to calculate the inertial efforts on the blade in the fixed rotor frame R_f.

AERODYNAMIC FORCES ACTING ON A BLADE

At this point, attention is devoted to the portion of the dynamic resultant due to the aerodynamic efforts $\vec{F}_{aerodinâmico}$ applied to the blade, generated in flight, and in reaction to the airflow in which it is immersed.

The first step is to obtain the velocity of a current point M of the blade ($\overrightarrow{V}_{M\ Pa/Rg}$) concerning Galileo's frame of reference R_g (O_g, X_g, Y_g, Z_g), because, if referring to the ground, one is stationary and immersed in an undisturbed atmospheric flow that blows on the blade. Considering the hypothesis of stabilized horizontal forward flight (with constant speed), for simplification purposes, the aerodynamic reference frame and the Galilean frame are made to coincide ($R_a \equiv R_g$) under the null wind assumption, that is, the velocity of the undisturbed flow that arrives at the blade is the V_x=V itself (the displacement of the aircraft), and there are no lateral or vertical components. Hence it can be assumed that: $\overrightarrow{V}_{M\ air/Rg} = \overrightarrow{V}_{air/Rg} = \overrightarrow{V_{X/Rg}} = \left(\overrightarrow{V}_{blade_V}\right)_{Ra}$. Considering $\overrightarrow{OM}$ the Rf frame of reference, the velocity of the blade point M, reasoning from R_f to R_g, can be decomposed into the sum of the velocity due to blade rotation, flapping, and lead-lag movements ($\overrightarrow{V}_{M\ blade/fixed\ rotor} = \overrightarrow{V}_{blade_{\Omega,\beta,\delta}}$), added to the speed due to the forward flight ($\overrightarrow{V}_{M\ fixed\ rotor/air} = \overrightarrow{V}_{blade_V}$), plus the induced velocity ($\overrightarrow{V}_{M\ air/Rg} = \overrightarrow{V}_{blade_{Vi}}$), where the first term was previously obtained as Equation (3).

With the same notation as before, even with the given assumptions of stabilized flight (without accelerations), straight flight (contained in the XZ plane), and level flight (contained in the XY plane), one cannot consider $R_g \equiv R_f$ because constant pitch angles α_D are assumed in this model. Hence, from the derivative of the vector position, we have the velocity of the blade in terms of its degrees of freedom given as the previously obtained Equation (4). The same treatment can be done for the velocity due to the forward flight $\vec{V}_{pá_V}$ in the aerodynamic frame of reference R_a (O, X_a (positive against the movement of the aircraft, hence V negative), Y_a, Z_a (inclined pitch and $\alpha_D<0$ relative to the Z-axis)). A rotation ($\alpha_D>0$), i.e, a linear transformation via director cosines, around $\vec{Y}_a = \vec{Y}$ (as the element $W_{3,3}$ is unitary) leads this velocity from R_a to R_f, as previously shown in Equation (5). It is now necessary to consider the point M with its degrees of freedom (ie, to take from the current R_f to $R_{p'}$).

Similarly, a rotation ($-\psi i$, counterclockwise, by the design of the AS355 F2 aircraft, represented in this work) around $\vec{Z} \equiv \vec{Z_i}$ leads $\vec{V}_{pá\,\Omega,\beta,\delta} + \vec{V}_{pá\,V}$ from R_f to R_t. Subsequently, a rotation of β (descending blade) around $\vec{Y_i} = \vec{Y'_p}$ leads it from R_t to R_p, and a rotation of $-\delta$ (blade retreating in ψ) around $\vec{Z'}_p \equiv \vec{Z}_p$ leads it to $R_{p'}$ (flapping followed by lead-lag movement), leading to the previously obtained Equation (6). Finally, since V_i is a consequence of the blade motion, whatever the blade position is (ψ, β, and δ), the blade's relative motion (here in the frame $R_{p'}$) due to the induced velocity V_i is given, as before, by Equation (7), and the blade velocity is given, as before, by Equation (8). Figure 9 in Section 3 shows the wind direction concerning the fixed rotor reference frame R_f (O, X, Y, Z). $V=V_{ar/Rg}$ before reaching the blade. Figure 9 also shows the decomposition of the wind speed U in the rotating blade reference frame $R_{p'}$(O, $X_{p'}$, $Y_{p'}$, $Z_{p'}$) into a velocity component tangential to the rotor plane and perpendicular to the blade span (U_T), and another velocity component perpendicular to the first one (U_P).

The resultant speed is $U = \sqrt{U_T^2 + U_P^2}$, with $\tan\phi \approx \phi \approx U_P/U_T$, where ξ = blade angle of attack; Φ = induced angle; and θ = pitch angle. The wind velocity $\vec{V}$ in the blade reference frame $R_{p'}$ is given by the previously obtained Equation (9) (where $\psi = 0^o$ is the phase reference for the blade). There is a third component of U (radial U_r or $U_{xp'}$) along the blade span, that is, along with X_p, whose value of contribution to the lift (L) and the drag (D) is assumed to be negligible.

Noting the assumption of a two-dimensional aerodynamics problem ($C_l=C_{l0\alpha}$) for the profile of the current point M of the blade (at position $\psi = 180^o$), with the direction of U_P and U_T previously shown in Figure 9. The speed U of the impacting flow will be taken as the composition of U_T and U_P. Satisfying this hypothesis for C_l and C_{l0}, it is assumed a high aspect ratio for the profile, and the absence of stall and compressibility phenomena (Johnson, 1980). These assumptions, together with the tangential and vertical velocity components in $R_{p'}$ given as before, and with the previously adopted assumption of small angles for β and δ, lead to the previously obtained Equation (10).

Hence, it is noted that the velocity component U_T is the sum of the velocities due to the blade rotation (Ω.r) and the translation (tangential component) of the helicopter $(V.\cos\alpha_D.\text{sen}\psi_i + V\cos\alpha_D \cos\psi_i\ \delta)$. The velocity component U_P is the sum of the velocities due to the helicopter translation (vertical component), plus the induced velocity $(V\ .\ \text{sen}\alpha_D + V_i)$, the flapping velocity (derivative in β), and the translation of the helicopter (tangential component) $(V\ .\ \cos\alpha_D\ .\ \cos\psi_i\ \beta)$.

The elementary lift (L) and drag (D) forces are, respectively, perpendicular and parallel to the plane of the resultant velocity U, $\left(\vec{U}\right)_{R_p}$ (now known after transferring R_f to $R_{p'}$), and are given as previously obtained Equation (11).

The drag on the main rotor produces the torque associated with it. Figure 23 shows the elementary lift and drag forces on an infinitesimal element of the blade radius.

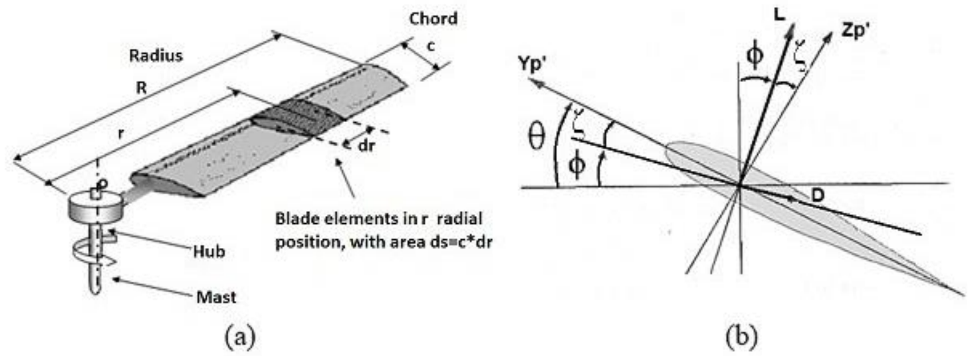

Figure 23: Elementary lift and drag in a blade section at ψ =90º immersed in flow: (a) blade view; (b) section view – adapted from (Gessow & Myers, 1952)

In the reference frame Rp', for blade *i*, the vector force in the element is given by the previously obtained equation (12). It is now necessary to go from $R_{p'}$ to R_f: a rotation of δ, blade advancing in ψ, around $Z_p \equiv Z_{p'}$ leads it to $R_{p'}$. A rotation of $-\beta$ (blade rising) takes it to R_t. With ξ, β and δ being small angles, we have: $\sin\xi \approx \xi = \theta - \phi \approx \theta - \tan\phi = \theta - Up/UT$; $\cos\xi \approx 1$; $\sin\beta \approx \beta$; $\sin\delta \approx \delta$; $\cos\beta \approx 1$; $\cos\delta \approx 1$; $\sin\xi\ \sin\delta \approx 0$; $\sin\delta\ \sin\beta \approx 0$; $\sin\xi\ \sin\beta \approx 0$. Assuming: $U^2 = U_T^2 + U_p^2 \approx U_T^2$, as $U_p << U_T$, and $a + C_{d0} \approx a$, as $C_{d0} << a$, leads to previously obtained Equations (13) and (14). For simplification, the following dimensionless coefficients are introduced:

- $\mu = \ = \dfrac{V\cos\alpha_D}{\Omega R}$ is called lead ratio, and is defined as the relationship between the velocity component parallel to the disc and the speed of the blade tip;
- $\lambda = \dfrac{V\text{sen}\alpha_D + V_i}{\Omega R}$ is a parameter of the axial flow, also called induced velocity, throughout this text, and is defined as the relationship between the velocity component perpendicular to the disk and the speed of the blade tip;
- $\chi = r / R$ and $\chi_e = e / R$.

$\theta(\psi)$ is expanded in components of a Fourier expansion: $\theta = \theta_{con} + \dfrac{r}{R}\theta_{tw}$, with θ_{tw} being the fixed torsion (by design) and $\theta_{con} = \theta_0 + \theta_{1c}\cos\psi_i + \theta_{1s}\ \text{sen}\psi_i$. These last interventions lead to the previously obtained Equation (15), still in the reference frame R_t.

For the evaluation of the axial flux parameter $\lambda(\psi)$, the Meijer-Dress formulation (Meijer Drees, 1949) allows the consideration of a cyclic variation of the parameter λ in reference frame R_t, according to azimuth ψ. This formulation leads to the previously obtained Equations (16) and (17), which give the cyclic components as previously obtained in Equation (18). The value of λ_0 is calculated by an iterative method (Newton-Raphson), and the values of λ_{1c} and λ_{1s} are calculated by replacing λ with the value λ_0. The element forces dF_{xia}, dF_{yia}, dF_{zia} are spatially integrated along the blade (from 'e' to 'R'), still in reference frame R_t. The dynamic pressure is adopted as $S = \rho ac(\Omega R)^2$, leading to the previously obtained Equation (19).

In general, the ratio *e/R* is small. We have for the AS355 F2 aircraft: R = 5.34 m and e = 0.67 m, which leads to e/R = 0.12. The simplifying hypothesis $R^n - e^n \approx R^n$ is carried out (n being a natural number). In this way, except for R - e ≈ R, the result leads to an error of less than 0.12% in the effort calculations, which is neglected.

RESULTANT FORCE APPLIED TO THE ROTOR HUB

The resultant is obtained from the previously established relationship:

$$\overrightarrow{\left(\frac{dH}{dt}\right)}_{hub/Rg} = \overrightarrow{M}_{blade\rightarrow hub} + \overrightarrow{M}_{fuselage\rightarrow hub}\,.$$

However, it is necessary to change the reference frame to the fixed R_f, for the aerodynamic efforts (since these were calculated in the rotating rotor frame R_t). The efforts of the blade on the hub were previously obtained as Equation (20). Substituting F_{xia}, F_{yia}, and F_{zia}, we obtain, in the reference frame R_f, the components of the resultant force on the rotor hub.

RESULTING MOMENTS IN THE ROTOR HUB

As previously presented, the moment in the rotor hub $\overrightarrow{M}_{blade\rightarrow hub}$ (concerning point O) due to the forces F acting on the blade, in the reference frame R_f, is determined with components given as

$$M_x = \left[\overrightarrow{OK_i}\Lambda\vec{F}_{blade\rightarrow hub}\right].\vec{X} = e\ \mathrm{sen}\psi_i F_z$$
$$M_y = \left[\overrightarrow{OK_i}\Lambda\vec{F}_{blade\rightarrow hub}\right].\vec{Y} = e\ \cos\psi_i F_z$$
$$M_z = \left[\overrightarrow{OK_i}\Lambda\vec{F}_{blade\rightarrow hub}\right].\vec{Z} = e\ \cos\psi_i F_y - e\ \mathrm{sen}\psi_i F_x + K_{i\delta} + C_{i\delta}\dot{\delta}_t$$

In the first vector of this dot product, the arm is OK and the inverted "V" denotes the cross product. Thus, the three components $\overrightarrow{M}_{blade\rightarrow hub}$ in the reference frame R_f are obtained directly.

RESULTING WRENCH IN THE HUB OF A N-BLADE ROTOR

The six expressions just established are equally valid for each of the blades that make up the rotor (so far they are periodic in ψ and therefore non-linear expressions). The global wrench of the efforts is obtained as the sum of these rigid body components, according to the number of blades, as previously obtained in Equation (21).

BLADE DISPLACEMENTS EQUATION - FLAPPING DEGREE OF FREEDOM

Applying Newton's 2nd Law in the reference frame R_g to the simply articulated blade, now taking moments concerning K, as seen in Figure (11), in flapping, followed by lead-lag, we obtain: $\overrightarrow{\left(\frac{dH}{dt}\right)}^{K_i}_{blade/Rg} = \overrightarrow{M}^{K_i}_{\substack{\text{external forces}\\ \text{on the blade}}} = \int_e^R (\overrightarrow{K_i M} \wedge \overrightarrow{\gamma_M})dm_i$, where the moment of the external forces is $\int_e^R (\overrightarrow{\gamma_M})dm_i$ and $dm_i = mdr$.

This time, the time derivative of the angular momentum ($H=I\Omega$) is not zero, since it considers the product of the moment of inertia by the time derivative of the product of the radius and the linear velocity (in the X_iZ_i plane) of the point M on the blade, which is equal to the angular velocity Ω. The value of 'I' is derived, internally, from the integral of the linear acceleration in *m*, and is assumed to be constant (rigid body). Then the calculation of the integrand follows the previously obtained Equation (22).

Through the linear transformation matrix corresponding to a rotation ($-\psi$) around Z, we move to the rotating rotor reference frame R_t. Considering small-displacement angles in β, δ, and θ (with the corresponding simplifications), and also neglecting the triple products between the angles β, δ and their derivatives, when compared to their double products, given that these are small angles, after some intermediate steps, we have, finally, in the reference frame R_t the derivative concerning the time of the product of the radius times the linear velocity of point M over the blade, as previously obtained in Equation (23).

Flapping movement equations

With the above-calculated integrand in hand, we focus on the movement around the flapping axis in K, $\overrightarrow{Y}_p \equiv \overrightarrow{Y}_t$. Hence, for the projection on the Y_i axis, the 2nd Law applied to the joint at K (in flapping), in the reference frame R_t, gives, with $dm_i = mdr$:

$$\overrightarrow{\left(\frac{dH}{dt}\right)}_{\text{blade i/Rg}} = \vec{M}_{\substack{\text{forces on blade i}\\ \text{flapping around K}}} = \int_e^R (\overrightarrow{K_i M} \wedge \overrightarrow{\gamma_M})_Y \mathrm{d}m_i.$$

The dynamic momentum theorem, in a projection on the y_i axis, after some intermediate calculations, leads to the previously obtained Equation (24). Considering the static moment and the flapping inertia for the blade as defined, the dynamic moment formulation leads to the Eq. (25). By using the aerodynamic forces on blade *i*, on axis Z_t, dFz_i^a as previously obtained, calculating the integral on the blade, assuming the cyclic nature of ψ, as well as the truncation of the Fourier series expansion of each term

$$\theta_{con} = \theta_0 + \theta_{1c}\cos\psi_i + \theta_{1s}\operatorname{sen}\psi_i,$$

$$\beta = \beta_0 + \beta_{1c}\cos\psi_i + \beta_{1s}\operatorname{sen}\psi_i \text{ , and}$$

$$\delta = \delta_0 + \delta_{1c}\cos\psi_i + \delta_{1s}\operatorname{sen}\psi_i,$$

leads to the previously obtained Equation (26). Equation (26) identifies the consecrated form of the vibration equation, of a Mass-Spring-Damper System, by its resulting terms of stiffness and damping due to mass (inertia), where the latter is in the second coupled member with the forcing term (equally divided by the inertia term). To eliminate the periodic nature of these ODE obtained above, a change of their domain from *t* (in ψ) to that of frequency (in cyclic θ) is made through the Coleman operators (Coleman & Feingold, 1957), as one of the so-called linear Fourier Transforms, through the Method of Operators. This method consists of the simultaneous application of each member of the flapping equation within the parentheses of each of the following operators: $\frac{1}{2\pi}\int_0^{2\pi}(\dots)d\psi$, $\frac{1}{2\pi}\int_0^{2\pi}(\dots)cos\psi d\psi$ and $\frac{1}{2\pi}\int_0^{2\pi}(\dots)sin\psi d\psi$. In practice, as mentioned before, the advantage achieved is shown in converting that ODE into several separable algebraic equations according to each of the constant components (β_0, β_{1C}, and β_{1S}) independent of ψ. The double products of angles compared to the angles themselves are neglected. In this way, the influence of the lead-lag angle on the beating movement will be neglected, which means to neglect δcosψ or δsinψ in this equation. Following the same steps, with intermediate calculations as in Section 3, three algebraic equations are then obtained, independent of ψ, as coupled functions of the constant components β_0, β_{1C}, and β_{1S}. However, it is worth introducing, for simplification, the Lock Number $\gamma = \rho ac\frac{R^4}{I_\beta}$ (parameter of the blade that relates aerodynamic forces with inertia forces), leading to the previously obtained flapping Equation (27).

BLADE DISPLACEMENTS EQUATION: LEAD-LAG DEGREE OF FREEDOM

In this case, the aim is to move around the lead-lag axis at joint K, that is, we have that $\vec{Z}_p \equiv \vec{Z'}_p$. But in order not to change the referential of the previous results, the 2nd Law in rotational movements is applied again in the reference frame R_t, for the component around $Z_i(R_t)$, assuming that the restoring moment due to the frequency adapter (which avoids ground or air resonance by reducing the blade frequency in lead-lag, moving it away from the fuselage resonance frequency value) is also by the Z_i axis, as considered before for the calculation of M_Z. This theorem gives, in projection onto the Z_i axis, the moment of the drag forces of the blade around point K as in the previously obtained Equation (28). This degree of freedom is maintained under mechanical artificial damping for reasons of dynamic stability (associated with ground and air resonances, which can destroy the aircraft in a few seconds). The restoring moment due to the frequency adapter in lead-lag is: $K_{i\delta}\ \delta_i + C_{i\delta}\ \dot{\delta}_{it}$. Given that $I_\beta = I_\delta = \int_e^R (r-e)^2 mdr$ (since the blade is assumed to be modeled as a line independent of axes and there is no cross-section), introducing the obtained expression for dF_{yi}^a leads to the previously obtained Equation (29).

After calculating the integral on the blade, making the assumptions $R^n - e^n \approx R^n$, the truncation in the Fourier Series expansion previously described in Equation (30), and neglecting the triple angle terms (eg: $\theta_0 .\beta_{1c} .\delta_{1s} \approx 0$, etc.) against the double products, given that θ, β, and δ are small angles, one can resort once again to the application of the operators in the differential equation (29) (again representative of a Mass-Spring-Damper System), whose result is, finally, the algebraic equations of lead-lag motion previously obtained in Equations (31) (for δ_0), (32) (for δ_{1c}), and (33) (for δ_{1s}), which describe the lead-lag angle $\delta(\delta_0,\delta_{1c}\ e\ \delta_{1s})$ as a function of the pitch angle $\theta(\theta_0,\theta_{1c}\ e\ \theta_{1s})$ and the flapping angle $\beta(\beta_0,\beta_{1c}\ e\ \beta_{1s})$.

ROTOR-FUSELAGE SYSTEM MODELING EQUATION (STATIONARY)

THE HYPOTHESES

We return to the six expressions of the wrench of the efforts on the rotor, as previously calculated, and apply them to the case of a rotor composed of N blades considered strictly identical. In this way, this wrench can be considered constant over time, and thus can be treated as stationary.

THE PARAMETERS

Added to the displacements θ, β, and δ (referring to the rotor state), α, ψ, and T_{RC} are considered to correspond to the fuselage attitude, with small angles which are used in the numerical simulation in radians. Thus, the parameters treated are the flight parameters $(\lambda_0,\lambda_{1c},\lambda_{1s},\beta_0,\beta_{1c},\beta_{1s},\theta_0,\theta_{1c},\theta_{1s},\delta_0,\delta_{1c},\delta_{1s})$, which are added to the fuselage attitude ($\theta_0,\theta_{1c},\theta_{1s},\alpha_f,j_f,T_{Ra},\beta_0,\beta_{1c},\beta_{1s},\delta_0,\delta_{1c},\delta_{1s}$).

APPLICATION OF THE COLEMAN TRANSFORMATION

In this step, the same integral operators are applied to the six expressions of the previously calculated wrench of the efforts on the rotor, as they are then periodic functions, to obtain a linear formulation whose effect on each component F and M is its description in the form of a linear combination of the flight parameters $(\lambda_0,\lambda_{1c},\lambda_{1s},\beta_0,\beta_{1c},\beta_{1s},\theta_0,\theta_{1c},\theta_{1s},\delta_0,\delta_{1c},\delta_{1s})$. Next, for simplification purposes, the triple products of angles are neglected against the double products in the expressions of F_x, F_y, and M_z, as well as the double products of angles, are neglected against the angles themselves in the expressions of F_z, M_x, M_y.

The efforts F and M of the rotor hub are expressed, therefore, as a function of the different flight parameters, post-Coleman Transformation (Coleman & Feingold, 1957) - now in the frequency domain and constant in time, where:

- the induced velocity coefficients $(\lambda_0,\lambda_{1c},\lambda_{1s})$ (response or output) are determined by the Meijer-Dress formulation (Meijer Drees, 1949);
- the torsion θ_{tw} is an adopted design data (a built-in fixed-parameter);
- the coefficients of the flapping movement $(\beta_0,\beta_{1c},\beta_{1s})$ (response or output) are calculated using the equilibrium equations as a function of $\theta_0,\theta_{1c},\theta_{1s}$ (and other parameters already known or calculated);
- the coefficients of the lead-lag movement $(\delta_0,\delta_{1c},\delta_{1s})$ (response or output) are calculated using the equilibrium equations as a function of ($\theta_0,\theta_{1c},\theta_{1s}$) and $(\beta_0,\beta_{1c},\beta_{1s})$.

The six equations of wrench (the efforts F and M) on the rotor hub are therefore functions of only three parameters: $\theta_0,\theta_{1c},\theta_{1s}$ (excitation or input, as a pilot control action through collective and cyclic commands).

(STATIC) BALANCE OF THE ROTOR-FUSELAGE SYSTEM

Assumptions:

- known/adopted design parameters: dimensions and limits (in this case, for AS 355F2).
- the fuselage, moving immersed in the air, does not produce L but produces D (from pressure and friction).
- the negative lift effect of the horizontal empennage 'T_{eh}', assumed modeled as $T_{eh} = 1/2\rho V^2(C_zS)_{eh}$, where $(C_zS)_{eh}$ is the equivalent lift area factor, assumed independent of the empennage profile (C_l and S).
- Tail rotor anti-torque thrust (T_{RC}), counterclockwise, is necessary to balance the rotor-fuselage system in reaction to the action of the main rotor on the fuselage. The value of T_{RC} is obtained corresponding to a directional lateral attitude in yaw (γ_f) null, that is, without skidding of the fuselage in forward flight.
- the negative value: installation of the Squirrel's tail rotor being on the right side (a second puller).

The following variables are still unknown: the efforts F and M of the rotor hub are a function of the three parameters $\theta_0, \theta_{1c}, \theta_{1s}$ (excitation or input, as the pilot control action through collective and cyclic commands). The attitudes (responses or outputs) of the fuselage are: longitudinal in pitch (α_f), lateral in roll (ψ_f). The rotor anti-torque thrust (T_{RC}) (obtained by assuming zero yaw lateral (γ_f)). In the case to be studied (stationary stabilized horizontal forward flight with constant speed), the aerodynamic reference frame and the Galilean frame are confounded Ra≡Rg but, due to the pitch α_f, Rh≠Rg.

As the rotor hub efforts F and M were initially expressed in the fixed rotor frame R_f, a linear transformation is necessary according to a rotation ($-\alpha_m$) around Y_f. With this, the wrench is transformed from the fixed rotor reference R_f into the helicopter reference frame R_h, as previously shown in Equation (34).

Analogously:

- as the forward flight speed V was expressed in the aerodynamic reference R_a, a rotation (α_f) around Y_f is applied. From there, V is leaded from the aerodynamic reference frame R_a to the helicopter reference frame R_h, as previously shown in Equation (35), where: $\alpha_f = \alpha_D - \alpha_m$.
- the helicopter's weight (descending) is passed from the Galilean frame R_g to the helicopter frame R_h by a rotation ($-\alpha_f$) around $Y_g = Y_h$. In continuation, another rotation ($-\varphi_f$) around X_h follows, as previously shown in Equations (36) and (37).

The balance of F along the three axes, in the R_h helicopter frame, leads to the previously shown Equation (38).

The equilibrium of moments M around the rotor hub, relative to which the fuselage rotation is zero, in the helicopter reference R_h, gives: $\sum \overrightarrow{M}_0 = 0$, leading to the previously shown Equation (39).

And we finally arrive at the six homogeneous equations, previously shown in Equation (40), representing the balance of the fuselage in R_h. As this is an equilibrium equation, there are no accelerations (which arise with the introduction of defects in the discussion that follows).

The previous hypothesis of small angles is maintained to facilitate the mathematical treatment of the solution, and we have the wrench of the applied efforts on the rotor hub in the R_h reference frame, as previously shown in Equation (41).

Adding the three equations of flapping, the three equations of lead-lag, and the six equations of the rotor wrench, we have a system of twelve non-linear algebraic equations in the twelve unknowns ($\theta_0, \theta_{1c}, \theta_{1s}, \alpha_f, \varphi_f, T_{Ra}, \beta_0, \beta_{1c}, \beta_{1s}, \delta_0, \delta_{1c}, \delta_{1s}$).

4.3 Introduction of anisotropies in the main rotor (Direct Problem)

Here the model of the direct problem is addressed, meaning that here the defect is introduced, leading to changes in the vibration signature. The disturbance of equilibrium discussed above, by inserted anisotropies, from here on, also treated as defects. Therefore, as a system response, the vibrations are measured in the aircraft structure thanks to the associated accelerations. All anisotropies inserted in the blades are considered as if they were "equivalent" anisotropies to the different ones that are corrected by adjustments to the blade inertia (m_i) and/or the aerodynamic performance of its profile (θ_i).

From the previous equilibrium equations, it is known that, in the case of the conventional isotropic rotor, the Coleman Transformation (Coleman & Feingold, 1957) provides that the efforts *F* and *M* in the rotor hub, as well as the twelve flight parameters (response) θ, β, δ (these in their three cyclic components) and α_f, ψ_f, T_{Ra}, are constant concerning time for each equilibrium position (since it eliminates periodic terms sine(ψ_i) and cosine(ψ_i)). These efforts applied to a fuselage assumed to be rigid and in balance with external forces applied to the fuselage, in the conditions of the stationary flight, or forward flight at constant speed. Consequently, in both cases, all the predicted accelerations of the fuselage (the linear accelerations of its CG and the angular accelerations around it) are null. From this equilibrium position (as static equilibrium), the values of the resulting attitude of the fuselage are obtained: longitudinal pitch (α_f); lateral or roll (φ_f); and yaw (ψ_f).

The introduction of anisotropies for a blade *i* (while the other blades are assumed to be unchanged) and the calculation of their new angular displacements θ, β, and δ on the rotor leads to new forces in the hub, which are no longer constant (being functions of ψ_i), that is, they are time-varying efforts according to the frequency 1Ω. Hence, the fuselage equilibrium equations are no longer homogeneous (as previously calculated), as the 2nd part (the right-hand side of the equation) leads to fuselage accelerations of the same frequency. It is worth mentioning that the displacement of each blade is a result of the contribution of constant efforts in time (isotropic equilibrium) and of efforts in these variables under 1Ω frequency (small variations around that equilibrium position, with the defects generating accelerations). From this point of view, the movement of each blade can then be decomposed into the movement of the blade itself (translated by the three angular displacements in flapping and the three angular displacements in lead-lag) added to that of the fuselage with which the blade is linked (translated by the displacements of the rotor - angular displacements α_f, φ_f, T_{RC}, and the input θ_0, θ_{1C}, θ_{1S}). In this oscillation, it is assumed that a new attitude of the fuselage assumes another variable portion, added to the previous one (isotropic equilibrium), which is unique and assumed unchanged after the introduction of anisotropies. This means that the defects do not alter the fuselage equilibrium attitudes but introduce variations around 1Ω them. In this way, the accelerations do not have permanent terms in time and are constituted only by periodic parcels (since in the isotropic case they are null) in $\psi(t)=\Omega_t$, for the six degrees of freedom (DoF) about the fuselage CG, as previously shown in Equation (42).

INFLUENTIAL PARAMETERS

It is worth remembering that any azimuthal position (ψ_i) of a blade corresponds to the angular space (involving the angular frequency of the rotor) associated with time by the relation $t = \psi_i / \Omega$, counted from the moment of the passage of the blades through the reference position, $\psi_i = 0$.

This reference, in practice, corresponds to the synchronism signal given by the magnetic sensor installed on the fixed plateau of the main rotor mast. To calculate the torque of the forces acting on the rotor hub updated with defects, it is necessary and sufficient to know the corresponding new values of $\lambda(\psi_i),\theta_i(\psi_i),\beta_i(\psi_i),\delta_i(\psi_i)$, the mass of the blades (m_i), the static moment of the blades (m_{si}), and the inertia of the blades ($I_{\beta i}$). It is considered that there were no changes in the parameters of the blades (R, e, c) and their profile (C_{d0}, a), and neither in the advancing rate μ nor the air density ρ.

Regarding the before-mentioned parameters, one has that:

• mass of the blades: $m_i = \int_e^R dm_i = \int_e^R m dr$. An anisotropy in m_i (and consequently in m_{si} and $I_{\beta i}$) can be considered as an "equivalent" mass change in the radial position of the rotor, where the equilibrium mass (balance platelets, in this case) can be added.

• static moment of the blades: $m_{si} = \int_e^R r dm_i = \int_e^R r m dr$, where m is the blade mass;

• blade inertia: $I_{\beta_i} = \int_e^R r^2 dm_i = \int_e^R r^2 m dr$. The three parameters m_i, m_{si}, and $I_{\beta i}$ can be different for each blade, due to the anisotropies. Furthermore, they are interdependent, that is, a variation of m_i implies a corresponding variation of the values of m_{si} and $I_{\beta i}$. The insertion of an equilibrium mass (Δm_i), associated with its RME (distance of the balance plate mounting to the rotor hub), leads us to changes in the parameters of blade *i*, based on the isotropic values of m_{si} and $I_{\beta i}$ ("iso" index, below):

$$m_{\rho_i} = m_{\rho_{iso}} + \Delta m_i$$
$$m_{s\rho_i} = m_{s\rho_{iso}} + \Delta m_i \, x \, RME$$
$$I_{\beta_i} = I_{\beta_{iso}} + \Delta m_i \, x \, RME^2$$

• air density (ρ): this parameter is provided, for example, from the standard atmosphere tables, and depends on pressure-altitude and temperature.

• advancing rate (μ): Dimensionless parameter of the helicopter's speed about the air (V) and of the rotor disk inclination (α_D) in pitch, which depends on the longitudinal position of the cyclic control. The fuselage pitch angle (α_f) depends on the inclinations of the disc, rotor (α_D), and mast (α_m) so that $\alpha_f = \alpha_D - \alpha_m$ (it is seen that α_f is smaller than α_D, justifying the compensation of α_m to meet maneuverability/flight quality requirements);

• the parameters of the blades (R, e, c) and their profile (C_{d0}, a): Although they also constitute possible anisotropies, within the scope of this study, they are considered constant and independent of the blades;

• The induced speed $\lambda_i(\psi_i)$: Proportional to the advancing rate (μ) - hence, to the rotor disk inclination (α_D); to the thrust coefficient (C_T) (which is due to the helicopter's thrust - Fz); the air density (ρ); and the azimuthal position (ψi). As it is assumed that there is no anisotropy on the induced velocity, λ does not depend on blade *i*;

• The blade pitch $\theta_i(\psi_i)$: As already introduced, anisotropies linked to the blade profiles can be considered as "equivalent" variations of the blade pitch $\theta_i(\psi_i)$, which varies according to the azimuthal position (ψi) of the blade and to the balance of the fuselage, in the cases considered of stationary flight or forward flight at a constant speed (μ = constant, non-zero).

For the case of fuselage equilibrium, it is assumed, as external forces acting:

- the rotor hub efforts;

- the weight of the helicopter applied at the CG position of the fuselage;

- the fuselage lead-lag, assumed to be applied at a fixed point (A) and acting independently of the fuselage pitch;

- the negative lift of the horizontal empennage assumed to be applied at a fixed point and acting independently of the fuselage pitch; and

- The anti-torque thrust of the rotor, is necessary to balance the torque applied by the main rotor. $\theta_i(\psi_i)$ can be changed through the length of the blades' control rods (which changes the collective pitch θ_0 of blade i); and/or

- the tab angle adjustment, whose profile bending creates an aerodynamic moment around the elastic axis of the blade (transmitting forces to the fuselage through the rods), is proportional to the forward flight speed. Hence, the tab angle adjustment does not affect the taper (β_0) of the rotor in stationary flight, however, it is proportional to μ, being more pronounced on the forward blade side than on the retreating blade. In this work, the tab angle adjustment is simulated as an anisotropy θ_{is}. Therefore, making $\theta_{is} \neq 0$ (and other parameters equal to zero) in the flapping motion equations, for stationary flight ($\mu = 0$), that is, hovering or vertical flight, one obtains: $\beta_0=0\ ;\ \beta_{1c} » -\theta_{1s}\ ;\ \beta_{1s}=0$. Analogously, for the forward flight condition ($\mu \neq 0$), we have $\beta_0 = \mu - \theta_{1s}$, which points out to an increase in taper (β_0) proportional to θ_{is} (rotor pitch in forward flight) and μ, as wished. The calculation of $\theta_i(\psi_i)$ is divided into two steps:

1 - in the absence of anisotropies on the rotor, the blade pitch (θ_0, θ_{1c}, θ_{is}) comes from the isotropic rotor equilibrium equations, as previously seen;

2 - the anisotropies are introduced on a blade by adding the desired increment (according to only to θ_{0i}, θ_{1si}), under the assumption that the pitch of the other blades is not altered. Then, the resulting pitch of the blades (θ_0, θ_{1c}, θ_{is}) is calculated again, assuming that there is no influence on the pitch of the other blades.

• The flapping movement $\beta_i(\psi_i)$: As seen before, β_i depends on the azimuthal position (ψ_i), the pitch $\theta_i(\psi_i)$, the induced velocity $\lambda(\psi_i)$, the air density (ρ), the parameters of the blade (R, e, c, a, m_{si}, $I_{\beta i}$), and of the advancing rate (μ). Analogously to the previous parameter, the calculation of $\beta_i(\psi_i)$ is divided into two steps:

1 - in the condition of the absence of anisotropies on the rotor, all blades have the same mass (m), static moment (m_s), a moment of inertia (I_β), and pitch (θ) (obtained from the helicopter equilibrium, as seen before). Thus, we have an expression of $\beta(\psi_i)$ which is valid for all blades.

2 - the three types of anisotropies adopted as equivalent defects on a blade (i) are introduced, namely:

- balance mass on the blade handle (change of m_i, m_{si}, $I_{\beta i}$)
- adjustment of the blade control rod (full change of θ_i, as it acts on all ψ)
- the tab angle adjustment (change of θ_{1si}, as it acts according to the flow)

Then, the flapping of this blade ($\beta_i(\psi_i)$) is calculated again, assuming that there is no influence on the flapping movements of the other blades.

• The lead-lag movement $\delta_i(\psi_i)$: As seen before, δ_i depends on ψ_i, θ_i, λ_i, β_i, the air density (ρ), the advance rate (μ), and the blade parameters (R, e, c, a, m_{si}, $I_{\beta i}$).

The displacement δ can also be changed due to anisotropies in the frequency adapter (either in its stiffness $K_{\delta i}$, or in its damping, $C_{\delta i}$).

Like what was done for θ_i and β_i, this calculation is divided into two steps:

1 - in the condition of the absence of anisotropies on the rotor, the lead-lag (δ_0, δ_{1c}, δ_{1s}) comes from the isotropic rotor equilibrium equations, as seen before;

2 - the anisotropies considered on a blade *i* are introduced, assuming that there is no influence on the lead-lag movements of the other blades.

CORRECTIONS APPLICABLE TO THE MAIN ROTOR

This item addresses the nature of the defects inserted in the mathematical model in use, which is adopted according to the corrections available in this research. The defects to be introduced are among the following:

- Inertia or mass defects: change in m_i, $m_{si,}$ and $I_{\beta i}$;
- Defects in the aerodynamic performance of the profile;
- Length of the pitch link (pitch rod): change in θ_{0i}; and
- Adjustments in the angle of tab: change in θ_{1si} (not adopted in this work).

The above discussion referred to the Direct Problem, in which a change is made, leading to changes in the vibration signature. In the case of the Inverse Problem, changes in the signature lead to the possible rotor variables that may have caused that change, and to a suggestion of the possible corrections/adjustments to be performed, to correct the unbalance and/or out-of-track blade. It is important to mention that the correction values to be suggested (as a diagnosis of defects) according to the results of the Inverse Problem must be submitted to the limits recommended in the Manufacturer's Manual, beyond which the foreseen action is the replacement of the defective item indicated by the algorithm.

RESULTANT EFFORTS WRENCH IN THE ANISOTROPIC ROTOR HUB

Carrying out the same calculations as previously described, for blade *i*, now after introducing the defects (using the new values of m_i or θ), the new pitch angles (θ_i), flapping angles (β_i), and its associated lead-lag (δ_i). The efforts F and M on the rotor hub are due to these new angles. These efforts are updated according to the previously derived expressions for forces *F* and moments *M*, so the resultant output (associated accelerations) has components in $\sin\psi$ and $\cos\psi$ (cyclic terms, truncated in 1Ω) added to the 1st constant component (index zero - the same as in the case of the isotropic rotor equilibrium), leading to the previously derived Equation (43). As before, we will apply to the expression of efforts of the operators: $\frac{1}{2\pi}\int_0^{2\pi}(...)\sin\psi d\psi$ and $\frac{1}{2\pi}\int_0^{2\pi}(...)\cos\psi d\psi$ to the periodic components in $\sin\psi$ and $\cos\psi$ of the blade *i*, culminating in the constant terms 1C and 1S. These transformations lead to the twelve expressions previously obtained in Equations (44) to (55) (constant terms 1C and 1S), where the index "*i*" of the various angles (the pitch, flapping, and lead-lag) is suppressed for simplicity of notation. To apply the sum of the forces acting on each blade, at this time one proceeds differently from Section 3. In the case study (N = 3 blades), the azimuth of each of the three blades must be considered, as they are now distinguished from each other, so it is not enough just to multiply by N. Adopting $\psi 1 = \psi$ (red blade), $\psi 2 = \psi + 2\pi/3$ (blue blade), and $\psi 3 = \psi + 4\pi/3$ (yellow blade), leads to:

$$Fx_1 = Fx_{01} + Fx_{1c1}\cos\psi + F_{x1s1}\mathrm{sen}\psi$$

$$Fx_2 = Fx_{02} + Fx_{1c2}\cos(\psi + 2\pi/3) + Fx_{1s2}\mathrm{sen}(\psi + 2\pi/3) = Fx_{02} + Fx_{1s2}\cos\psi - Fx_{1c2}\mathrm{sen}\psi$$

$$Fx_3 = Fx_{03} + Fx_{1c3}\cos(\psi + 4\pi/3) + Fx_{1s3}\mathrm{sen}(\psi + 4\pi/3) = Fx_{03} - Fx_{1c3}\cos\psi - Fx_{1s3}\mathrm{sen}\psi$$

Finally, by harmonic balance, we have:

$$\{Fx_{1c}\}_{rotor} = Fx_{1c1} + Fx_{1s2} - Fx_{1c3} \qquad \{Mx_{1c}\}_{rotor} = Mx_{1c1} + Mx_{1s2} - Mx_{1c3}$$

$$\{Fx_{1s}\}_{rotor} = Fx_{1s1} - Fx_{1c2} - Fx_{1s3} \qquad \{Mx_{1s}\}_{rotor} = Mx_{1s1} - Mx_{1c2} - Mx_{1s3}$$

$$\{Fy_{1c}\}_{rotor} = Fy_{1c1} + Fy_{1s2} - Fy_{1c3} \qquad \{My_{1c}\}_{rotor} = My_{1c1} + My_{1s2} - My_{1c3}$$

$$\{Fy_{1s}\}_{rotor} = Fy_{1s1} - Fy_{1c2} - Fy_{1s3} \qquad \{My_{1s}\}_{rotor} = My_{1s1} - My_{1c2} - My_{1s3}$$

$$\{Fz_{1c}\}_{rotor} = Fz_{1c1} + Fz_{1s2} - Fz_{1c3} \qquad \{Mz_{1c}\}_{rotor} = Mz_{1c1} + Mz_{1s2} - Mz_{1c3}$$

$$\{Fz_{1s}\}_{rotor} = Fz_{1s1} - Fz_{1c2} - Fz_{1s3} \qquad \{Mz_{1s}\}_{rotor} = Mz_{1s1} - Mz_{1c2} - Mz_{1s3}$$

(DYNAMIC) BALANCE OF THE ROTOR-FUSELAGE SYSTEM

The previously-derived balance equations of the rotor-fuselage system are no longer homogeneous after the introduction of rotor defects, hence the classification of the balance as dynamic. The balance of external forces is presented in the previously derived Equation (56). One can observe in Equation (56) that the 2nd term (the right-hand side) is the product of the total mass of the aircraft by the periodic acceleration of the CG along each axis.

The equations of moments were previously obtained with the equilibrium about the rotor hub. As the focus is on the motion of the CG of the aircraft, these equations must be rewritten to consider the wrench of the external efforts applied to the rotor hub (index zero) and this CG. Furthermore, there is a need to know the fuselage moments of inertia (due to its rotating movements) about the CG, which change as a function of the aircraft centering. Thus, the moments of inertia in roll (I_{xx}), pitch (I_{yy}), and yaw (I_{zz}) are considered, as well as the product of inertia representing the yaw-roll coupling (I_{zx}), while the other couplings are assumed to be null.

From the moments and products of inertia and the mass M, the radii of gyration ρ are obtained as a function only of the centering X_G and Y_G by the expression $I = M\rho^2$. The balance of moments about the CG is described by $\sum M = I\alpha$, where M comes from the global wrench of efforts on the hub, the linear measures are the moment arms, which leads to the previously derived Equations (57) and (58).

One must note in these Equations (57) and (58) that α_{f0}, φ_{f0}, and T_{RA0} were obtained from the fuselage equilibrium with the isotropic rotor, as derived before. Also, $T_{RC\ 1C}$ and $T_{RC\ 1S}$ are the periodic components of the tail rotor thrust required to nullify the ψ_{f1C} and ψ_{f1S} components of the yaw motion (assumed constant). Since ψ_{f1C} and ψ_{f1S} were assumed not

to be zero in the calculation of the second derivative of ψ_f, then it is required that $T_{RC\ 1C} = T_{RC\ 1S} = 0$ (therefore, it is assumed that the tail rotor does not provide cyclic thrust that can cancel the cyclic motion in yaw).
To find the 12 unknowns of the fuselage accelerations (6 linear and 6 angulars): Ω^2 (x_{1c}, x_{1s}, y_{1c}, y_{1s}, z_{1c}, z_{1s}, α_{f1c}, α_{f1s}, φ_{f1c}, φ_{f1s}, ψ_{f1c}, ψ_{f1s}), one must apply again, to the variable equilibrium equations (thanks to the expansion of the three angular accelerations), the operators: $\frac{1}{2\pi}\int_0^{2\pi}(...)\sin\psi d\psi$ and $\frac{1}{2\pi}\int_0^{2\pi}(...)\cos\psi d\psi$. The efforts on the rotor hub already obtained, leads to the previously derived Equations (59) to (70).

TRANSFER OF THE CG ACCELERATIONS TO FUSELAGE POINT 'M'

The accelerations of the rigid fuselage, excited by the rotor and by external forces applied to the fuselage, are known and they are applied to CG. Now, they need to be transported to the fuselage points indicated by manufacturers in which accelerometers are intended to be placed, and the vibration quantities are intended to be obtained. In this context, we have the position vector GM of a point (*M*) of the fuselage about its CG (origin as point G) of the helicopter reference frame R_h. From which, through linear transformations based on rotations of ($-\psi_f$), ($-\alpha_f$), and ($-\varphi_f$), as shown previously in Equation (71), the same vector position is written in the Galileo reference frame, parallel to the aerodynamic frame ($R_g \equiv R_a$), with X, Y, Z values of the coordinates of the points in the helicopter frame (R_h). Carrying out the necessary algebra, the vector is derived twice concerning time t to provide accelerations. Considering, in Galileo's frame of reference, a point G' coincident with point G, we have that the acceleration of the CG (point G) has only linear terms (because it is a point), and is given by previously obtained Equation (73). The acceleration of point *M*, in reference frame R_h is given by previously obtained Equation (72). From this frame, transforming to the helicopter frame, again, we have $(d^2GM/dt^2)_{Rh}$, as previously shown in Equation (74). Small angles ψ_f, α_f, and φ_f is again used and, for simplification, the triple products of angles are also neglected concerning the double products, leading to the previously obtained Equation (75). Considering in X that: $d^2X_M/dt^2 = \Omega^2 X_M = \Omega^2(-X_{M1c}\cos\psi - -X_{M1s}\sin\psi)$, we will also have the analogue for Y and φ. To find the six unknowns of the three linear accelerations of the fuselage point *M*, we will apply, as before, the operators to these three equations. The six unknowns were previously detailed in Equation (76).

AMPLITUDE AND PHASE OF THE RESULTING ACCELERATIONS

The efforts on the rotor hub are expressed as a function of the azimuth coordinate of the red blade: $\psi_1 = \psi = \Omega_t$, where t represents the time after the red blade passes through the nose of the helicopter (home position $\psi = 0$) when the magnetic sensor triggers the timing signal. From this moment (then t = 0), the Theory of Complex Numbers, applied to the amplitudes of the sine and cosine vibration measured in the fuselage, allows the acceleration to be expressed in terms of amplitude and phase. Thus, from the measured information on x (x_{1s}, x_{1c}), y (y_{1s}, y_{1c}), and z (z_{1s}, z_{1c}), we have the amplitudes at the CG and point *M*, as previously detailed in Tables 2 and 3.

4.4 Validation of the calculation code

APPLICATION OF THE MODEL: COMPUTATIONAL SIMULATION

This computational resource constitutes a valuable tool for simulating the model's responses to the excitations associated with introduced anisotropies equivalent to typical defects, such as main rotor unbalance and out-of-tracking blades. Thus, the original computational code in FORTRAN for a 4-blade helicopter (Jorge, 1992) was written in MATLAB$^{(R)}$ for a 3-blade helicopter (González, 2012).

Within the so-called Direct Problem, the code is divided into two parts, as shown in Figure 24, by the structuring of the work: a first part for the calculation under the modeling of the fuselage-rotor system in equilibrium (this one called isotropic) in terms of the twelve parameters $\alpha(\psi)$, $\beta(\psi)$, $\delta(\psi)$, $\theta(\psi)$, $\varphi(\psi)$, T_{RC}, β_{0i}, β_{1ci}, β_{1si}, δ_{0i}, δ_{1ci}, δ_{1si}, θ_{0i}, θ_{1ci}, and θ_{1si}; and a second part to calculate the vibratory responses as variations (concerning the isotropic case), due to anisotropies, according to the amplitude and phase as obtained at a point *M* on the fuselage.

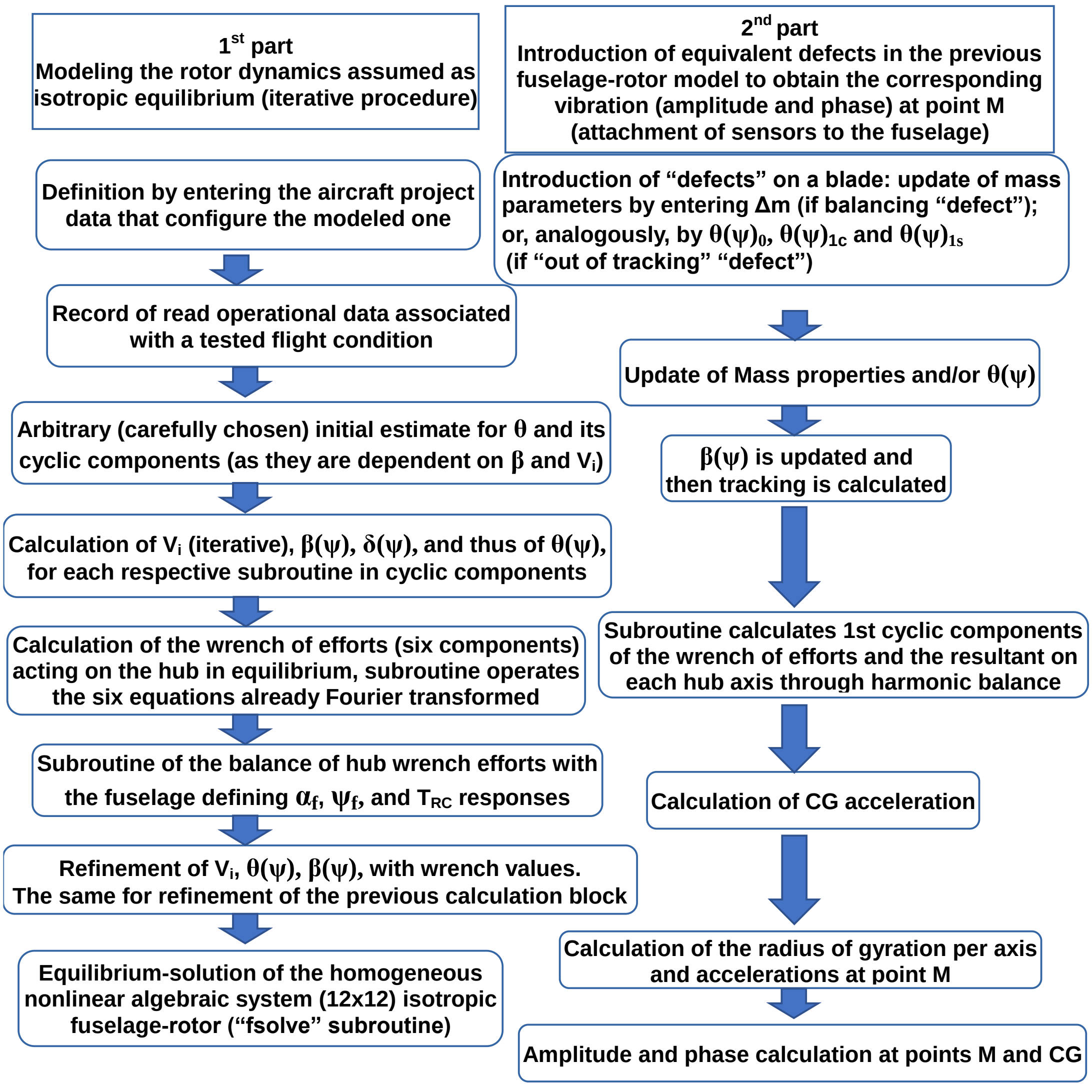

Figure 24: Flowchart of the subroutines of the computational code for the Direct Problem [Adapted from (González, 2012)]

The first part deals with the numerical resolution of a multidimensional system of twelve nonlinear algebraic equations (to twelve unknowns) governing the movement of the rotor-fuselage system, in the frequency domain (after applications of Fourier Integral Transform according to Coleman operators, as seen above). This first part requires a lot of iterations to define the proper input vector, as the components are linearly dependent and unknown. Internally, the solution process of this algebraic system includes its linearization by subroutines of the computational algorithm "fsolve", selected as the most adequate among the options available in the MATLAB$^{(R)}$ software environment.

Structured with aircraft design information, the resolution of these equations uses data from the executed flights as input and then reveals the dynamic behavior of the analytical model adopted according to small vibrations around the equilibrium. Briefly describing the code, Figure 24 presents a flowchart for the code. The code starts with the definition of the aircraft design data adopted, as previously presented, followed by the recording of obtained data associated with a flight condition. Once these data are gathered, a subroutine is activated that operates the previously discussed Meijer-Dress formulation, iteratively, according to the Newton-Raphson numerical method, to obtain the first estimate of the induced velocity Vi, as it is a requirement for the next task, which is to obtain, via the dedicated subroutines, the values of $\beta(\psi)$, $\delta(\psi)$ and $\theta(\psi)$, according to their cyclic components. These subroutines are initialized from a free but careful initial estimate for θ, whose value depends on β and Vi, which are not yet available, proving to be quite a sensitive part of the code. Numerical methods are expected to allow modeling with minimal simplifications while preserving the precision of the result. However, this approach requires a good initial estimation of the input vector to further find the solution to the system. In this case, although θ represents the command (from the pilot), around which the rotor needs to adapt, the convergence of the method of the 'fsolve' subroutine is sensitive to large variations, even though its internal algorithm predicts eventual problems of a distant estimate of the real root. These four variables are then used in the next subroutine that calculates the six components of the wrench acting on the hub in equilibrium, operating the post-Fourier Transform equations (six equations). In sequence, subroutines are called to provide the values of α_f, φ_f, and T_{RC}, based on the three equilibrium equations of the rotor-fuselage system. With these data, it is possible to recalculate, in a refinement step, the values of the first four variables before the next step: the calculation of the equilibrium of the fuselage-isotropic rotor nonlinear algebraic system. The best result of the 'fsolve' subroutine comes from the internal application of numerical optimization techniques that impose robustness to Newton's method in the calculation of each step, as offered by the MATLAB$^{(R)}$ software, and which makes use of its Jacobian matrix, previously evaluated as Equation (77), also provided by a specific subroutine. The result of this algorithm converges to the output vector composed of the twelve mentioned values. It is worth mentioning here the sensitivity of the functional parameters requested by this subroutine (according to the internal algorithm, the "fsolve" and the residual error), for each flight condition, to verify the convergence of the numerical method. Most optimization subroutines adopt a termination criterion, to end the calculation when the residual error (the difference between two successive iterations roots) and/or the difference between each iterative step are less than a value specified by the user. Hence, if this value is too large, the subroutine does not manage to find a solution that can effectively nullify the system of equations. Otherwise, if it is too small, the algorithm reaches the maximum number of iterations before the difference between two successive iterations, to obtain the root, has been reached. Having obtained the established scenario for the equilibrium behavior of the system in context, we move on to the second part of the Direct Problem, which does not require iterations: the introduction of primary anisotropies, that is, one at a time. Firstly, this is done by updating the mass parameters (if the balance "defect" is adopted) or the three cyclic components of θ (such as in the case of an out-of-tracking type of "defect") of the selected blade, using the sum of increments associated with the last values obtained (these three ones, again, by initial estimates).

From this point on, it is possible to recalculate the first cyclical components of the forces and moments that are applied to each blade according to the three adopted Cartesian axes, which, as mentioned before, are no longer constant. The following steps are analogous calculations of the resulting wrench of efforts on the hub, according to similar terms in sine and cosine (harmonic balance); the CG acceleration; the radius of gyration of the fuselage, needed to obtain, in the subsequent step, the accelerations at the CG and point M; and, finally, the amplitude and phase calculation at these points (the CG and point M).

VALIDATING THE MODEL: FLIGHT TESTS

In the task of demonstrating the applicability of the proposed mathematical model, we choose to compare the simulated response with real experimental data. Among possible sources of the same, it was decided to start a flight test campaign on a platform with the same parameters of the considered model. The platform adopted is an Aerospatiale-AS 355 F2 Squirrel Twin Engine, a representative model of a series, and belonging to the then Special Group of Flight Tests - GEEV (currently called Flight Tests and Research Institute - IPEV), one of the military organizations of the Department of Aerospace Science and Technology - DCTA, located in São José dos Campos, SP, Brazil.

The tests performed were a valuable instrument to support the research in context, as they met the test requirements, and were performed in compliance with the established provisions of the test order, which presented the complete analysis of the main risks, with a description of the causes, consequences, and the mitigating actions to be taken, as well as the emergency procedures to be adopted. The flight test schedule established the following registration points, corresponding to the flight profiles provided in the MET 62.10.00.603 Maintenance Manual for the aircraft (HELIBRAS, 1994):

- ground turn with the throttle adjusted to flight setting;
- hovering IGE (in ground effect) at 2 m above the ground, heading with the wind;
- leveled forward flight in maximum power continuous (PMC); and
- forward flight at the PMC, underside turns, left and right, leaning 45°.

Through these points, representative of the basic operating conditions, the aim is to collect vibration characteristics (amplitude and phase) of this aircraft, corresponding to balancing and tracking conditions at 1Ω frequency: first, in the condition within the tolerances recommended in the MET; and then outside them, as follows:

- yellow blade: two fewer balance platelets; all other blades balanced and inside tracking;
- analogous procedure with the red blade; and finally
- again with the rotor balanced, only the yellow blade is out of the ideal tracking.

The following references from the MET were adopted, for the case of rotor balanced, with adjusted tracking, for 1Ω: (with IPS being: " inches per second")

- ground turning and hovering at 2 m: in the Y direction < 0.2 IPS and tracking < 6 mm;
- level forward flight in PMC: in the Z direction < 0.2 IPS and tracking < 20 mm; and
- forward flight with lateral turns at ±45° incline in PMC: in Z < 0.35 IPS.

For the vibration data acquisition, a portable equipment ACES P2020 was used, coupled to two sets of accelerometers in positions defined in the maintenance manual: one accelerometer to capture the amplitudes of the accelerations in the Y-axis (located horizontally on the mast of the main rotor – it is a rigid point); another accelerometer to capture the accelerations on the Z-axis (vertically on the left front floor); and a magnetic sensor located on the fixed plateau to measure the phases, when it passes through the magnetic switch (emitter) permanently affixed to the mobile plateau. Figure 25 shows the equipment used (except the magnetic sensor) (images taken during the tests).

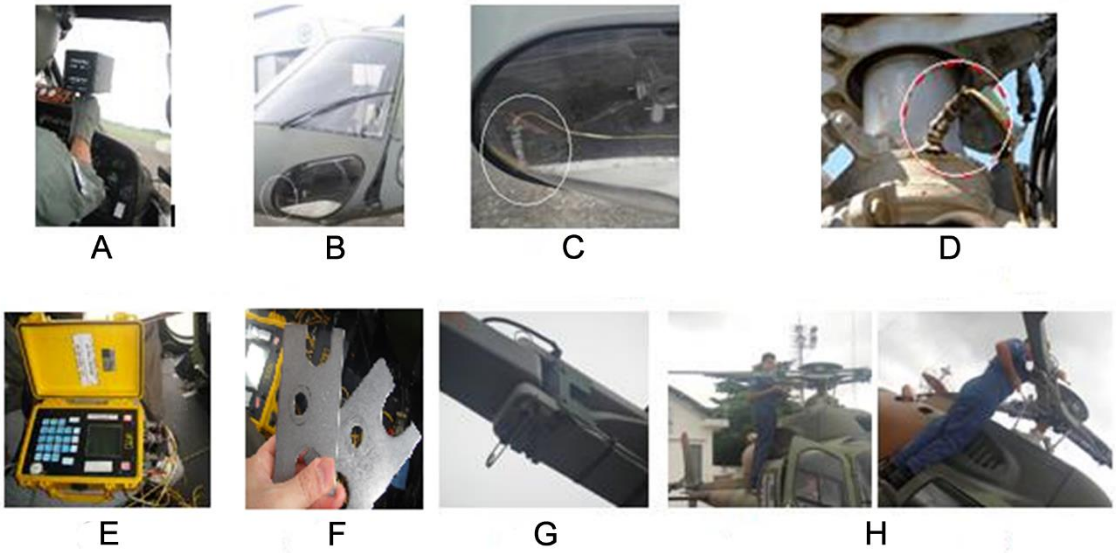

Figure 25: Flight test instrumentation: (A) strobex; (B), (C) Z-axis accelerometer; (D) Y-axis accelerometer; (E) ACES P2020 analyzer; (F) balance sheet; (G) platelets fixed to the blade handle; (H) change in platelet configuration [Adapted from (González, 2012)]

ASSESSMENT OF THE (PRELIMINARY) FLIGHT TEST RESULTS

As for the computational resource adopted to verify the model, the simulation would provide better results if the real design values (unavailable) were used. It is noteworthy that the consideration of flight conditions becomes a problem, given that, for each case of mass and balance, for example, it would be necessary to effectively evaluate the value of the initial θ fixation to be provided at the beginning of the code for the isotropic case. Therefore, for a more comprehensive simulation in terms of flight conditions/phases and the flight envelope of the aircraft, it would be necessary to build a numerical solution more adapted in robustness to this specific problem. Nevertheless, in the case limited to the range of this initial estimated of θ, as stated above, the code showed convergence after twelve iterations, consuming insignificant computational time, whose values were subjected to comparisons with the results of the flight tests. Tables 4 and 5 present a comparison between flight test and numerical simulation results, for 16 test points (cases in which flight tests were originally scheduled). For better use of the evaluation, and by the recommendations of the MET, the end signal of each installed accelerometer is considered. Therefore, in Tables 4 and 5, the data indicated is highlighted in the grids. In each cell corresponding to the reading at a test point, there are two lines for comparisons between test data (top line) and numerical simulation (bottom line). The grids guide the consideration of lateral vibrations Y (in the rotor plane) for test points 1 and 2, and vertical vibrations Z (orthogonal to the rotor plane) for the others, only.

Table 4: Comparison of flight test results and numerical simulation: test points 1 to 8 [Adapted from (González, 2012)]

Data	1	2	3	4	5	6	7	8
1Ω Z (IPS)	0,38 0,347	0,35 0,351	0,08 0,349	0,14 0,349	0,30 1,033	0,08 1,051	0,34 1,406	0,12 1,411
Phase Z (°)	326,50 -89,97	359,50 89,95	273 -89,953	309 -89,908	202,5 -55,581	185 -55,271	204,50 -49,200	189,50 -49,342
1Ω Y (IPS)	0,18 1,478	0,47 1,491	0,05 1,484	0,20 1,162	0,26 2,022	0,44 2,062	0,28 2,898	0,46 2,902
Phase Y (°)	358,50 - 83,530	8,50 -83,601	358,50 -83,512	22,50 -83,475	16 -30,800	9,50 -30,181	6 -18,777	13 -18,942
Red Blade	-0,5 0.474	-1,3 0.473	No data 0.4763	0,7 0.478	No data 1.444	-5,8 1.462	No data 1.459	-6,6 1.899
Yellow blade	0,0 0.475	0,0 0.473	No data	0,0 0.478	No data 1.444	0,0 1.462	No data 1.459	0,0 1.899
Blue blade	0,0 0.475	2,0 0.474	No data	0,5 0.478	No data	-7,8 1.462	No data 1.459	-5,5 1.899

Table 4 additional details: Flight tests (1st day) Test point & description. Condition & description
1. Point 1: Ground turn. Condition 1: Rotor balanced and tracking adjusted - test/code.
2. Point 1: Ground turn. Condition 2: Yellow blade with two fewer platelets - test/code.
3. Point 3: Hover IGE. Condition 1: Rotor balanced and tracking adjusted - test/code.
4. Point 3: Hover IGE. Condition 2: Yellow blade with two fewer platelets - test/code.
5. Point 4: Level forward flight at PMC. Condition 1: balanced and tracking adjusted - test/code.
6. Point 4: Level forward flight at PMC. Condition 2: Yellow blade with two fewer platelets - test/code.
7. Point 5: Forward flight + Curves $\phi = 45°$ at PMC (Right Turn). Condition 1: balanced and tracking adjusted - test/code.
8. Point 5: Forward flight + Curves $\phi = 45°$ at PMC (Right Turn). Condition 2: Yellow blade with two fewer platelets - test/code.

Table 5: Comparison of flight test results and numerical simulation: test points 9 to 16 [adapted from (González, 2012)]

Data	9	10	11	12	13	14	15	16
1Ω Z (IPS)	0,16 0,343	0,04 0,339	0,06 0,349	0,03 0,340	0,37 1,345	0,33 1,356	0,40 1,356	No data
Phase Z (°)	333 -89,96	25,5 89,944	262 89,990	125 -89,96	172,5 - 9,5583	114 - 48,974	170,50 - 49,537	No data
1Ω Y (IPS)	0,08 1,142	0,21 1,125	0,09 1,172	0,26 1,103	0,24 2,827	0,30 2,817	0,33 2,849	No data
Phase Y (°)	319 -83,531	116 -83,629	97 -83,541	122,50 -83,540	22 - 18.845	55 - 18.400	358 - 18.807	No data
Red Blade	1,0 0.473	-0,7 0.467	0,0 0.476	1,0 0.471	-4,8 1.874	-0,2 1.890	-5,0 1.882	No data
Yellow blade	0,0 0.473	0,0 0.4677	0,0 0.476	0,0 0.471	0,0 1.874	0,0 1.890	0,0 1.882	No data
Blue blade	1,0 0.473	0,0 0.467	-1,7 0.476	-1,7 0.471	-5,6 1.874	-4,0 1.890	-4,6 1.882	No data

Table 5 additional details: Flight tests 2nd day. Test point & description. Condition & description
9. Point 1: Ground turn. Condition 1: Rotor balanced and tracking adjusted - test/code.
10. Point 1: Ground turn. Condition 2: Yellow blade with two fewer platelets - test/code.
11. Point 3: Hover IGE. Condition 1: Rotor balanced and tracking adjusted - test/code.
12. Point 3: Hover IGE. Condition 2: Yellow blade with two fewer platelets - test/code.
13. Point 4: Level forward flight at PMC. Condition 1: balanced and tracking adjusted - test/code.
14. Point 4: Level forward flight at PMC. Condition 2: Yellow blade with two fewer platelets - test/code.
15. Point 5: Forward flight + Curves $\phi = 45°$ at PMC (Right Turn). Condition 1: balanced and tracking adjusted - test/code.
16. Point 5: Forward flight + Curves $\phi = 45°$ at PMC (Right Turn). Condition 2: Yellow blade with two fewer platelets - test/code.

The flight test campaign could not complete the schedule in its entirety due to a failure related to the operation of the Main Gear Box (MGB) (presence of swarf/filings in the dedicated magnetic sensor), which also contributes to vibrations. This occurrence made the aircraft unavailable for a long period, in addition to what was compatible with this research work. Thus, there are no data tested from test point 16 (Table 5), nor the tracking variation per action in the pitch control rod length adjustments. It is worth mentioning the difficulties of the mechanics for the sensitive readjustments of the pitch rod to its original position, which is decisive for reference flights.

As for the flight tests, even though they are the best alternative in terms of the wealth of information, they also presented, in smaller numbers, some adverse results than expected (for example: in the evolution of trials 5 to 6; and 7 to 8; 13 to 14 - decrease instead of the expected increase in the amplitude of the oscillatory response. These inconsistencies are attributed to the complexity of the atmospheric environment in which the flight dynamics are immersed; to the instantaneous variation of aircraft parameters, including those sensitive to the recording instant (eg: speed and vibration reading, which are related to the test pilot's ability to identify and sustain the desired condition then reached); and to possible disturbances associated with the acting defect and only then detected. All these facts can be mitigated by considering an average of a large number of similar flights, which was not possible in this research.

As for the simulations, the same inconsistencies were manifested in the evolution of tests 3 to 4; 9 to 10; 11 to 12. It is attributed to the series of simplifying considerations that were necessary for this study as a determining influence on the small values of the variations and to the large ones in the module of the results of the amplitudes relative to the experimental data, as well as the large phase variations. Also noteworthy is the influence of the rigid blade hypothesis and the absence of relevant real project values, as these would be the only guarantee that the same tested aircraft is being simulated.

The results obtained are preliminary. A few results were encouraging, such as the evolution of flight tests 1 to 2; 3 to 5; and 7 to 8 – confirming the increasing trend in the amplitude of the oscillatory response. Especially in evolution 1 to 2 and 5 to 6 the phase change trend aligned with the experimental test data (taken as a reference for this reading).

A comment on the vibration absorbers in Z- and Y- directions

In the flight tests carried out, the accelerometer in the vertical Z-direction was located in the front section of the cabin, as shown in Figure 25, reasonably far away from the most rigid section of the fuselage (which would be near the station just below the main rotor).

This front section, at the nose of the aircraft, is a region that oscillates (and therefore has important natural modes of vibration) in this Z-direction (due to the elasticity of the structure). A suggestion for future work would be to choose a location to install the accelerometer and collect vibration data in the Z-direction as another point, in a more central region, perhaps near the vertical station below the main rotor.

Another important aspect is that under the floor of the Squirrel, more or less in the region below the pilot's seat, there is a vertical vibration absorber, tuned to the 3Ω frequency, as shown in Figure 26. This absorber is located in a station about halfway between the main rotor station and the region near the nose of the aircraft, where the accelerometer was placed in the flight tests that were carried out.

Typically, a linear absorber would not have an important effect on frequencies away from its design frequency (in this case, 3Ω), but, in the case of non-linearities in the vibration absorber behavior, there is a possibility (to be investigated) that this vibration absorber could have influenced the signal in 1Ω captured by the accelerometer.

The two reasons above (the location of the accelerometer at a forward station near the nose of the aircraft; and the presence of a nearby Z-direction vibration absorber) may have contributed to the discrepancy found between the flight test results (lower Z-vibration amplitudes) and the numerical model (higher Z-vibration amplitudes), in this cockpit accelerometer, installed in the vertical direction.

The vibration amplitude measured in the flight tests was about one order of magnitude lower than the vibration amplitude calculated by the numerical model, giving a hint that maybe some part of the vibration in 1Ω was also attenuated, maybe by some non-linear behavior of this vertical vibration absorber in 3Ω.

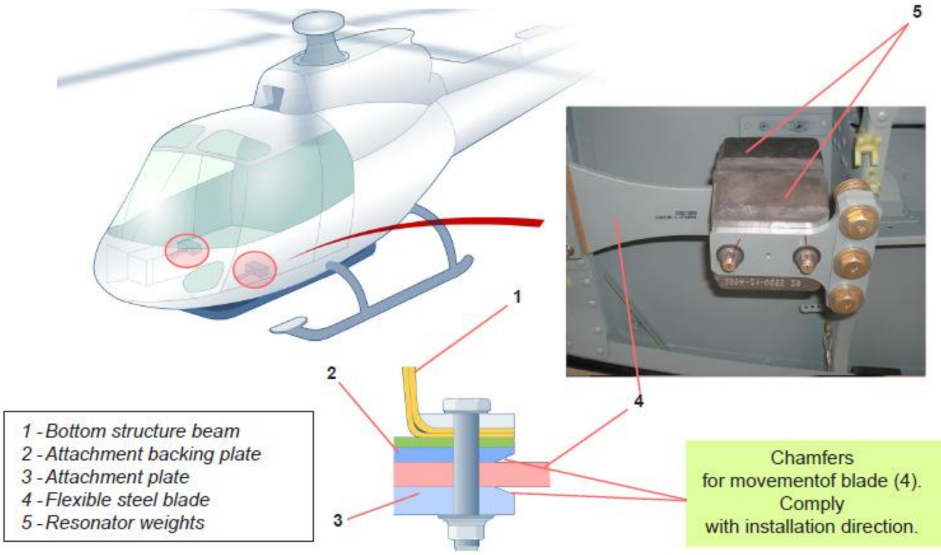

Figure 26: (AS 350B3 Squirrel) Z-direction vibration absorber (floor below pilot) – adapted from (EUROCOPTER, 2010)

As for the accelerometer in the Y-direction (therefore, practically in the rotor plane), it was correctly placed in a more central region, but because the location of this accelerometer was at a height very close to the rotor plane, the vibration measured in the Y-direction could have been influenced by the presence of the main rotor vibration absorber, with its resonator weights, as shown in Figure 27.

These resonator weights, inside the fairing, form a tuned set to absorb vibrations in the rotor plane at the 3Ω frequency. Thus, like the case of the absorber of vertical vibrations under the pilot's floor, this in-plane absorber may have influenced the Y-vibration measured results. Again, the Y-vibration amplitude measured in the flight tests was one order of magnitude lower than the Y-vibration amplitude calculated by the numerical model, giving a hint that maybe some part of the vibration in 1Ω was also attenuated, maybe by some non-linear behavior of this vibration absorber in 3Ω.

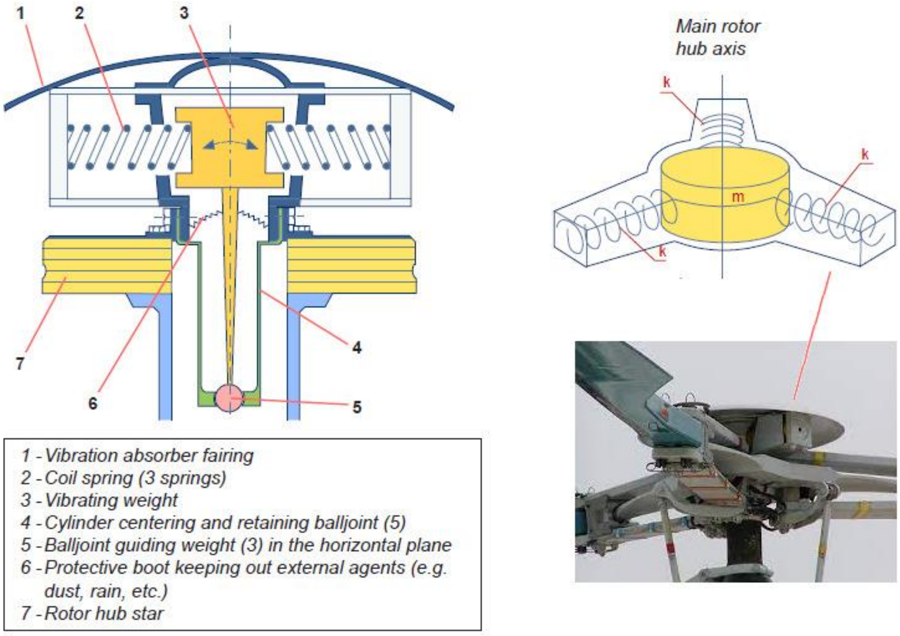

Figure 27: (AS 350B3 Squirrel) Y-direction vibration absorber (rotor hub) – adapted from (EUROCOPTER, 2010)

The presence of these vibration absorbers in Z- and Y- directions near the location of the corresponding Z- and Y- accelerometers may have contributed to the lower amplitudes in the vibration signal obtained in the flight tests, when compared to the corresponding amplitudes calculated using the numerical model and may help to explain the differences in amplitudes that were found.

Thus, the presence of a Z- or Y- vibration absorber, in the vicinity of an accelerometer in the same Z- or Y- direction, requires further investigation and would demand a change in the location of the accelerometer in future test flights, and/or an improvement in the numerical model, to include the presence of such vibration absorbers.

4.5 Possibilities for future work

As suggestions for further work, one can consider:

- a thorough review of the model and its assumptions, to be able to refine and adapt the model to attain a higher level of fidelity of the model concerning the real aircraft, to properly represent the dynamics of the rotor-fuselage system, including the above-mentioned vibration absorbers in Z- and Y- directions (see Figures 26 and 27);
- real aircraft data is required to be used in the model, again to increase model fidelity concerning a real aircraft. Proper aircraft parameters must be given, and/or identified using data science/pattern recognition techniques (Artificial Neural Networks, for example), and must be validated before their use in the numerical model;
- the numerical model and the flight tests need to represent the same flight conditions, to validate the comparisons between numerical and experimental results. The observed trends for the code results as compared to the flight test results should present similar behavior, to provide evidence of the potential for this model to be used as a tool to help maintenance procedures of balancing and tracking of the helicopter main rotor, based on vibration measurements in the fuselage.
- after the model for the Direct Problem (given defects in the main rotor, leading to vibration changes (amplitude and phase) at particular fuselage points) is revised and validated, the research may concentrate on adequate approaches (optimization methods, identification approaches) for the Inverse Problem (vibration changes (in amplitude and phase) at particular fuselage points leading to detection/localization/classification/identification of defects in the main rotor, and, in consequence, leading to the suggestion of corrective maintenance procedures, such as the proper adding/subtracting of balance masses, or the increasing/decreasing of the pitch rod length).

5 Concluding Remarks

In this chapter helicopter, vibration reduction techniques were discussed, focused on balancing, and tracking the helicopter rotors, and concentrated on a discussion of model-based parameter identification for balancing and tracking a helicopter main rotor using once-per-revolution vibration data. Details of the models were presented for two study cases: a 4-blade main rotor, and a 3-blade main rotor. Simulation results were obtained in both cases from the models that were derived in this work. These results were compared, for the 4-blade rotor case, with the charts available in the maintenance manual, and for the 3-blade rotor case, with some preliminary flight tests that were performed under flight profiles recommended in the maintenance manual (MET), as an experimental phase of the work.

The results obtained for both cases showed that the models derived in this study, even with all the assumptions and simplifications in the derivation of the equations, are promising, and pointed out in the proper direction.

For the 4-blade case, the model has indicated a correction to be done in the proper blade and in the proper direction (for example, for correctly adding or subtracting balancing masses). Only the amount of mass to be added/subtracted differs slightly from the model to the experimental case.

For the 3-blade case, the computer code exhibited significant sensitivity to changes in flight conditions and, certainly, was influenced by the deficiency of real design data in the simulation, which could have limited the performance of the numerical results. Also, environmental factors during the experimental flight, as well as the instantaneous parameters in continuous variation, may have contributed to compromise the intentions of formal validation of the model.

The perspectives regarding the potential of the model derived in this work were deemed satisfactory, with a valuable experience arising from the investigation and analysis of the comparative results, with insights, such as the need to take into account the presence of the Z- and Y- vibration absorbers, in the vicinity of the accelerometers in the same Z- or Y- direction.

As suggestions for future work, the coefficients of the obtained equations could be seen as parameters to be identified in an inverse problem. With this approach, the values of the mass, centering, etc., will be identified for the actual helicopter, and used as the parameters in the derived equations, instead of using, in these equations, the average/typical values that were used in this work. Doing this model-based parameter identification for an already-derived equation should be more efficient and less time-consuming, when compared to the signal-based identification of the helicopter and rotor parameters from scratch, in which only input and output data would be available, without any prior knowledge of the mechanics of the system.

Acknowledgments

The authors would like to acknowledge the support from the Brazilian Navy (Naval Aviation), Airbus Helicopters (France), and the Institute for Research and Flight Tests (IPEV-DCTA, Brazil).

References

Beer, F., Johnston, E., Mazurek, D., Cornwell, P., & Self, B. (2019). *Vector Mechanics for Engineers: Statics and Dynamics* (12th ed.). Mc Graw Hill.

Ben-Ari, R., & Rosen, A. (1997). Mathematical Modelling of a Helicopter Rotor Track and Balance: Results. *Journal of Sound and Vibration*, *5*(200), 605–620.

Benoit, B., Dequin, A.-M., Kampa, K., Grunhagen, W. von, Basset, P.-M., & Gimonet, B. (2000). HOST, a General Helicopter Simulation Tool for Germany and France. *American Helicopter Society 56th Annual Forum,* 1–23. https://www.researchgate.net/publication/224792351_HOST_a_General_Helicopter_Simulation_Tool_for_Germany_and_France

Bielawa, R. L. (2006). *RotaryWing Structural Dynamics and Aeroelasticity*. AIAA.

Bramwell, A. R. S., Done, G., & Balmford, D. (2001). *Bramwell's Helicopter Dynamics* (2nd ed.). Butterworth-Heinemann.

Coleman, R. P., & Feingold, A. M. (1957). *Theory of self-excited mechanical oscillations of helicopter rotors*.

Damy, L. F. (2017). *Contribution to the development of helicopter tail rotor balancing techniques: proposition of an adaptive method and stochastic modeling (In Portuguese)* [Instituto Tecnológico de Aeronáutica]. http://www.bdita.bibl.ita.br/tesesdigitais/lista_resumo.php?num_tese=73533

EUROCOPTER. (2010). *THM AS 350B3 Squirrel: Mechanics Instruction Manual*.

EUROCOPTER. (2012). *Dynamics, Vibrations and Internal Noise: Module Presentation OFFSET BRASIL* (p. 127).

Friedmann, P. P., & Hodges, D. H. (2003). Rotary Wing Aeroelasticity—A Historical Perspective. *Journal of Aircraft*, *40*(6), 1019–1046.

Ganguli, R., Chopra, I., & Haas, D. J. (1998). Helicopter rotor system fault detection using physics-based model and neural networks. *AIAA Journal*, *36*(6), 1078–1086. https://doi.org/https://doi.org/10.2514/2.483

Gessow, A., & Myers, G. C. (1952). *Aerodynamics of the Helicopter*. McMillan.

González, R. de A. (2012). *Helicopter Main Rotor Failure Analysis using vibration and HUMS philosophy (In Portuguese: Análise Preditiva na Detecção de Falhas no Rotor Principal com Foco na Vibração em um Helicóptero Segundo a Filosofia HUMS)*. Instituto Tecnológico de Aeronáutica (ITA), Brazil.

HELIBRAS. (1994). *MET - Maintenance Manual 62.10.00.603 of AS355F2 helicopter*.

Johnson, W. (1980). *Helicopter Theory*. Dover Publications.

Johnson, W. (2013a). *Rotorcraft Aeromechanics*. Cambridge University Press.

Johnson, W. (2013b). A History of Rotorcraft Comprehensive Analyses. *AHS 69th Annual Forum*, 1–22. https://ntrs.nasa.gov/api/citations/20130014338/downloads/20130014338.pdf

Jorge, A. B. (1992). *Fault detection system of a helicopter rotor from the vibration level (In French: Systeme de detection de defauts d'un rotor d'helicoptere a partir du niveau vibratoire)*. Ecole Nationale Superieure D'ingenieurs de Constructions Aeronautiques (ENSICA), Toulouse, France.

Jorge, A. B., & Torres Filho, A. S. (1989). Vibration in Helicopters. Causes and Consequences on Equipment. How to live with the problem? (In Portuguese: Vibração em Helicópteros. Causas e Consequências nos Equipamentos. Como conviver com o problema?). *BISAFO - Boletim Informativo Segurança de Aviação Em Foco, SIPAERM, Brasil*, *23*, 16–22.

Kunz, D. L., & Newkirk, M. C. (2009). A generalized dynamic balancing procedure for the AH-64 tail rotor. *Journal of Sound and Vibrationnd Vibration*, *326*, 353–366. https://doi.org/10.1016/j.jsv.2009.04.043

Meijer Drees, J. (1949). A theory of airflow through rotors and its application to some helicopter problems. *Journal of the Helicopter Association of Great Britain*, *3*(2), 79–104.

Miller, N. A., & Kunz, D. L. (2008). A comparison of main rotor smoothing adjustments using linear and neural network algorithms. *Journal of Sound and Vibration*, *311*, 991–1003. https://doi.org/10.1016/j.jsv.2007.09.041

Mobley, R. K. M. (1999). *Root Cause Failure Analysis*. Butterworth-Heinemann.

Müller, M., Arnold, U. T. P., & Morbitzer, D. (1999). On the Importance and Effectiveness of 2/REV IBC for Noise, Vibration and Pitch Link Load Reduction. *25th European Rotorcraft Forum*.

Padfield, G. D. (2007). *Helicopter flight dynamics: the theory and application of flying qualities and simulation modeling* (AIAA (Ed.)).

Padfield, G. D. (2018). *Helicopter Flight Dynamics - Including a Treatment of Tiltrotor Aircraft* (3rd ed.). Wiley.

Prouty, R. W. (1985). *Helicopter Aerodynamics*. Phillips Pub.

Rabe, D., & Wilke, G. (2018). Parametric Design Studies of the Helicopter Rotor Noise using Variable-Fidelity Methods. *AHS International 74th Annual Forum & Technology Display*, 1–20. https://elib.dlr.de/125009/1/AHS-74-Paper.pdf

Rosen, A., & Ben-Ari, R. (1997). Mathematical Modelling of a Helicopter Rotor Track and Balance: Theory. *Journal of Sound and Vibration*, *5*(200), 589–603.

Venkatesan, C. (2015). *Fundamentals of Helicopter Dynamics*. CRC Press.

Ventres, S., & Hayden, R. E. (2000). Rotor Tuning Using Vibration Data Only. *VFS Annual Forum & Technology Display, Forum 56*.

Wang, S., & Danai, K. (2003). A probability-based approach to helicopter track and balance. *AHS 59th Annual Forum*, 1–10.

Wang, S., Danai, K., & Wilson, M. (2005). Adaptive Method of Helicopter Track and Balance. *Journal of Dynamic Systems, Measurement, and Control*, *127*, 275–282. https://doi.org/10.1115/1.1913683

Wilke, G. A. (2017). *Aerodynamic Optimization of Helicopter Rotor Blades using Variable Fidelity Methods* [TU Braunschweig]. https://core.ac.uk/download/pdf/158058408.pdf